11.04 Geophysical Properties of the Near Surface Earth: Electrical Properties

PWJ Glover, University of Leeds, Leeds, UK

11.04.1 Introduction to the Electrical Properties of Near-Surface Rocks

11.04.1.1 Importance

The electrical properties of near-surface geomaterials have been hugely important in the development of many modern well-developed countries, and will play a leading role in the further development of those less well-developed countries which are currently emerging as possible future economic powers. The effect is, of course, most obvious in the exploitation of hydrocarbon resources, where Archie's laws have been at the heart of oil and gas reserves calculations for every field that has been produced since their inception (Archie, 1942). This amounts to more than 1.5 trillion barrels of oil and 7.5 trillion cubic feet of gas (Bentley, 2002). These resources have driven the global economy of the last 50 years (Glover, 2009; Speight, 2011). The impact of oil and gas is overwhelming. According to the International Energy Agency's Energy Balance data, hydrocarbons heat the majority of all we heat, transport most of that that is transported, and make a significant proportion of our manufactured goods. Modern health, for example, would be impossible without the sterile plastic consumables upon which it depends.

However, it would be a mistake to consider the role of electrical conduction in near-surface materials to be confined to the oil and gas industry. There are significant applications in mining (e.g., Friedrichs et al., 1999); soil remediation (e.g., Pearce and Zuluaga, 2004; Rojo et al., 2014); waste management (domestic, industrial, toxic, and radioactive) (e.g., Lesparre et al., 2013); civil engineering, where the artificial rock concrete is a major factor in the development of our modern landscape (e.g., Susanto et al., 2013; Weiss et al., 2013); treatment of natural hazards including rock and mud slides (e.g., Jackson et al., 2002); and earthquakes and volcanic activity (e.g., Di Maio and Patella, 1991, 1994; Fujinawa et al., 1992; Mizutani et al., 1976; Revil et al., 2002, 2010).

In a more academic sphere, the applications of the concepts described in this chapter are used for understanding the continental crust (e.g., Glover, 1996; Glover and Adám, 2008; Glover and Vine, 1992, 1995; Glover et al., 2000b; Yang, 2011) and oceanic crust (e.g., Baba, 2005; Gung et al., 2003; Key et al., 2013; Yoshino et al., 2008); the triggering of natural and synthetic earthquakes (e.g., Chelidze et al., 2003; Cyr et al., 2010); volcanic activity monitoring (e.g., Revil et al., 2010); the properties of lunar (e.g., Li et al., 2005), Martian (e.g., Carter et al., 2009), and asteroidal (e.g., Wittmann et al., 1999) materials; and soil science (e.g., Robinson et al., 2003; Peplinski et al., 1995). Counterintuitively, perhaps, some of the electrical conductivity models have been applied in fields as varied as catalysis research (e.g., Zhang and Catchmark, 2011) and food engineering (e.g., Jha et al., 2011; Jindal et al., 2013). Certain concepts such as cation-exchange capacities (CECs) even find themselves useful in farming and gardening (e.g., Banton et al., 1997; Green, 1997; Oliver et al., 2013). Electrical measurements are also used by archaeometrists to search for buried archaeological remains (e.g., Gaffney, 2008; Glover, 2010a), as well as in the study and conservation of items of cultural heritage (e.g., Maurício et al., 2005; Sass and Viles, 2010; Zhao et al., 2012).

11.04.1.2 Scope

The electrical properties of rocks describe how charge is transported through them. The transport of charges may be in response to a steady-state or time-varying electric field, giving rise to a steady-state resistivity and conductivity or a complex

impedance or admittance. In each case, the charge carriers may be electrons or ions.

Electrons are the charge carriers that mediate conduction in metals and semiconductors. It is the conduction mechanism when conduction takes place in minerals at high temperatures and pressures and falls outside the scope of this volume (please see Chapter 2.25).

Ions are the charge carriers that mediate conduction in pore fluids, in the electrical double layer that exists at the mineral/pore fluid interface, and in melts. All three situations are common in near-surface rocks and are considered in detail in this chapter. In the steady state, we consider the electrical resistivity and conductivity, but use complex impedance and admittance when discussing the frequency-dependent conduction, each of which is composed of an in-phase resistivity or conductivity and an out-of-phase or quadrature resistivity or conductivity.

There may be net transport of ionic charges in the absence of an electric field. For example, preferential advection of positive and negative ions may take place due to the flow of fluids. The preferential advection then causes a separation of charge that results in a current source. The streaming potential is the electric field associated with that current source. This creation of an electric potential in response to a fluid flow in the absence of an external applied electric field is an example of an electrokinetic process. Electrokinetic processes are described towards the end of this chapter.

11.04.1.3 Objectives

This chapter has the following objectives:

- To describe the fundamental physics that underlies the steady-state conduction of electric currents in geomaterials including conduction mechanisms.
- To examine the electrical properties of the various materials that contribute to the electrical properties of geomaterials.
- To review briefly the range of resistivity and conductivity values found in common geomaterials.
- To introduce Archie's laws in detail, noting their important and wide-ranging academic and industrial applications in understanding near-surface geomaterials.
- To examine theoretical and empirical models for steady-state conduction in geomaterials including those for partially saturated and shaley rocks.
- To examine the origins, role, and implications of surface conduction in geomaterials and to review briefly some applications for clean and shaley geomaterials.
- To describe the measurement, modeling, and range of frequency-dependent conduction in geomaterials, including a review of the dispersion processes that control the overall dielectric properties of the geomaterial, measurement, and modeling, together with the range of dielectric properties of geomaterials and the materials that compose them.
- To describe the electrokinetic processes that couple the electrical properties of rocks to fluid flowing through them and the main parameters that affect the electrokinetic coupling.
- To describe the measurement and modeling of these electrokinetic properties both in the steady state and as a function of frequency.

11.04.1.4 Structure of the Chapter

This chapter is in six parts. Section 11.04.1 serves as a short general introduction. Section 11.04.2 describes steady-state electrical properties, starting with Ohm's law, discussing the properties that affect the electrical properties of rocks, introducing Archie's laws, and examining the range of electrical properties encountered in rocks and minerals in the natural world.

There are many mixing models that aim to provide the conductivity or resistivity of a geomaterial once the conductivity or resistivity of its components and their volume fractions are known. Section 11.04.3 examines mixing models in detail, making a distinction between geometric arrangements of phases and those that invoke parameters to describe the connectedness of each phase.

Section 11.04.4 examines surface conduction in detail, introducing the electrical double layer and describing the basic theory of surface conduction and its applications to clean and clay-containing geomaterials.

Steady-state conduction is a special case of conduction where the electric potential and current remain constant with time. In general, this is not so. Electromagnetic fields may vary harmonically at a given frequency or transiently. Section 11.04.5 describes frequency-dependent conduction in geomaterials, starting with an understanding of the dielectric properties of geomaterials and how they provoke polarization mechanisms within geomaterials and how conduction and displacement currents contribute to the overall complex electrical properties of the geomaterial. Mixing models, theoretical modeling, and measurement (impedance spectroscopy) of the complex electrical properties of geomaterials are also considered before examining the range of dielectric properties of geofluids and geomaterials.

If a porous medium has an electrical double layer at the fluid–matrix interface, it develops a finite surface conduction. When fluid flows in such a medium, there is an electrokinetic coupling that generates an electrical streaming potential. Section 11.04.6 examines the origin, properties, measurement, and modeling of the electrokinetic properties of geomaterials.

Finally, Section 11.04.7 provides a brief summary.

11.04.2 Steady-State Electrical Properties

11.04.2.1 Basic Physical Relationships

11.04.2.1.1 Ohm's law

Ohm's law is the fundamental physical law that relates the current flowing through a material to the difference in potential across it.

The law states that in an electrical circuit, the current (I, in A) passing through a conductor between two points is directly proportional to the difference in electric potential (V, in V) between the two points and inversely proportional to the resistance of the material (R, in Ω) between the two points:

$$I = \frac{V}{R} \quad [1]$$

The potential difference represents the electric force that causes a flow of charge carriers that forms the current. The resistance is that property of the material which resists the flow of the charge carriers, and limits current density proportionally to the electric potential difference.

11.04.2.1.2 Ohm's law in a continuous medium

At any point in a continuous medium, Ohm's law can be written as

$$\vec{J} = \sigma \vec{E} \quad [2]$$

where $\vec{J}$ is the current density, in A m^{-2}; σ is the conductivity of the material, in S m^{-1}; and $\vec{E}$ is the electric field, in V m^{-1}.

The conductivity, σ, is usually a scalar function that may vary with angular frequency, but can be a nonlinear tensor function of temperature, pressure, and deformation as well as being a tensor due to anisotropy.

If the material moves with a velocity $\vec{v}$, relative to a magnetic field $\vec{B}$, the current density is augmented by a contribution that is induced in the material by the magnetic field:

$$\vec{J} = \sigma\left(\vec{E} + \vec{v} \times \vec{B}\right) \quad [3]$$

This relationship is not developed in the remainder of this chapter, but is an important starting point for understanding geophysical techniques such as magnetotellurics.

11.04.2.1.3 Resistance and resistivity

The resistance (R) is the ability of a material to impede the passage of an electric current. It is measured in ohms (Ω). The resistance depends upon the size and shape of the material in which the current flows. Doubling the distance through which the current flows doubles the resistance, while doubling the cross-sectional area of material perpendicular to flow halves the resistance. Hence, resistance is partly due to some intrinsic property of the material and partly due to the geometry of the material relative to the two points between which the current flows and the electric potential is applied.

The resistivity (ρ) describes only the intrinsic resistive properties of the material to the flow of charge carriers and is not affected by the geometry of the sample. It corresponds to the resistance of a sample 1 m long with a constant cross-sectional area for current flow that is 1 m^2. Resistivity has units of ohm meters (Ωm).

For a continuous current that passes through a homogeneous and isotropic material with a length L and a cross-sectional area A, the resistance and resistivity are related by

$$\rho = R\frac{A}{L} \quad [4]$$

We can define the resistivity of a material as

$$\rho = \frac{\vec{E}}{\vec{J}} \quad [5]$$

where $\vec{E}$ is the magnitude of the electric field applied to the material (in V m^{-1}) and $\vec{J}$ is the magnitude of the current density that results (in A m^{-2}).

Resistivity depends on temperature. As a general rule, the resistivity of a metal increases with temperature, while that of a semiconductor decreases with temperature. The resistance of minerals at high temperatures is beyond the scope of this chapter (see **Chapter 2.25**). The resistivity of aqueous fluids, which occupy the pores of near-surface rocks and form one of the main conduction pathways in such rocks, decreases with increasing temperature at about 4% per °C at low temperatures (around 5 °C), at about 2% per °C at room temperatures, and at about 1% per °C as the temperature approaches 100 °C (Sen and Goode, 1992a,b). This is a significant sensitivity to temperature and implies that all electrical measurements should be made at a stable temperature, and care is taken comparing measurements made at different temperatures. Conversely, some field applications use resistivity to infer the in situ temperature, for example, some geothermal applications and the monitoring of groundwater-surface water exchange.

Figure 1 shows the electrical resistivity of several types of Earth material. It is worth noting that the range of measured resistivities is extremely large from $10^{-7}\Omega$m for copper to $10^{18}\Omega$m for diamond (Pierson, 2004). However, electrical resistivity measurements may be made in the laboratory with a precision of several decimal places. Hence, electrical

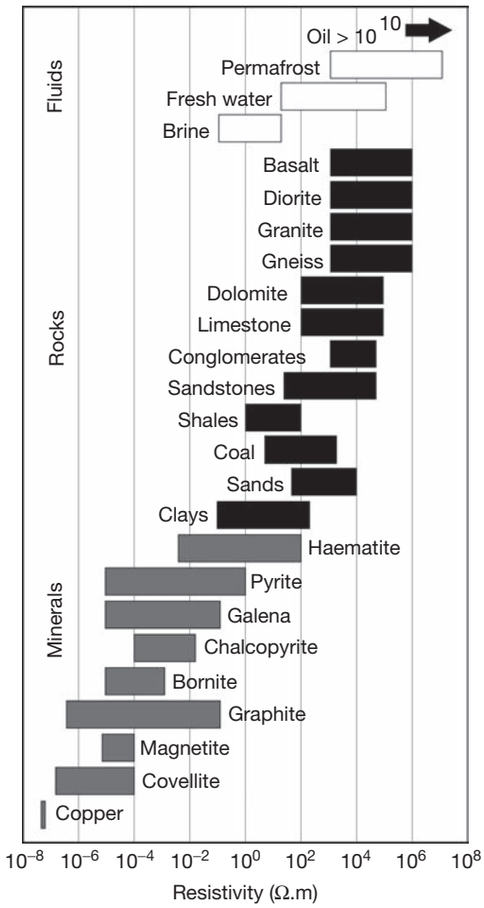

Figure 1 Electrical resistivity of several geomaterials (compiled from Guéguen and Palciauskas, 1994; Schön, 2004; Keller, 1989).

properties offer a very precise way of differentiating geomaterials and can be used to develop probes, which are highly sensitive to changes in rock structure and composition. However, many geomaterials have a large natural range of electrical properties that arise from their natural heterogeneity and anisotropy. When this is the case, even highly sensitive electrical techniques cannot differentiate between them.

Electrical measurements have the additional advantage in that they can often be made remotely. A small-scale example is the electrical induction downhole tool, which can be used to measure the conductivity of a formation even though the well is filled with an insulating oil-based mud. A large-scale example would be the magnetotelluric method that allows the conductance of layers deep in the Earth to be measured. In both cases, a current is induced in the material that is to be measured using an electromagnetic field. The current that flows induces a secondary field, which itself can be measured in order to obtain the resistance of the remote material.

11.04.2.1.4 Conductance and conductivity

Conductance (G_c), which is expressed in siemens (S), is the inverse of resistance (R). Hence (Guéguen and Palciauskas, 1994),

$$G_c = \frac{1}{R} \quad [6]$$

Conductance represents the ability of a material to let charges flow through it freely.

Conductivity (σ) is, therefore, the inverse of resistivity:

$$\sigma = \frac{\vec{J}}{\vec{E}} \quad [7]$$

where $\vec{J}$ is the current density that flows in the material, in A m^{-2}, and $\vec{E}$ is the electric field, in V m^{-1}. Conductivity is expressed in siemens per meter (S m^{-1}).

11.04.2.1.5 Conductivity and charge carriers

Consider charge carrier i with a charge $Z_i e$, where Z_i is the valency of the charge carrier and $e \approx 1.6022 \times 10^{-19}$ C is the elementary charge (Lide, 2012). If the charge carrier is in an electric field $\vec{E}$, the force on the charge carrier is $Z_i e \vec{E}$. In a steady state, the force results in a uniform charge carrier velocity:

$$\vec{v} = \mu_i \vec{E} \quad [8]$$

where μ_i is the mobility of the charge carrier, in m^2 V^{-1} s^{-1}, and is dependent upon its type, the medium, and temperature. Since the electric current density is the charge that crosses a unit surface area per second and n_i is the number of charge carriers of type i per unit volume,

$$\vec{J} = n_i Z_i e \vec{v} \quad [9]$$

Combining [7] to [9] gives an expression for conductivity as

$$\sigma_i = n_i Z_i e \mu_i \quad [10]$$

The conductivity is directly proportional to (i) the number of charge carriers per unit volume, (ii) the charge that each carries, and (iii) the mobility of the charge carriers. This basic statement is true for electronic conduction in solids; ionic conduction in solids, aqueous fluids, and melts; and for ionic conduction within the electrical double layer at the mineral/fluid interface.

11.04.2.1.6 Electronic conduction

All materials contain electrons. However, not all electrons are mobile. In solids, electrons have well-defined energy states that form bands. These bands are separated by disallowed energy states. Electrons may be mobile if they occupy a partially filled band of energy states. Then, externally applied energy, for example, from the ambient temperature ($=k_b T$) or an externally applied electric field ($= e\vec{E}$), can promote an electron to a higher energy, which is reflected in its kinetic energy (i.e., its motion).

Good conductors such as metals have a partially filled energy band, and the addition of externally applied energy results in the motion of electrons in this 'conduction' band (Poirier, 2000). By contrast, insulators have a full energy band so no externally supplied energy can be gained by electrons, and consequently, electrons cannot move. Moreover, the disallowed energy states that exist between the full band and the next, empty, conduction band is so large that electrons cannot be promoted to it and hence cannot gain kinetic energy of movement (Poirier, 2000).

For semiconductors, the energy band is also full. However, the energy gap between it and the next allowed energy band is small and electrons may be promoted into the higher-energy conduction band (Poirier, 2000). At a given temperature T, a number n_e of electrons can be promoted (excited thermally) into the conduction band according to

$$n_e \approx \exp\left\{-\frac{E_g}{k_b T}\right\} \quad [11]$$

where E_g is the width of the energy gap between the bands. If $E_g \gg k_b T$, there are very few electrons in the conduction band and the conductance is negligibly small. For minerals with $E_g \approx 0.5$ eV such as olivine ($E_g = 0.5$ eV; Guéguen and Palciauskas, 1994) or galena ($E_g = 0.37$ eV; Xu and Schoonen, 2000), there is only one promoted electron per 300 hundred million atoms of the mineral at 25 °C, but this rises to one promoted electron per 223 atoms at 800 °C, while a mineral with a large bandgap such as diamond ($E_g = 5.5$ eV; Guéguen and Palciauskas, 1994) or zirconia ($E_g = 5.0$ eV; Xu and Schoonen, 2000) has fewer than one conduction electron per 10^{12} atoms for all temperatures less than 2000 °C.

Hence, the electronic conductivity of a solid depends very much upon the size of the bandgap and the temperature, which control the number of electrons that are mobile and can take part in conduction according to eqn [10]. This equation shows that the conductivity also depends on the mobility of the electrons.

The electron mobility is given by

$$\mu_e = \frac{e\tau}{m_e} \quad [12]$$

where τ is the time between collisions between the electrons and the lattice and m_e is the mass of the electron. Collisions become more frequent with increasing temperature, and consequently, electron mobility diminishes. However, this effect is much smaller than the effect of temperature on the number of

electrons available for conduction, and hence, the overall trend is that the conductivity of solids increases strongly with temperature.

The conductivity of insulators and semiconductors also increases slightly with pressure due to a reduction in the band-gap energy. The effect of pressure is extremely small compared with that of temperature, and can be neglected in the Earth's crust (Dai and Karato, 2009; Xu et al., 2000). If one takes a typical geotherm of 30 °C km^{-1} and a typical geobar of 30 MPa km^{-1}, the effect of pressure is less than 1% of the effect of temperature at upper crustal conditions.

11.04.2.1.7 Ionic conduction

Transport of charge is mediated by ions. Ionic conduction is different from electronic conduction in that there are fewer ions available to carry charges than there are electrons in a metal or semiconductor, and since ions of different charge impede each other and even bond to each other, their mobilities are smaller.

Conduction in pore fluids is mediated by charged ions. In an aqueous solution of NaCl, for example, there are finite nonzero concentrations of the charged ions H^+, H_3O^+, OH^-, Na^+, and Cl^-, all of which transfer charge when an electric potential difference is applied to the fluid.

The general equation for describing the flow of charge carriers in a direction x (or indeed any particle, whether charged or not, and whether of ionic size or macroscopic size) is given by

$$\vec{J} = -D_i \frac{\partial n_i}{\partial x} + \bar{v} n_i \qquad [13]$$

where the first term is a statement of Fick's law, n_i is the number density of ionic species i, and D_i is the diffusion coefficient of the charged species, in m^2 s^{-1}, while the second term is due to fluid advection in direction x with a mean velocity $\bar{v}$. If we imagine a steady-state regime where $\vec{J} = 0$, hence,

$$D_i \frac{\partial n_i}{\partial x} = \bar{v} n_i \qquad [14]$$

and that is in thermodynamic equilibrium so that the spatial charge carrier distribution follows Boltzmann's law:

$$n(x) = n_o \exp\{-\varphi / k_b T\} \qquad [15]$$

where $k_b \approx 1.3806 \times 10^{-23}$ m^2 kg s^{-1} K^{-1} is Boltzmann's constant (Lide, 2012) and φ is either the chemical potential or the electric potential, leading ultimately to the equation

$$\frac{dn}{dx} = -\frac{n}{k_b T}\frac{d\varphi}{dx} = \frac{nF}{k_b T} \qquad [16]$$

where $F = -d\varphi/dx$ is the applied force responsible for the advective transport. Combination of [14] and [16] leads to the Nernst–Einstein equation (Poirier, 2000):

$$\frac{\bar{v}}{D} = \frac{F}{k_b T} \qquad [17]$$

Since the applied force for the advective transport $F = Z_i e \vec{E}$, we can combine [17] with [8] to obtain the ionic mobility as

$$\mu_i = \frac{Z_i e D_i}{k_b T} \qquad [18]$$

11.04.2.1.8 Conductivity of pore fluids

By combining [9] with [18], we may obtain the electrical conductivity for an ion in solution that is based on the Nernst–Einstein relationship:

$$\sigma_i = \frac{D_i Z_i^2 e^2 N n_i}{k_b T} \qquad [19]$$

where i represents the ith charge carrier; D_i is the diffusion coefficient of the charged species, in m^2 s^{-1}; Z_i is the valency of the charge carrier; $N \approx 6.022 \times 10^{23}$ mol^{-1} is Avogadro's number; n_i is the concentration of the charge carrier in mol l^{-1} (Lide, 2012); and T is the absolute temperature, in kelvin (K). It is worth noting that this equation shows an apparent inverse dependence on temperature, but at temperatures lower than about 250 °C, the conductivity of pore fluids increases with temperature because other terms in eqn [19] are also dependent on temperature, more than counteracting the explicit inverse dependence.

In a pore fluid, the current is carried by anions and cations traveling in opposite directions. In a steady state, the driving electric force $Z_i e \vec{E}$ is exactly balanced by the viscous drag on the hydrated ion $6\pi\eta r \vec{v}$ that is, according to Stokes' law, proportional to the velocity of the ion $\vec{v}_i$ (in m s^{-1}) and its hydrated radius r_i (in m) as well as the viscosity of the fluid η (in Pa s). Hence (Guéguen and Palciauskas, 1994),

$$Z_i e \vec{E} = 6\pi\eta r_i \vec{v}_i \qquad [20]$$

Comparison of this equation with [8] shows that the ionic mobility can be written as

$$\mu_i = \frac{Z_i e}{6\pi\eta r} \qquad [21]$$

Hence, eqn [21] shows that the individual ionic mobilities depend upon the viscosity of the fluid. This will have importance later in this chapter when we discuss how the increasing viscosity as one approaches the Stern plane will reduce the ionic mobilities in the electrical double layer that exists at the mineral/pore fluid boundary. It should be noted that while both eqns [18] and [21] are often applied to ionic solutions such as pore fluids, eqn [21] relies on the assumption that the hydrated ions behave as spherical particles moving slowly through a fluid, and this is not necessarily the case at high salinities.

Equation [21] can be used with eqn [10] to obtain the conductivity of the ion in the solution:

$$\sigma_i = \frac{n_i Z_i^2 e^2}{6\pi\eta r} \qquad [22]$$

This equation is important as it clearly shows that the conductivity is

- directly proportional to the number density of charge carriers available to transport charge,
- directly proportional to the square of the charge carried ($Z_i^2 e^2$),
- inversely proportional to the radius of the hydrated ion, and
- inversely proportional to the viscosity of the fluid.

Hence, eqn [22] lays the foundation for having different conductivity contributions from anions and cations of different hydrated radius.

While eqns [19]–[22] describe the conductivity of a pore fluid formally, in practice, it is often obtained using plots, nomograms, and empirical formulae. Perhaps, the most common and useful empirical formula for the conductivity of an aqueous solution of NaCl is given by Sen and Goode (1992a,b), noting that the second of the two references corrects an important error in the relationship presented by the first. The relationship is

$$\sigma_f(T, C_f) = \left(d_1 + d_2 T + d_3 T^2\right) C_f - \left(\frac{d_4 + d_5 T}{1 + d_6 \sqrt{C_f}}\right) C_f^{3/2} \qquad [23]$$

where $d_1 = 5.6$ $(\mathrm{S\,l\,m^{-1}\,mol^{-1}})$, $d_2 = 0.27$ $(\mathrm{S\,l\,m^{-1}\,mol^{-1}})/°\mathrm{C}$, $d_3 = -1.51 \times 10^{-4}$ $(\mathrm{S\,l\,m^{-1}\,mol^{-1}})/°\mathrm{C}^2$, $d_4 = 2.36$ $(\mathrm{S\,m^{-1}}/(\mathrm{mol\,l^{-1}})^{3/2})$, $d_5 = 0.099$ $(\mathrm{S\,m^{-1}}/(\mathrm{mol\,l^{-1}})^{3/2}/°\mathrm{C})$, $d_6 = 0.214$ $((\mathrm{mol\,l^{-1}})^{-1/2})$, T is in °C, and C_f is the salinity of the bulk pore fluid $(\mathrm{mol\,l^{-1}})$.

Hilchie's equation (Hilchie, 1984) is another method for calculating the conductivity of an NaCl fluid, but in this case, the equation is capable of converting fluid conductivities between temperature and salinities rather than being a formula for giving the conductivity directly.

Figures 2 and 3 show the values of eqn [23] for a range of fluid salinities that are found in the Earth's crust. Both salinity and temperature have a significant effect. Figure 2 shows the overwhelming effect of the number density of ions on the pore fluid conductivity. Fluids that are more saline have a greater number of ions and hence a greater conductivity. However, at very high salinities, interaction between ions begins to reduce their mobility, which reduces the rate of increase of conductivity with salinity.

The variation with temperature (Figure 3) is more complex. At low temperatures ($T < 140$ °C), the viscosity decreases with temperature and that leads to an increase in conductivity with temperature. At high temperatures ($T > 400$ °C), which is outside the range covered in Figure 3, the viscosity increases with-temperature leading to a decrease of conductivity with temperature.

It should be noted that eqn [23] and Figures 2 and 3 are for aqueous solutions of NaCl only. Equation [22] indicates that different anions and cations will have different contributions to the overall conductivity of a solution because they have different hydrated radii.

The overall conductivity of a solution composed of a complex mixture of ions can be found by defining an equivalent

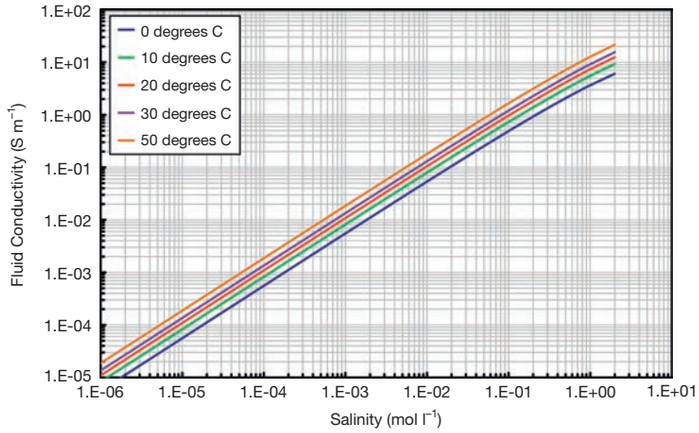

Figure 2 Conductivity of pore fluids as a function of salinity and temperature according to the empirical model of Sen and Goode (1992a,b).

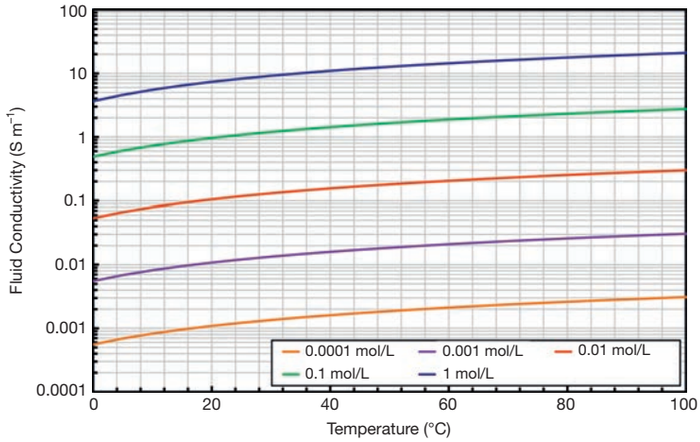

Figure 3 Conductivity of pore fluids as a function of temperature and salinity according to the empirical model of Sen and Goode (1992a,b).

NaCl solution that has the same conductivity as the complex solution. One of the most practical ways to do this is to define a multiplier for each of the ions in the solution except the Na^+ and Cl^- ions. These multipliers are called Dunlap coefficients. Because the salinity dependence of the conductivity of aqueous solutions of other ions is different from that of an NaCl solution, the multipliers also vary with salinity. **Figure 4** shows the diagram that is used to choose these multipliers (Dunlap and Hawthorne, 1951; Schlumberger, 2013). It is best understood by taking an example: consider a solution that contains 20 000 ppm (parts per million) of NaCl, 10 000 ppm of KCl, and 1000 ppm of $MgSO_4$. The multipliers are Na(1.00), Cl(1.00), K(0.9), Mg(1.63), and SO_4(0.64), and the total NaCl equivalent solution is $(20\,000 \times 1 + 20\,000 \times 1 + 10\,000 \times 0.9 + 10\,000 \times 1 + 1000 \times 1.63 + 1000 \times 0.64)/2 = 30\,635$ ppm NaCl. Note that the sum of the products of the multipliers with the dissolved solids is divided by two because the calculation is carried out for both anions and cations. If there are dissolved salts that have two cations per anion or vice versa, the calculation becomes a little more complex. The value 30 635 ppm NaCl can now be entered into eqn [23] to obtain the conductivity of the complex pore fluid as a function of temperature.

Figure 4 covers the range 10 mg kg^{-1} to 300 000 mg kg^{-1}, which is approximately 0.0002–5 mol l^{-1}, taking NaCl as a typical reference.

In general, the use of **Figure 4** followed by the application of the Sen and Goode equation is considered to be valid in this range of salinities. However, **Figure 4** treats each ion as independent. In reality, different mixtures of ions interact to different extents and would lead to different effective NaCl concentrations. Furthermore, **Figure 4** does not take into consideration that the multipliers will change with temperature. Hence, an effective NaCl concentration at the temperature for which **Figure 4** is valid (25 °C) will be used in the Sen and Goode equation invoking a temperature of, say, 150 °C. An error inevitably results. Unfortunately, we only have one **Figure 4** and it is for 25 °C.

One way of resolving the problem is to develop an electrochemical theory for the concentration dependence of ionic conductivity. This has been the subject of much study and the resulting Debye–Hückel theory is generally valid up to 10^{-2} mol l^{-1}.

Hence, if accurate values of conductivity are required up to 10^{-2} mol l^{-1}, the Debye–Hückel theory may be invoked, while for values in the range given by **Figure 4**, the empirical Sen and Goode method can be used providing that it is understood that its results are approximate.

Figure 5 shows the conductivity of pore fluids as a function of salinity for different pore fluid compositions derived from experimental measurements. It is clear that the general trend is sublinear with some electrolytes such as NaCl deviating from linear behavior at the highest salinities, while others such as KCl do not. It is worth noting that there is a variation of more than one order of magnitude in conductivity between the electrolytes included in this diagram at any given salinity. It is important, therefore, that the true composition of the pore fluid is taken into account in any laboratory or field measurement, especially if it changes spatially or temporally.

The small value of conductivity in bulk fluids at low salinities becomes important in geologic porous media because at these salinities, conduction through the electrical double layer becomes greater than that through the bulk fluid (see **Section 11.04.2.4**). The sensitivity to changes in temperature is also important because it implies that any experimental measurement of pore fluids or rocks saturated with pore fluids must be carried out at the same monitored temperature or be corrected to a standard temperature.

11.04.2.2 Parameters Affecting the Electrical Conductivity of Rocks

The electrical conductivity of rocks depends critically upon how current is carried through the rock. Deep in the Earth at high temperatures, conduction occurs through the solid minerals by electronic conduction, with minerals acting as semiconductors.

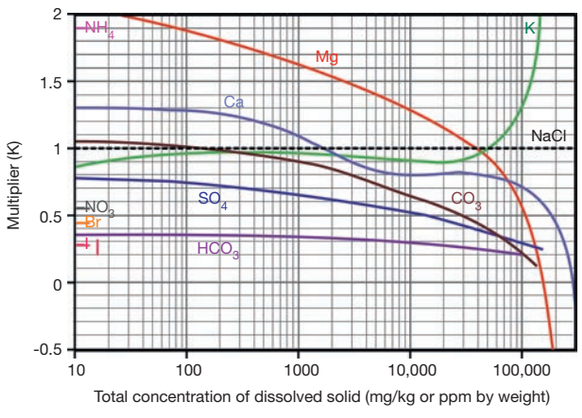

Figure 4 Graph of the multipliers used to convert a pore solution with a complex composition to an NaCl equivalent composition for the purposes of calculating the electrical conductivity of the solution. See the text, for example, of its use (Dunlap and Hawthorne, 1951; Schlumberger, 2013).

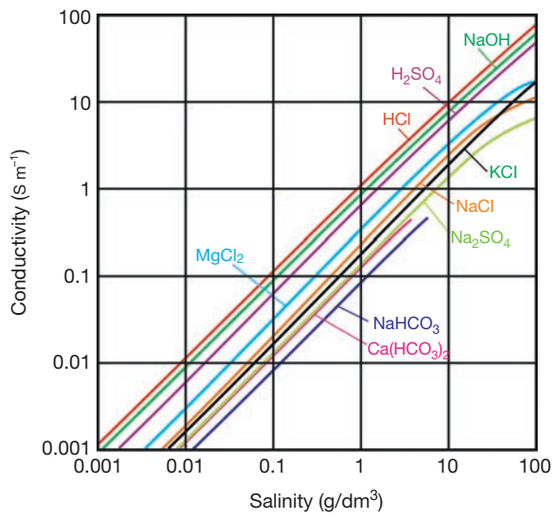

Figure 5 Conductivity of pore fluids as a function of salinity for different pore fluid compositions at 25 °C. Modified after Keller GV and Frischknecht FC (1966) *Electrical Methods in Geophysical Prospecting*, Pergamon Press, 517 pp.

In the upper crust, there are a number of ways in which conduction occurs. The most common is through the movement of charged ions in the pore fluid which either fully or partially saturates the pores of the rock. If the rock is composed of insulating minerals such as silicates, mineral conduction is negligible ($10^{-14} < \sigma_r < 10^{-10}$ S m^{-1}). By contrast, the conductivity of the pore fluids which they contain is much larger ($10^{-3} < \sigma_r < 1$ S m^{-1}). Hence, conduction takes place exclusively through the pore fluid by the movement of charged ions. Consequently, the conductivity of the rock is controlled by the way the pore fluids are connected throughout the rock, and this depends on the rock's microstructure.

The conductivity of the rock depends on

- the conductivity of the fluid that occupies the pores,
- the porosity of the rock,
- the degree to which the porosity is saturated with fluid, and
- the connectedness of pathways available for electrical conduction.

Each of these is discussed in turn:

Fluid conductivity. For most geomaterials, especially those at shallow levels in the crust where temperature and pressures are low, the matrix is effectively insulating and the bulk fluid provides the major contribution to the conductivity of the rock. Hence, we can say that the more saline the pore fluid, the higher the conductivity of any geomaterial saturated with it (Guéguen and Palciauskas, 1994).

Porosity. If the conductivity of a geomaterial depends upon conduction through the pores, it is intuitive that increasing the porosity will increase the electrical pathways available for conduction, and hence increase the electrical conductivity of the geomaterial (Guéguen and Palciauskas, 1994).

Saturation. A rock may have a large porosity, but the electrical conductivity of the whole rock may be very low if the pores are full of insulating fluid such as oil or gas. Hence, the degree to which the pores of the rock are saturated with a conducting fluid (usually brine) is also important, with higher conductivities occurring for higher water (brine) saturations (Guéguen and Palciauskas, 1994).

Connectedness. This is the last of the basic parameters affecting the conductivity of a geomaterial. Though critical to the final rock conductivity, it is unfortunately often overlooked. Rocks may have a large porosity that is completely saturated with a high-salinity fluid, yet have a low conductivity because the conducting pores are not connected (Guéguen and Palciauskas, 1994). This parameter is described by the connectivity of the geomaterial (Glover, 2009).

These four controlling parameters were brought together for the first time by Archie (1942), who developed a number of empirical laws to describe electrical conduction in reservoir rocks, which are described in subsequent sections of this chapter.

Another source of conduction involves conduction through the electrical double layer that is formed at the interface between the bulk fluid and the mineral surfaces (Adamson, 1976; Davis and Kent, 1990; Dukhin and Derjaguin, 1974; Glover et al., 1994; Hunter, 1981; Pride, 1994; Revil and Glover, 1997, 1998; Revil et al., 1999a,b; Sposito, 1989). This mechanism is more dominant at low bulk fluid salinities, where it provides more conduction than the weak bulk fluid, and also when the rock contains a significant fraction of clay minerals, which provide a greater surface area for surface conduction (see **Section 11.04.2.4**).

Surface conduction depends upon

- the specific conductance of the mineral surface/bulk fluid interface,
- a parameter describing the characteristic pore size of the rock, and
- the connectedness of surface conduction pathways.

Minor sources of conduction in the upper crust are associated with the presence of highly conducting phases such as graphite (Glover, 1996; Glover and Adám, 2008; Glover and Vine, 1992; Selway, 2014; Yang, 2011; Yoshino and Noritake, 2011) or sulfides (Duba et al., 1994; Einaudi et al., 2005; Glover and Vine, 1994), the latter of which rarely have sufficient connectedness to contribute significantly to the overall conductivity of the rock.

In particular areas, partial melting might be the cause of local high-conductivity anomalies (Glover et al., 2000b). Electrical conduction in melts is mediated by ions. The application of Archie's laws to these scenarios is difficult, but alternative methods now exist to allow there to be more than one conducting phase in a rock. These models are discussed in more detail in **Section 11.04.3.3**. Conduction through semiconducting minerals or through melt depends upon

- the conductivity of each of the phases present (melt, matrix, and conducting mineral),
- the volume fraction of each of the phases, and
- the electrical connectedness of each of the conducting phases.

In all of the cases listed earlier, we can note that the parameters that affect the electrical conductivity of the rock correspond to answers to the following questions:

- How conductive are the phases in the rock that conduct?
- How much of each phase is there?
- How connected is each of the phases?

11.04.2.3 Archie's Original Empirical Laws

Archie's laws were introduced in 1942 (Archie, 1942). We are introducing them here, before the section on mixing models, because of their importance, which was touched upon in the introduction.

It should be noted strongly that Archie's laws were originally empirical and had a small range of validity. However, it became increasingly clear that they could be applied successfully outside their initial range of validities and finally were proved analytically as an extension of the Lichtenecker and Rother (1931) mixing law (LR equation). The derivation can be found in a number of works including Glover (2010b). However, there are some questions concerning the theoretical derivation of the LR equation (Reynolds and Hough, 1957), and although the LR equation has recently been given a greater theoretical pedigree from effective medium approaches (Zakri et al., 1998), it would be fair to say that Archie's laws cannot be said to have an undisputed theoretical basis quite yet. However, recently, it has become clear that the simple Archie's laws are simply a special case of a more general mixing law that will be introduced in **Section 11.04.3.3**.

11.04.2.3.1 Formation factor and connectedness

Archie began by considering a porous medium of porosity ϕ, and naming the unitless ratio of the resistivity of the fully saturated rock ρ_o to that of the pore fluid saturating the pores ρ_f as the formation factor, F (which is sometimes called the resistivity formation factor):

$$F = \frac{\rho_o}{\rho_f} \quad [24]$$

(It should be noted that the symbols commonly used in the oil and gas industry are R_o in place of ρ_o, and R_w in place of ρ_f.)

The term formation factor was used because it was approximately constant for any given formation. The formation factor varies from unity, $F = 1$, which represents the case where $\rho_o = \rho_f$ (i.e., when $\phi \to 1$), and increases as the porosity decreases, with $F \to \infty$ as $\phi \to 0$. The formation factor can be less than unity, but only when the rock matrix is less resistive than the pore fluid and this is extremely rare (Glover, 2009).

The inverse of the formation factor is the ratio of the conductivity of the fully saturated rock to that of the fluid. This parameter is called the 'conductivity formation factor' or the 'connectedness' of the rock (G, no units) (Glover, 2009, 2010b). It has recently found utility in the extension of Archie's first law to n-conducting phases (**Section 11.04.3.3**). The symbol G should not be confused with conductance, which shares the symbol, but is rarely used in petrophysics, and is given the symbol G_c in eqn [6] earlier in this chapter to avoid confusion.

11.04.2.3.2 Archie's first law

The first experiments by Archie led him to the conclusion that the formation factor depends upon porosity in the form of an inverse power law (Archie's first law):

$$F = \phi^{-m} \quad [25]$$

with an exponent $-m$ (no units). He called the exponent the cementation exponent (factor or index) because he believed it to be related to the degree of cementation of the rock fabric. Higher values of m make the formation factor, and hence the rock conductivity, more sensitive to changes in porosity (Ellis and Singer, 2007). **Figure 6** shows the results of eqn [25].

The range of values for the cementation exponent is relatively small. A value of $m = 1$ is not observed for real rocks and represents a porous medium composed of a bundle of capillary tubes that cross the sample in a straight line. Rocks with a low porosity but a well-developed fracture network sometimes have cementation exponents that approach unity because the network has flow paths that are fairly direct. Here, we get the first taste that the cementation exponent has something to do with the connectedness of the pore and fracture network (where, for the time being, connectedness is considered to be a qualitative term for the general availability of pathways for transport). A cementation exponent equal to 1.5 represents the analytic solution for the case where the rock is composed of perfect spheres (Mendelson and Cohen, 1982; Sen et al., 1981). In fact, $m = 1$ (which is the trivial parallel conduction case) and $m = 1.5$ (Sen et al., 1981) were, until recently, the only two cases where an analytically derived value of the cementation exponent was known. A series of papers from 2004 onward have shown that Archie's law can be derived by applying continuum percolation theory to fractal porous media (e.g., Ewing and Hunt, 2006).

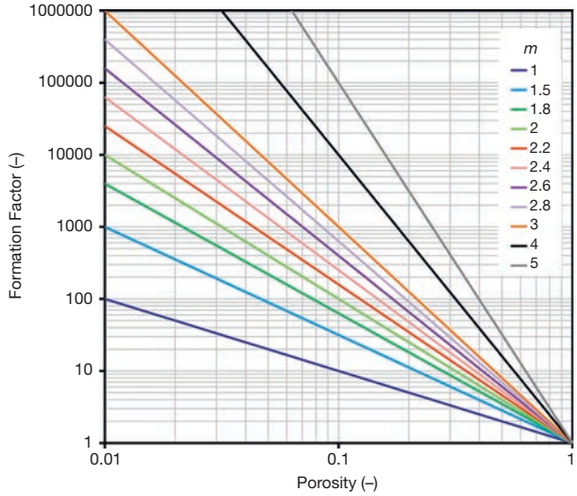

Figure 6 Formation factor as a function of porosity according to Archie's first law. The negative of the gradient of each curve provides the cementation exponent.

Most porous arenaceous sediments have cementation exponents between 1.5 and 2.5 (Glover et al., 1997). Values higher than 2.5, and as high as 5, are generally found in carbonates where the pore space is less well connected (Tiab and Donaldson, 2011). In general, the value of the cementation exponent increases as the degree of connectedness of the pore network diminishes, which rather supports it being called the cementation exponent. Incidentally, values of the cementation exponent less than unity are possible, arise when the matrix itself has a significant conductivity, and are observed in the modified Archie's law for two conducting phases (Glover et al., 2000a) (see **Section 11.04.3.3**).

The best method for obtaining a mean value of the cementation exponent of a set of rocks from the same formation is from the negative gradient of the graph of $\log(F)$ against $\log(\phi)$ (Tiab and Donaldson, 2011), which the oil and gas industry calls a Pickett plot, while values for individual samples can be found using

$$m = -\frac{\log(F)}{\log(\phi)} \quad [26]$$

Equations [24] and [25] are often combined under the name of Archie's law to give

$$\rho_o = \rho_f \phi^{-m} \quad [27]$$

which is an extremely useful form of the law. Here, $\rho_o \to \rho_f$ either as $\phi \to 1$ (i.e., the 'rock' is 100% pore fluid) or if $m = 0$ irrespective of the value of porosity. Even though $m = 0$ does not fall within the useful range for reservoir rocks, this result is a further indication that low values of cementation exponent represent good connectedness, and in the limit (i.e., when $m \to 0$), the connectedness of the conducting phase in the rock is optimal.

It should be noted that the correct use of Archie's first law requires accurate determinations of (i) the resistivity of the fully saturated rock, (ii) the resistivity of the fluid in the pores, and (iii) the relevant porosity for electrical transport

Figure 7 A cell for measuring fluid resistivity. Each end has a coaxial connection to a blacked platinum gauze electrode. There are two fluid ports for removing bubbles and a thermocouple well. The cell's geometric factor should be obtained by calibration with known fluids at each of the frequencies for which it will be used.

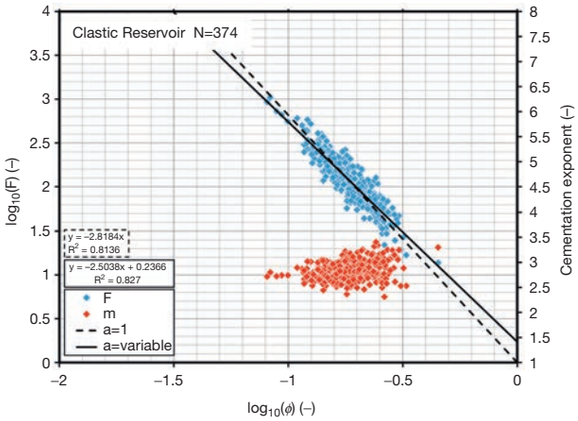

Figure 8 Formation factor (blue symbols) as a function of porosity for 374 samples from a single formation in a reservoir from the North Sea, UKCS. Two models have been fitted to the data. The dashed line is Archie's first law [25], while the solid line is Winsauer et al.'s (1952) modification with the '*a*' factor. Both seem to fit the data well according to the R^2 values, but the result is significantly different cementation exponents; Archie's first law [25] gives $m=2.81814$, while Winsauer et al.'s modification gives $m=2.5038$.

through the rock, which should be the effective porosity that contributes to the electrical conduction. Accurate determination of the resistivity of the fully saturated rock implies good control of the geometric factor that allows it to be calculated from the measured resistance, as well as certainty that the rock is fully saturated.

It is important that the resistivity of the brine in the pores is measured as there is a discrepancy between the salinity of brine in the stock saturating solution and that in equilibrium with the pores. At low salinities, the pore solution may be ten times more saline than that of the stock solution (Walker et al., 2014), leading to gross errors in the use of Archie's law if the values for the stock solution are used.

The resistivity of the solutions should be carried out in a specially designed cell with a known geometric factor (Figure 7) or a benchtop conductivity meter. The former is the better solution as it allows fluid resistivity measurements to be made at the same frequencies as the rock measurements if impedance spectroscopy is being performed, but the latter is acceptable providing the measurement is made in sufficient fluid with the electrode in the center of the beaker and a stirrer being employed. As with all electrical measurements, the temperature should be noted with the measurement, and corrections to a standard temperature carried out if required.

The accuracy of the porosity is more difficult. If one carries out porosity by helium pycnometry, by fluid saturation and by mercury injection porosimetry on the same sample, the measured porosities will be different in decreasing order. The question, that is still debatable, is which is the best measurement of porosity to use, especially as there are many other sources of porosity measurement too (i.e., by image analysis of thin sections, x-ray computed tomography (CT) and micro-CT scanning, positron emission tomography (PET) scanning, and nuclear magnetic resonance (NMR) spectroscopy)? At the moment, the most appropriate seems to be the fluid saturation approach. This approach at least has the advantage of employing fluids similar to those in the rock. It might be thought, therefore, that the same volume of pause might be saturated by using a reservoir fluid in the laboratory as occurred in the reservoir. At least, sufficiently similarly to make the measured porosity more relevant than that provided by other techniques.

It should be strongly noted that an extremely common form of Archie's first law contains an empirical factor *a* according to $F=a\phi^{-m}$ and hence $\rho_o=a\rho_f\phi^{-m}$. This empirical factor did not appear in Archie's original paper (Archie, 1942) and does not arise in the literature until Winsauer et al.'s (1952) and Wyllie and Gregory's (1953) papers (Winsauer et al., 1952; Wyllie and Gregory, 1953). The use of the empirical factor is retained by many researchers because it improves the fit to sparse and low-quality datasets (Glover, 2012, pers. comm.). However, its use is analytically wrong because it implies that as the porosity tends to 100% (i.e., the sample has no matrix but is just the pore fluid), the sample has a resistivity $a\rho_f$. There is a contradiction here, because such a sample is solely pore fluid with a defined resistivity of ρ_f. Hence, the original equation is not generally valid unless the value of $a\equiv 1$. While the use of the empirical factor may have once been acceptable when Archie's first law had only an empirical pedigree, recent research indicates that nonunity values of *a* probably result from unresolved systematic errors in the porosity or resistivity measurements.

Figure 8 shows typical data from a reservoir in the North Sea. The data come from one well-defined sandstone formation. When the formation factor is plotted against porosity on logarithmic axes, two straight lines can be fitted. The dashed line represents Archie's first law [25], while the solid line incorporates the empirical factor *a*. In each case, the gradient represents the cementation factor *m* and it is instructive how different these are in the figure despite the goodness of fit R^2 value for the two fits being so similar. Here, the solid line provides the best assessment of the cementation exponent. In fact, for most data, the presence of the Winsauer *a*-factor allows a reasonably accurate cementation exponent to be calculated even if the data are not of the highest quality, and I would recommend its use in such cases, despite its non-analytical nature. Furthermore, the *a*-factor can be used as an indication of data quality (if close to unity, the quality of the data is good). The red points in Figure 8 show calculations of the cementation exponent on a plug-by-plug basis using eqn [25].

11.04.2.3.3 Resistivity index

Archie also examined the work of other investigators who did experiments on the resistivity of partially saturated sandstones. He observed that the bulk resistivity ρ_r of a rock that is partially saturated with an aqueous fluid of resistivity ρ_f is directly proportional to the resistivity of the rock when it is fully saturated with the same fluid, ρ_o:

$$I = \frac{\rho_r}{\rho_o} \quad [28]$$

(Once again, it should be noted that the symbols commonly used in the oil and gas industry are R_o in place of ρ_o and R_t in place of ρ_r.)

The constant of proportionality I is called the resistivity index and describes the effect of partial desaturation of the rock. The resistivity index varies between unity and infinity depending upon the degree of saturation of the rock.

11.04.2.3.4 Archie's second law

Archie observed that the following relationship exists empirically for sandstones (Archie's second law):

$$I = S_w^{-n} \quad [29]$$

where S_w is the fractional water saturation of the rock porosity and n is the saturation exponent.

The best method for obtaining a mean value of the saturation exponent of a sample in the laboratory is from the negative gradient of the graph of $\log(I)$ against $\log(S_w)$ (Tiab and Donaldson, 2011). This is a time-consuming measurement that involves the progressive desaturation of a core plug.

If we assume that a certain water saturation S_w is obtained by displacing some of the water from a previously fully saturated rock in a uniform manner, the volume fraction of water in the rock goes from ϕ to ϕS_w, and we can use eqn [27] to calculate the effective resistivity of the rock as $\rho_r = \rho_f(\phi S_w)^{-m}$ by assuming that the nonconducting fluid acts like the nonconducting rock matrix. Substituting this into eqn [28] and using eqn [27] again, but this time for the fully saturated rock, we get

$$I = \frac{\rho_r}{\rho_o} = \frac{\rho_f(\phi S_w)^{-m}}{\rho_f \phi^{-m}} = S_w^{-m} \quad [30]$$

This is a demonstration of the analytic origin of Archie's second law, and predicts that the saturation exponent should be the same as the cementation exponent of the first law.

Equation [30], however, represents an oversimplification. The derivation of eqn [30] makes the assumption that we can replace ϕ in eqn [27] with ϕS_w while retaining the exponent $-m$. However, this is only possible if the connectedness of the phase ϕS_w is exactly the same as that of the previous phase ϕ. Of course, this is extremely unlikely to be the case. Imagine, for example, methane replacing water in a water-wet rock. The methane will preferentially occupy the center of the pores, and the water will preferentially occupy the pore space next to the mineral surfaces. The connectedness of the water in this partially saturated rock will be different, and generally less, than in the fully saturated case. Hence, we can say that $n \neq m$ generally because the connectedness of the fluid phase is a function of its volume fraction, and as the water is displaced from the pore space, the saturation exponent increases.

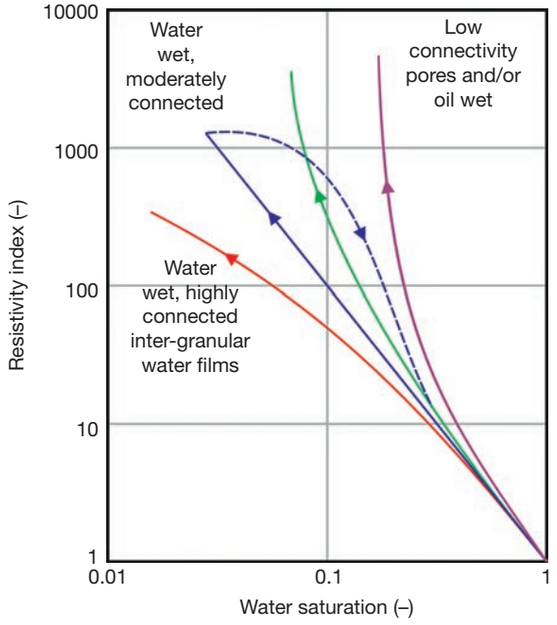

Figure 9 Resistivity index (as defined in eqn [28]) as a function of water saturation for a rock saturated with water and oil. Solid lines indicate drainage. The dark blue line, which represents Archie's second law ($n = 2$), is only valid for clean, water-wet moderately well-connected rocks. Rocks with higher connectivity due to the presence of intergranular water films tend to follow the red curve, while low connectedness or oil-wet rocks follow the green and purple trends. It should be noted that imbibition can often produce a nonlinear curve (dashed) due to the development of oil-wet patches in the rock.

The latest Archie's formulations that are generalized to take account of any number of conducting phases not only explicitly treat this problem (Glover, 2010b) but also show that both the first and the second Archie's laws are in fact the operation of the same general law but applied to a different frame of reference (see **Section 11.04.3.3**).

Since the laboratory determination of the saturation exponent is time-consuming and costly, it is common to hear that the saturation exponent has been taken to be equal to 2 in calculations. While it is true that there seems to be a strong preference for values of saturation exponent near 2 ± 0.5 for most water-wet rocks, oil-wet rocks show much higher values (4–5) (**Figure 9**) (Montaron, 2009; Sweeney and Jennings, 1960). Hence, it is extremely important to obtain accurate and representative values of this parameter for use in reserves calculations.

Once more, eqn [28] and eqn [29] can be combined to give

$$\rho_r = \rho_o S_w^{-n} \quad [31]$$

Archie's second law can be expressed in graphical form, as shown in **Figure 9**. Equation [29] is shown by the straight blue line on this diagram. Clean rocks at high water saturations generally fall along such straight lines, with their slope representing the value of the saturation exponent. However, there also exist data that fall significantly off such lines. It is thought that data following the red line on the diagram represents rocks that have extremely high water connectedness due to the presence of intergranular water films, while data following the

green to purple trends (e.g., Sweeney and Jennings, 1960) represent low water connectedness particularly in oil-wet rocks. All of the solid curves are for drainage conditions. It has also been noted that it is possible to generate imbibition curves with different behaviors such as the dashed curve in the figure, which are believed to be caused by the development of patches of oil-wet rock that reduce the connectedness of the water phase and ensure that the saturation exponent is a function of the water saturation history of the rock (Montaron and Han, 2009).

11.04.2.3.5 Combined Archie's laws

The two Archie's laws can be combined into one equation:

$$\rho_r = \rho_f \phi^{-m} S_w^{-n} \quad [32]$$

This equation is of the greatest utility in the calculation of hydrocarbon reserves. In this application, values of porosity, pore fluid resistivity, and rock resistivity from borehole measurements are combined with the determinations of the cementation and saturation exponents, which are most often made in the laboratory on representative rock samples to calculate the water saturation. The water saturation can then be used with formation thickness, areal extent, and porosity to calculate the volume of hydrocarbons in the reservoir.

11.04.2.3.6 Electrical tortuosity and connectivity

In the discussion of Archie's laws, we have eluded to the importance of how well connected, or otherwise, a conducting phase, such as an aqueous fluid, is in the rock. This has traditionally been described by an electrical tortuosity. Electrical tortuosity τ_e is most often written as

$$\tau_e = F\phi \quad [33]$$

which, although useful does not show its origins clearly. It is possible to rewrite [33] as

$$F = \phi^{-1}\phi^{1-m} \quad [34]$$

where it can be recognized that the resistivity formation factor has a contribution arising purely from the presence of a scalar porosity and another that arises from the way that porosity is arranged, and which also depends upon porosity. This latter contribution is called the tortuosity, τ_e. Hence, the electrical tortuosity can also be expressed as

$$\tau_e = \phi^{1-m} \quad [35]$$

A full discussion of tortuosity can be found in the comprehensive review by Clennell (1997) and in the work of David (1993).

It should be noted that electrical tortuosity is not the same as hydraulic tortuosity, τ_h. Hydraulic tortuosity is defined as the mean flow path length between two points in a porous medium divided by the direct distance between those two points. The electrical tortuosity is often expressed as being equal to the square of the hydraulic tortuosity. Since there can be significant confusion between the two terms, it is always useful to define explicitly which type of tortuosity is meant, and to be certain which is being referred to when only the generic term 'tortuosity' has been used.

The inverse of electrical tortuosity is called the electrical connectivity χ. The conductivity formation factor G, which is sometimes called the connectedness, is related to the porosity and electrical connectivity by

$$G = \phi^m = \phi\chi \quad [36]$$

where it is clear that the overall connectedness of the rock depends on the porosity of a fully saturated pore space and its arrangement, the latter of which is given by the connectivity. Hence, the connectedness can be thought of as a measure of how the presence of the pores, when filled with a fluid of a given conductivity, controls the conductivity of the whole rock.

11.04.2.3.7 Validity of Archie's laws

Archie's laws came into being as empirical relationships that were formally valid only for the range of lithologies, temperatures, porosity, and pore fluids used to make the experimental measurements. However, very quickly, it became clear that the laws could be applied very successfully outside these initial ranges, and that has been confirmed by subsequent analytic derivations of Archie's first law.

Archie's laws, however, are subject to several restrictions:

- Archie's laws can only be used with a single conducting phase. Hence, the laws cannot be used at high temperatures in the presence of a melt because the rock matrix conducts significantly, or if there is a significant contribution from highly conducting accessory minerals. This restriction has been removed by the development of a version of Archie's first law for two conducting phases (Glover et al., 2000a,b, c) and then for any number of phases (Glover, 2010b).
- Archie's laws fail where the lithology contains minerals, usually shales, that provide a significant surface conductance and when the salinity of the pore fluids is low. Recent studies show that surface conduction effects can be very significant for a wide range of rocks and sediments especially at lower frequencies. However, Archie's laws can be used approximately in these cases if the pore fluid salinity is sufficiently high that it provides a conductance that is significantly larger than the surface conduction. Since the presence of shale surface conductance has always been important in the hydrocarbon industry, a number of modifications to Archie's first law have been proposed that are discussed in **Section 11.04.2.4** in the succeeding text, the most famous of which is by Waxman and Smits (1968).
- There is some question about the validity of Archie's laws at the extremes of the porosity range. At low porosities, there may be a fraction of the porosity ϕ_o that does not take part in conduction, which may be taken into consideration using a percolation limit approach (Bernabé and Bruderer, 1998; Hunt, 2004; Kirkpatrick, 1973; Seager and Pike, 1974; Shah and Yortsos, 1996):

$$F = (\phi - \phi_o)^{-m} \quad [37]$$

At high porosities, there is a dearth of data with which to check Archie's first law, but effective media models indicate that the rate of change of conductivity with porosity is less than that predicted by Archie's law.

11.04.2.4 Empirical Modifications for Shaley Rocks

The simple forms of Archie's laws assume that the only source of conduction in the rock is provided by the pore fluid and that ionic conduction in the pore fluid is uniform throughout the saturated pore space. While this is true for sedimentary rocks that are clay-free, it became clear that Archie's laws did not work for rocks with a significant fraction of clay, where there was an additional conduction contribution that was associated with conduction along clay surfaces. Initially, it was thought that atoms of Al^{3+} that substitute for Si^{4+} in the mineral structure would lead to a charge imbalance. Such an imbalance would then lead to an additional adsorption of cations onto the surface, which subsequently move and give rise to a surface conduction. We now know that a complex electrochemical structure exists at the interface between the mineral and the pore fluid, which is sometimes modeled as an electrical double layer (e.g., Revil and Glover, 1998) or an electrical triple layer (e.g., Revil and Leroy, 2004). Several types of surface conduction can occur within these structures, which are dependent on many factors, the most important of which are fluid salinity and pH (Parks, 1965; Revil and Glover, 1997, 1998; Revil et al., 1999a,b).

Clay minerals have a particularly high surface conduction. This was once thought to be, due to clays having a greater surface adsorption site density compared to, say, silica. However, it is now known that clay minerals generally have a lower surface adsorption sites density than many other minerals, but a much greater internal surface area that more than makes up for this. The effect of surface conduction is extremely important and is covered in **Section 11.04.4** in the succeeding text.

Archie's first law may now be modified to give

$$\sigma_r = \frac{\sigma_f}{F} + \frac{\sigma_s}{f} \qquad [38]$$

where we have used rock conductivity ($\sigma_r = 1/\rho_r$) and pore fluid conductivity ($\sigma_f = 1/\rho_f$) in place of the associated resistivities, together with the surface conductivity σ_s, and F and f are the formation factors associated with the bulk fluid conduction and the surface conduction, respectively. This equation assumes that the bulk conduction and the surface conduction occur independently and in parallel, giving rise to the simple addition, but does not assume that the flow paths are the same, hence the separate formation factors. However, it is usually assumed that both formation factors are the same and given the symbol F^* while rewriting [38] as

$$\sigma_r = \frac{1}{F^*}\left(\sigma_f + \frac{2\Sigma_s}{\Lambda}\right) = \frac{1}{F^*}(\sigma_f + BQ_v) \qquad [39]$$

The first equation in [39] arises from the formal definition of the formation factor (e.g., Revil and Glover, 1997; Schwartz et al., 1989), which will be discussed in **Section 11.04.3** in the succeeding text. The term Λ, which was introduced by Johnson et al. (1986), is a characteristic length (in m) associated with the pore structure of the rock and may be considered to be an effective pore radius. It is approximately equal to twice the pore volume divided by the pore surface area. The parameter Σ_s is called the specific surface conductivity or surface conductance (in S). It should be noted that the $2\Sigma_s/\Lambda$ term depends upon an assumption that is explicit in the definition of Λ, which is that the interfacial conductivity extends only a short distance into the pores, which is the same as saying that the pore walls appear flat with respect to the thickness of the electrical double layer (i.e., a thin double-layer assumption) (Johnson et al. 1986).

Applying an analogy of [10] in two dimensions, we obtain $\Sigma_{si} = n_{si}Z_i eB_i$ for each of i types of ion on the surface, where Σ_{si} is the specific surface conductance of each type of surface ion, n_{si} is the surface number density of each type of surface ion, Z_i is the valency of each type of surface ion, and B_i is the surface mobility of each type of surface ion. Now, taking the mean behavior of all ions and including $\Lambda = 2V_p/S_p$ allows us to write $2\Sigma_s/\Lambda = BQ_v$, where $Q_v = n_s Z e S_p/V_p$ is the excess surface charge taking part in surface conduction per unit pore volume (Guéguen and Palciauskas, 1994).

It should be noted that the excess charge per volume is related to the traditional measurement of CEC. The CEC measurement (e.g., Ross and Ketterings, 2011) provides a chemical measurement of excess charge per weight of the sample. The value is commonly given in milliequivalents per gram (mequiv. g^{-1}) where, for NaCl solutions, 1 mequiv. $g^{-1} = 96\,320$ C kg^{-1} (e.g., Patchett, 1975). While CEC measurements are carried out on crushed samples, and one could question their validity for whole rock samples, it is possible to take the CEC measurement for a rock and calculate the equivalent value of Q_v providing the density and porosity of the rock are known.

The right-hand side of [39] was developed by Waxman and Smits (1968) and used as the standard shaley sand model for conductivity for many years. **Section 11.04.3.5** discusses models for shaley sands in more detail and compares the Waxman and Smits model with others that are more suited for application in the hydrocarbon industry.

11.04.2.5 The Range of Electrical Conductivity of Near-Surface Rocks

Huge numbers of experiments have been carried out on rocks from the upper crust in the last 70 years; many of them by the oil and gas industry. While most remain confidential, it is possible to get an extremely good idea of the range of electrical conductivities from extremely low-conductivity microgranites with vanishingly small porosities and almost no microfracturing (e.g., Ailsa Craig, which is still used to make curling stones), through reservoir rocks where the conductivity is controlled by the fluids in the pore spaces and clays, to veins of highly conducting minerals such as sphalerite or graphite. **Table 1** shows some typical ranges of conductivity and resistivity obtained from the literature, while some of the same information is available in **Figure 1**. It is not within the remit of this chapter to review the huge number of measurements that are available. However, good compilations exist in the literature, the foremost of which are by Keller (1989), while more data can be found in Schön (2004) and to a lesser extent in Guéguen and Palciauskas (1994).

A great number of processes have the potential to affect the conductivity of rocks. **Box 1** shows a compilation of the main processes and the direction in which each one influences the conductivity of the geomaterial.

Table 1 A summary table of the conductivities and resistivities of common rocks and minerals (at surface temperatures and pressures)

Rock	*Conductivity (S m^{-1})*	*Resistivity (Ωm)*
Granite	0.001–0.00001	1000–100 000
Gabbro	0.001–0.00001	1000–100 000
Basalt	0.1–0.0001	10–100 000
Andesite	0.001–0.00001	1000–100 000
Sand and gravel	0.05–0.002	20–5000
Sandstone	0.1–0.001	50–1000
Limestone	0.002–0.00001	5000–100 000
Dolomite	0.001–0.0002	1000–50 000
Conglomerate	0.01–0.0001	100–10 000
Coal	0.1–0.001	10–1000
Shales	0.001–1	50–1000
Clays	0.05–0.01	20–100
Graphite	100–0.01	0.01–100
Massive sulfides	1000–1	0.001–1
Salt water	10–1	0.1–1
Brackish water	1–0.1	1–10
Freshwater	0.1–0.01	10–100
Permafrost	0.02–0.00001	500–100 000
Sea ice	0.05–0.001	20–1000

Modified after Palacky GV (1987) Resistivity characteristics of geologic targets. In: *Electromagnetic Methods in Applied Geophysics*, *1. Theory*, p. 1351

Box 1 Effect of various processes upon the conductivity of geomaterials

Effect	Conductivity
Increasing porosity	↑
Increasing pore fluid salinity	↑
Increasing surface conductance	↑
Increasing connectedness	↑
Increasing connectivity	↑
Increasing cementation exponent	↓
Increasing clay alteration	↑
Dissolution	↑
Shearing/faulting	↑↓
Weathering	↑
Induration	↓
Carbonate precipitation	↓
Silicification	↓
Metamorphism	↑↓
Compaction	↓
Overpressure	↑
Increasing formation factor	↓
Increasing tortuosity	↓
Hydrocarbon production/imbibition	↑
Hydrocarbon emplacement/drainage	↓
Increasing saturation exponent	↓
Increasing thermal/microfracturing	↑
Increasing oil wettability	↓
CCS emplacement	↓
Hydrofracturing	↑
Formation temperature	↑
Increasing overburden pressure	↓

11.04.3 Mixing Models for the Electrical Conductivity of Geomaterials

Mixing models are incredibly important for the measurement and calculation of the electrical properties of all complex and porous media. In this section, we will review some of the main mixing models for the steady-state electrical conductivity of geomaterials, pointing out their advantages and disadvantages. Each can be written in terms of resistivities. Some of the models in this section are theoretical, while many are empirical and some empirical models have an increasingly good theoretical pedigree. Mixing models for the permittivity and complex electrical properties of rocks are left until **Section 11.04.5.5**.

The models fall into three main groups, which are described in each of the following subsections. A special subset of mixing models that includes variable water saturations has also been considered. Many of the models referred to in this section are presented in **Table 2** and are graphed in **Figure 10**.

11.04.3.1 Geometric Models

These models consider two, three, or more conducting phases and build the arrangement of those phases into the model itself. In other words, these are geometric models that are only valid if the arrangement of the conducting phases approximates to that of the model (first part of **Table 2**).

The parallel model can have many conducting phases with different phase conductivities σ_i and different phase volume fractions ϕ_i, but they all have to be arranged electrically in parallel. The equation for the resulting conductivity is the same as an arithmetic mean weighted by the volume fractions. By contrast, the perpendicular model considers the conductivities to be arranged in series and is expressed by a weighted harmonic mean. Here, the current flows perpendicularly to the layers of conducting phase crossing each of them in series. Clearly, these are extreme cases and the actual conductivity of a rock would fall somewhere in between these bounds.

In 1962, Hashin and Shtrikman (1962) produced two other bounding models that are more restrictive and hence more useful than the parallel and perpendicular cases. These are called the Hashin and Shtrikman upper and lower bounds or HS+ and HS−, respectively. Unlike the series and parallel models, however, the Hashin and Shtrikman bounds are only valid for two conducting phases. There is currently active, and extremely mathematical, research into the extension of the HS bounds to multiple phases and multiple dimensions (e.g., Liu, 2010).

Ten years after the publication of the Hashin and Shtrikman bounds, Waff (1974) produced a model that shares many of the basic structural qualities of a granular rock in that its two phases were considered to be in the form of conducting spheres with conducting spherical shells around them, which approximates to the scenario where grains are surrounded by a pore fluid. It turned out that the equation he produced is mathematically the same as the Hashin and Shtrikman upper bound, giving it more validity for use in granular porous media with subrounded grains.

The first part of **Figure 10** shows a comparison between the parallel, perpendicular, HS+/Waff, and HS− models for a two-phase mixture with the first phase having the nominal conductivity of 0.01 S m^{-1} and the second having the nominal

Table 2 Some of the most common mixing models for electrical conductivity in porous media

Name	Conducting phases: Min	Conducting phases: Max	Equation	References	Notes
Models without variable exponents					
Parallel model	1	Many	$\sigma_{\text{eff}} = \sum_{i=1}^{n} \phi_i \sigma_i$	Guéguen and Palciauskas (1994), Luo et al (1994), Somerton (1992)	Arithmetic mean. Parallel layers of constant arbitrary thickness with conductivity σ_i arranged axially to current flow
Perpendicular model	1	Many	$\frac{1}{\sigma_{\text{eff}}} = \sum_{i=1}^{n} \frac{\phi_i}{\sigma_i}$	Guéguen and Palciauskas (1994), Luo et al (1994), Somerton (1992)	Harmonic mean. Parallel layers of constant arbitrary thickness with conductivity σ_i arranged normally to current flow
Random model	1	Many	$\sigma_{\text{eff}} = \prod_{i=1}^{n} \sigma_i^{\phi_i}$	Guéguen and Palciauskas (1994), Luo et al (1994), Somerton (1992)	Geometric mean. Arbitrary shaped and oriented volumes of conductivity σ_i distributed randomly
Hashin–Shtrikman upper bound	2	2	$\sigma_{\text{eff}}^{+} = \sigma_2 \left(1 - \frac{3(1-\phi_2)(\sigma_2-\sigma_1)}{3\sigma_2 - \phi_2(\sigma_2-\sigma_1)}\right)$	Hashin and Shtrikman (1962)	Commonly denoted HS+. Derived from effective medium considerations
Hashin–Shtrikman lower bound	2	2	$\sigma_{\text{eff}}^{-} = \sigma_1 \left(1 + \frac{3\phi_2(\sigma_2-\sigma_1)}{3\sigma_1 + (1-\phi_2)(\sigma_2-\sigma_1)}\right)$	Hashin and Shtrikman (1962)	Commonly denoted HS−. Derived from effective medium considerations
Waff model	2	2	$\sigma_{\text{eff}} = \frac{\sigma_2 + (\sigma_1-\sigma_2)(1-(2\phi_2/3))}{1 + (\phi_2/3)(\sigma_1/\sigma_2 - 1)}$	Waff (1974)	Based on concentric spheres of varying sizes with volume of core (fractional volume of phase 1) to volume of shell (fractional volume of phase 2) ratio constant. Functionally equivalent to HS+
Brick-layer model	2	2	–	Beekmans and Heyne (1976)	Cubes of one phase arranged in a three-dimensional grid with a second phase occupying the gaps between the blocks. Only valid for small percentages of interblock phase
Modified brick-layer model	2	2	$\sigma_{\text{eff}} = \frac{\sigma_2\left(\sigma_2\left(\phi_1^{2/3} - 1\right) - \sigma_1\phi_1^{2/3}\right)}{\sigma_1\left(\phi_1 - \phi_1^{2/3}\right) + \sigma_2\left(\phi_1^{2/3} - \phi_1 - 1\right)}$	Schilling et al. (1997)	Modified to allow validity to be extended to cover the range $0.00 \le \sigma_1 \le 1.00$ (0–100%) Almost coincident with HS+
Models with variable exponents					
Lichtenecker–Rother equation	1	2	$\sigma_{\text{eff}} = (\sigma_1^{1/m}(1-\phi_2) + \sigma_2^{1/m}\phi_2)^m$	Lichtenecker and Rother (1931) Korvin (1982)	Derived from the theory of functional equations under appropriate boundary conditions. Formally, the same as Archie's law if $\sigma_1 = 0$
Bussian's equation	2	2	$\sigma_{\text{eff}} = \sigma_2\phi_2^m \left(\frac{1-\sigma_1/\sigma_2}{1-\sigma_1/\sigma_{\text{eff}}}\right)^m$	Bussian (1983)	Derived from effective medium theory
Conventional Archie's law	1	1	$\sigma_{\text{eff}} = \sigma_2\phi_2^m$	Archie (1942)	Derived empirically, but provable analytically for special cases
Extended and generalized models with variable exponents					
Lichtenecker–Rother equation (generalized)	1	Many	$\sigma_{\text{eff}} = \left(\sum_{i=1}^{n} \sigma_i^{1/m}\phi_i\right)^m$	Lichtenecker and Rother (1931) Korvin (1982)	Logical extension of the Lichtenecker and Rother model made in this work
Modified Archie's law	1	2	$\sigma_{\text{eff}} = \sigma_1(1-\phi_2)^p + \sigma_2\phi_2^m$ where $p = \frac{\log(1-\phi_2^m)}{\log(1-\phi_2)}$	Glover et al. (2000a)	Derived from conventional Archie's law by considering boundary conditions implied by geometric constraints
Generalized Archie's law	1	Many	$\sigma = \sum_i \sigma_i \phi_i^{m_i}$ where *exact solution* $m_j = \log\left(1 - \sum_{i\neq j} \phi_i^{m_i}\right) \Big/ \log\left(1 - \sum_{i\neq j} \phi_i\right)$ *first order approximation* $m_j = \sum_{i\neq j} \phi_i^{m_i} \Big/ \sum_{i\neq j} \phi_i$	Glover (2010b)	Derived from the conventional Archie's law by considering boundary conditions implied by geometric constraints

Notes. There is either 1 phase, 2 phases, or n phases each denoted by subscripts, with the subscript i denoting the ith phase in an n-phase set. Conductivities are noted as σ, while cementation and analogous exponents are denoted by m or p. The volume fraction of each phase is denoted by ϕ.

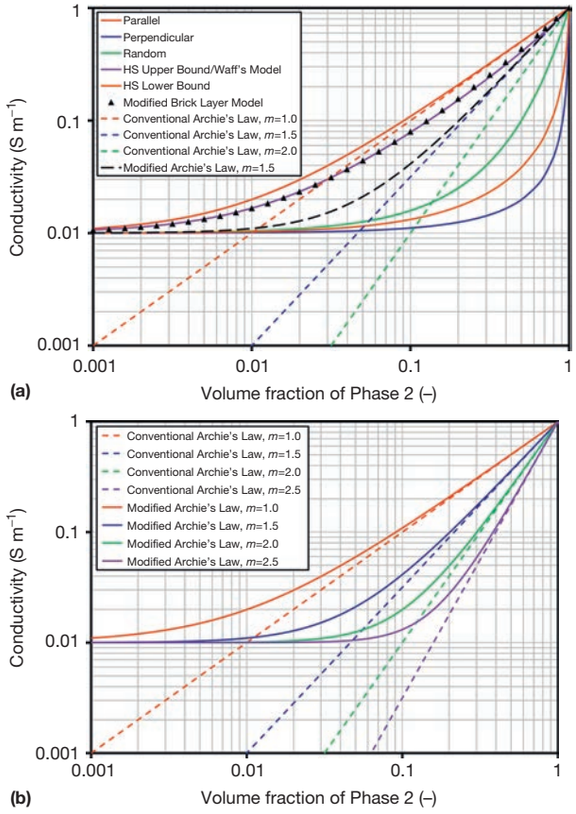

Figure 10 (a) Comparison of various mixing models as a function of the volume fraction of Phase 2. In this generic diagram conductivity of Phase 1 is $\sigma 1 = 0.01$ S m^{-1} and that for Phase 2 is $\sigma 2 = 1.0$ S m^{-1}. Geometrical models are shown by solid lines, except the modified bricklayer model which is shown by triangles because it is so similar to the HS upper bound, which it overlies. The three Archie's law implementations, for $m = 1.0$, 1.5, and 2.0, respectively, are shown by short dashed lines. The single implementation of the modified Arches law for m equals 1.5 is shown in black with a long dashed line. Note that the parallel and perpendicular models describe the extreme bounds of the conductivity for any given volume fraction of Phase 2, while the HS upper and lower bounds are more restrictive. (b) Comparison of the performance of the conventional Archie's law (Archie, 1942) with the modified Archie's law for two conducting phases (Glover et al., 2000). The conventional Archie's law is given by short dashed lines, while the modified Arches law by solid lines. Note that in no cases does the conventional Archie's law model the conductivity well at low volume fractions of Phase 2, while the modified Archie's law converges on the conductivity of Phase 1 as the volume fraction of Phase 2 goes to 0. In each case the modified Archie's law becomes asymptotic with the conventional Archie's law at large volume fractions of Phase 2. Reproduced from Glover PWJ, Hole MJ, and Pous J (2000). A modified Archie's law for two conducting phases. Earth and Planetary Science Letters 180: 369-383. http://dx.doi.org/10.1016/S0012-821X(00)00168-0.

conductivity 1 S m^{-1}, as a function of the volume fraction of the second phase. It is clear that the HS+ and HS− bounds fall between the values for the parallel and perpendicular models.

Another approach is to consider cubic bricks instead of spheres in a so-called brick-layer model (BLM). Beekmans and Heyne (1976) did this to produce a model for two phases with different conductivities and volume fractions. They considered the blocks to be solid grains with a given conductivity and the material between the blocks to be melt of a higher conductivity. Unfortunately, this model was only valid for the volume fraction of the interblock phase that amounted to less than a few percent (Barsoukov and Macdonald, 2005). The model was modified by Schilling et al. (1997) to be valid for all interblock volume fractions and is known as the modified brick-layer model (MBLM). Schilling et al. then used the MBLM to model the electrical conductivity of partial melting in laboratory tests very successfully (Partzsch et al., 2000), which implied that the structure of the melt and solids in their experimental samples must have been approximated by the blocky structure of the model. Plotting the MBLM in **Figure 10** shows it to be extremely similar to HS+, but not exactly the same.

Finally, an interesting model is based upon the weighted geometric mean. Although it cannot be proven analytically, this equation has been shown to arise naturally from a random three-dimensional mixture of phases of different conductivities σ_i and different phase volume fractions ϕ_i. One would think that such an equation would not be useful in the modeling of electrical conductivity in geomaterials, but it has already found application in calculating the permeability of a rock with different fractions of different grain sizes using electrical data (Glover et al., 2006a,b). **Figure 10** shows that the geometric mean (labeled 'random model' in **Figure 10**) is closer to the Hashin and Shtrikman lower bound (HS−) than the MBLM or Waff model.

The advantage of the geometric models is that in many cases, one can treat many different conducting phases. Their disadvantage is that they represent only one particular geometry.

11.04.3.2 Models with Variable Exponents

The second part of **Table 2** contains models with variable exponents.

The advantage that Archie's law and the other models in this subsection have over the geometric models is that they contain one or more variable exponents. These exponents are a measure of the connectedness of each of the conducting phases in the rock. The exponents not only give an extra degree of flexibility when fitting the equation to data but also can be inverted to provide the exponents, which can then be used as a measure of the connection of each phase in the rock.

The disadvantage with the original Archie's law is that only one conducting phase is allowed. This becomes clear in the top part of **Figure 10**, where each of the curves for Archie's cementation exponents $m = 1$, 1.5, and 2, respectively, tends to zero as the volume fraction of the second (conductive) phase tends to zero. If one were modeling a system with a conducting matrix (Phase 1) and a conducting fluid (Phase 2), the model would fail, particularly at low porosities and for low-conductivity fluids. **Figure 10(a)** shows such a scenario, where the conductivity of the matrix (Phase 1) is 0.01 S m^{-1} and that of the conducting fluid (Phase 2) is 1 S m^{-1}. Use of the conventional Archie's law as represented by the straight lines in the figure leads to errors. If we ask the conventional Archie's model to tell us what the conductivity of a rock composed of 1% fluid and 99% matrix is, we get 0.01, 0.001, and 0.0001 S m^{-1} for $m = 1$, 1.5, and 2, respectively. In all cases, the calculated conductivity is equal to or significantly lower than the conductivity of the rock matrix even though the rock matrix makes up 99% of the rock. This is an error that the geometric models do not make, tending to the conductivity of the matrix as the other phase

decreases to zero (Figure 10(a)). It is also an error that the modified Archie's law is not subject to (Section 11.04.3.3).

Although Archie's first law is probably the simplest of this group and was, as we have already seen, originally derived empirically, the Lichtenecker and Rother (1931) equation (LR equation) predated it by ten years. The LR equation is also more general, being valid for two or more phases, and indeed collapses to become formally the same as Archie's first law if all but one of the phase conductivities become zero. Initially, the LR equation was also empirical but has recently gained more theoretical pedigree (Zakri et al., 1998). It is also interesting in that in the LR equation, the conductivity terms have the exponents, not the phase fractions. Bussian's (1983) equation was derived from effective medium theory and was thought to be a good model for the complete range of parameters, but it has been shown recently that it diverges from experimental results at low fluid conductivities. In addition, it is difficult to solve because it is nonlinear. However, a conformal mapping code is now available to simplify the process (Glover et al., 2010).

11.04.3.3 Extended and Generalized Archie's Laws

In 2000, Glover et al. (2000b) needed to model the electrical conductivity of a rock where the solid grains had a finite conductivity because they were at high temperature but there was also a high-conductivity melt fraction of unknown geometry. Under these conditions, the modified brick-layer model cannot be used. Instead, they produced an extended version of Archie's law for two conducting phases where each phase had an exponent that described its degree of connection, and the two exponents were related to each other Glover et al. (2000a). This, so-called, modified Archie's law (MAL) not only has two conducting phases, but also allows the electrical connectedness of the two phases to be varied, so different geometries can be modeled.

The derivation of modified Archie's law is heuristic and makes an important assumption that electrical conduction in each of two conducting phases that completely describe the porous medium can be considered independently. In other words, any mathematical description does not contain a term describing the interaction between the phases. Formally, such a term is written as a Stieltjes integral. That the conduction in the two phases can be considered independently does not of course imply that the two conduction paths are independent. Conduction may start off in Phase 1 and cross over into Phase 2 and back again many times, just that when the conduction occurs in Phase 1, it is governed by Phase 1 properties and likewise for Phase 2. When current passes from Phase 1 to Phase 2, whatever perturbation that has on the conductivity of the whole rock is canceled out by the currents passing from Phase 2 to Phase 1 in other parts of the rock. It is hypothesized that this canceling of the interaction terms is fundamentally a consequence of Gauss' law. The result is that each of the phases can be described by an Archie-like term:

$$\sigma_r = \sigma_1 \phi_1^p + \sigma_2 \phi_2^m \qquad [40]$$

where there are two phases (subscripted 1 and 2), each phase has a volume fraction ϕ_1 and ϕ_2, respectively, and each has an intrinsic conductivity σ_1 and σ_2, respectively. Phase 1 has an exponent p and Phase 2 has an exponent m, using the symbology of the original paper (Glover et al., 2000a). In the usual interpretation, Phase 1 is the matrix and Phase 2 is the fluid that occupies the pores of the rocks; hence, eqn [40] becomes

$$\sigma_r = \sigma_{\text{matrix}}(1-\phi)^p + \sigma_f \phi^m \qquad [41]$$

where ϕ is the porosity of the porous medium, σ_{matrix} is the conductivity of the rock matrix, and σ_f is that of the fluid occupying the pores. The application for which the modified Archie's law was developed, however, did not have an aqueous pore fluid. For that application, Phase 1 was hot crustal rock whose conductivity was described using equations of the form of eqn [11] for continental crustal lithologies, and Phase 2 was melt (Glover et al., 2000b).

Table 3 Approximation of the modified Archie's law (MAL) for various exponents to other models

Approximate modified Archie's law exponents	
Model	m
Parallel model	1
Perpendicular model	3–5
Random model	1.7–2.2
Hashin–Shtrikman upper bound/Waff model	1.15–1.25
Hashin–Shtrikman lower bound	1.8–3
Modified brick-layer model	1.15

Where there is a range given, the lower values produce a good fit at low values of the volume fraction of the phase with the higher conductivity, and the higher values in the table produce better fits for high values of the volume fraction of the phase with the higher conductivity.

The modified Archie's law has two exponents, each of which describes the electrical connectedness of its phase, and this allows a range of behaviors including that which approximates to the HS upper bound/Waff model ($m = 1.15$–1.25) and the HS lower bound ($m = 1.8$–3). Table 3 shows a full set of approximations of the modified Archie's law to various other models. The first part of Figure 10 includes one curve using the MAL with a cementation exponent of the second phase equal to 1.5. It is interesting to note that the MAL behaves in general like the geometric models, but its position between the parallel and the perpendicular models is defined by the cementation exponent of the second phase. This behavior is shown clearly in the second part of Figure 10, which compares the behavior of the conventional and modified Archie's laws for four values of cementation exponent.

The two exponents in the modified Archie's law are not independent of each other. Just in the way that the volume fractions of the two phases always sum to unity, there is a finite connectedness available to the three-dimensional rock. This means that if one phase, say, Phase 1, increases its connectedness (i.e., the exponent p decreases), the connectedness of Phase 2 must increase (i.e., the exponent m increases), and vice versa. The two exponents are linked by the relationship

$$p = \frac{\log(1-\chi_2^m)}{\log(1-\chi_2)} \qquad [42]$$

The modified Archie's law has subsequently been used successfully from concrete to food engineering.

The question arose naturally whether a form of Archie's law for n-conducting phases existed. Following the development of the concept of connectedness in 2009 (Glover, 2009), such a law was formulated and partially validated using a numerical

approach (Glover, 2010b). This general law will probably only rarely find an application. However, interestingly, the generalized Archie's first law automatically generates the second Archie's (saturation) law and seems not to require the concept of percolation in order to be a complete description of the electrical conductivity of an n-phase material, geologic or not.

11.04.3.4 Empirical Models for Full Water Saturation

In the literature, there exist a large number of models that have been developed empirically for a particular company and even a particular oil or gas field. Once successful in a given field for a given company, they are often applied elsewhere without consideration of their validity. These equations should generally be avoided.

Company models are generally the same form as Archie's law, but with particular values for a and m. Examples include the 'Humble' formula ($a=0.62$, $m=2.15$), which was developed for the Humble Oil Company by Winsauer et al. (1952) from 30 samples (28 sandstones, 1 limestone, and 1 unconsolidated sandstone) and the Tixier equation ($a=0.81$, $m=2$), which uses the same data and forces $m=2$. Other equations which are based on more data include that of Carothers and his colleagues who used a database of 793 sandstone samples ($a=1.45$, $m=1.54$) and the Shell formula, which was developed for low-porosity (<9%) unfractured carbonates ($a=1$, $m=1.87+0.019/\phi$). This model is one of the many that use an empirical relationship to obtain the cementation exponent and then use that cementation exponent within Archie's law. Others include Focke and Munn (1987), Nugent et al. (1978), Nurmi and Frisinger (1983), and Rasmus (1983).

These models were often not intended for general application, but have subsequently been applied generally. They have no scientific merit in themselves, and most of them represent specific cases of Archie's first law. It is best to regard them as obsolete and use one of the other more appropriate models given in **Table 2**.

11.04.3.5 Shaley Sand Water Saturation Equations

Most shales have moderately low resistivities, which can be seen on any resistivity log, and log analysts explain the fact by attributing the extra conduction to absorbed waters on clay surfaces. This is a simplistic way of explaining effects that we now describe using electrical double- and triple-layer models (e.g., Revil and Glover, 1997, 1998; Revil and Leroy, 2004).

The presence of clays as a component of shaley sandstones introduces an extra conductivity contribution that should be combined with the conductivity of the pore formation water in detailed reservoir analysis. If no account is taken of the extra conductivity in a shaley sand zone by using the simple combined Archie's equation [32] to calculate water saturation, the result will be an overestimation of water saturation, since the resistivities have been reduced below their true values by the conductivity of the shale component. Hence, potentially economic hydrocarbon-bearing intervals may be missed.

There are two main families of resistivity model for partially saturated shaley sandstones. Both have developed from Archie's equations and accommodate the conductivity effects of clay minerals in order that more accurate water saturations may be computed (Worthington, 1985). All the models consider that the shale is a homogeneous conductive medium and add the conductivity of the shale fraction (V_{sh}) to Archie's law component of conductivity. These equations have the form

$$\sigma_t = \sigma_{clean} + \sigma_{shale} \quad [43]$$

where the total conductivity of the rock σ_t is composed of that which it would have if it were clay-free σ_{clean} plus that associated with the shales σ_{shale}. Although the physical basis of these models is incorrect because the shale and pore fluid contributions do not, in general, occur in parallel and independently, the equations often provide approximate solutions to water saturation, especially when the equation parameters are adjusted so that the results conform to local water saturation data measured from cores or production tests. **Table 4** shows some of the main models of this type.

All but two of the models in **Table 4** assume that pore fluid-mediated conduction and shale-mediated conduction (whatever its physical mechanism) are independent, occur in parallel, and hence can be described by a sum of conductivities. One would expect that these models perform better in laminar or layered shales. The two remaining models (Waxman and Smits (1968) and the dual-water model (Clavier et al., 1977; Coates et al., 1983)) are also formed by a sum of conductivities, which would imply parallel conducting mechanisms, but their use of different formation factors allows them to also perform well where the clay is distributed throughout the rock in a dispersed manner or is part of the rock structure.

It has been pointed out that none of these models are correct in a theoretical sense (Doveton, 2001), but in approximating the theoretical behavior, some can provide fairly accurate solutions for the hydrocarbon industry. Some of these equations are still widely used because of their relative simplicity and limited demands on additional input parameters.

One of the most commonly used equations of this type is the Simandoux equation (Simandoux, 1963). The original equation contained a factor ε, where $\varepsilon=1$ when $S_w=1$ and $\varepsilon<1$ when $S_w<1$. In fact, it is usually the modified Simandoux equation (Bardon and Pied, 1969) that is used these days. In this model, $\varepsilon=S_w$. The modified Simandoux equation can be written in a generalized polynomial form that makes it easier to implement numerically and accounts for saturation exponents other than $n=2$:

$$S_w^n + \left[\frac{V_{sh}\rho_w\phi^{-m}}{\rho_{sh}}\right]S_w - \frac{\rho_w\phi^{-m}}{\rho_t} = 0 \quad [44]$$

It is known that the Simandoux equation tends to underestimate the water saturation in oil reservoirs (Doveton, 2001; Smith and Rouleau, 1977). The underestimation of water saturation leads to an overestimation of the oil saturation that Doveton (2001) has suggested has been a possible reason for the popularity of the equation.

The Simandoux and Bardon and Pierre equations make a number of assumptions. First, the clean and shaley contributions can be considered to be independent and arranged electrically in parallel, leading to the conductivities being summed. Second, the shale fraction has a very good connectedness for both the shale volume and the water associated with that shale, as indicated by the unity exponents for V_{sh} and S_w in the second term (cf. **Table 4**). Examination of the other equations of this type shows the first assumption also applies to them, while the second assumption applies to most. The Hossin

Table 4 A selection of shaley rock water saturation models (arranged in chronological order)

Models	*Equation in terms of resistivity*	*Equation in terms of conductivity*	*Reference*
Poupon et al.	$\frac{1}{\rho_t}=\frac{(1-V_{sh})S_w^2}{F\rho_w}+\frac{V_{sh}}{\rho_{sh}}$	$\sigma_t=\frac{(1-V_{sh})S_w^2}{F}\sigma_w+V_{sh}\sigma_{sh}$	Poupon et al. (1954)
Hossin	$\frac{1}{\rho_t}=\frac{S_w^2}{F\rho_w}+\frac{V_{sh}^2}{\rho_{sh}}$	$\sigma_t=\frac{S_w^2}{F}\sigma_w+V_{sh}^2\sigma_{sh}$	Hossin (1960)
Simandoux	$\frac{1}{\rho_t}=\frac{S_w^2}{F\rho_w}+\frac{\varepsilon V_{sh}}{\rho_{sh}}$	$\sigma_t=\frac{S_w^2}{F}\sigma_w+\varepsilon V_{sh}\sigma_{sh}$	Simandoux (1963)
Waxman and Smits	$\frac{1}{\rho_t}=\frac{S_w^2}{F^*\rho_w}+\frac{BQ_vS_w}{F^*}$	$\sigma_t=\frac{S_w^2}{F^*}\sigma_w+\frac{BQ_vS_w}{F^*}$	Waxman and Smits (1968)
Modified Simandoux	$\frac{1}{\rho_t}=\frac{S_w^2}{F\rho_w}+\frac{V_{sh}S_w}{\rho_{sh}}$	$\sigma_t=\frac{S_w^2}{F}\sigma_w+V_{sh}\sigma_{sh}S_w$	Bardon and Pied (1969)
Indonesia equation	$\frac{1}{\rho_t}=\frac{S_w^2}{F\rho_w}+2\left[\sqrt{\frac{V_{sh}^{(2-V_{sh})}}{F\rho_w\rho_{sh}}}\right]S_w^2+\frac{V_{sh}^{(2-V_{sh})}S_w^2}{\rho_{sh}}$	$\sigma_t=\frac{S_w^2}{F}\sigma_w+2\left[\sqrt{\frac{\sigma_w\sigma_{sh}V_{sh}^{(2-V_{sh})}}{F}}\right]S_w^2+\sigma_{sh}V_{sh}^{(2-V_{sh})}S_w^2$	Poupon and Leveaux (1971)
Schlumberger	$\frac{1}{\rho_t}=\frac{S_w^2}{F(1-V_{sh})\rho_w}+\frac{V_{sh}S_w}{\rho_{sh}}$	$\sigma_t=\frac{S_w^2}{F(1-V_{sh})}\sigma_w+V_{sh}\sigma_{sh}S_w$	Schlumberger (1972)
Dual Water Equation	$\frac{1}{\rho_t}=\frac{S_w^2}{F_0\rho_w}+\frac{\left(\frac{1}{\rho_{bw}}-\frac{1}{\rho_f}\right)V_0Q_vS_w}{F_0}$	$\sigma_t=\frac{S_w^2}{F_0}\sigma_w+\frac{(\sigma_{bw}-\sigma_w)V_0Q_vS_w}{F_0}$	Clavier et al. (1977)
Juhasz	$\frac{1}{\rho_t}=\frac{S_w^2}{F\rho_w}+\left(\frac{1}{F_{sh}\rho_{sh}}-\frac{1}{\rho_w}\right)\frac{V_{sh}\phi_{sh}S_w}{\phi}$	$\sigma_t=\frac{S_w^2}{F}\sigma_w+\left(\frac{\sigma_{sh}}{F_{sh}}-\sigma_w\right)\frac{V_{sh}\phi_{sh}S_w}{\phi}$	Juhasz (1981)

ρ_t is the total resistivity of the material (Ωm), ρ_f is the resistivity of the aqueous pore fluid (Ωm), ρ_{sh} is the resistivity of the shale (clay) (Ωm), ρ_{bw} is the resistivity of the bound water in the dual-water model (Ωm), the analogous symbols with σ replacing ρ refer to the equivalent conductivities, S_w is the saturation of the aqueous fluid (dimensionless), V_{sh} is the volume fraction of shale (clay) in the material (dimensionless), V_0 is the volume of shale associated with one coulomb of excess charge ($m^3\ C^{-1}$), ε is an ad hoc constant in the original model (dimensionless), F is the formation factor (dimensionless), F^* is the shaley sand formation factor (dimensionless), F_0 is the formation factor associated with the total porosity (dimensionless), Q_v is the excess of surface charge due to adsorption of ions within the electrical double or triple layer normalized by pore volume ($C\ m^{-3}$), B is ionic surface mobility ($m^2\ s^{-1}\ V^{-1}$), ϕ is the porosity of the sample (dimensionless), and ϕ_{sh} is that of the shale component (dimensionless).

(1960) model is the exception, associating a smaller connectedness to the shale volume as indicated by the exponent 2.

The Waxman and Smits (1968) and dual-water (Clavier et al., 1977) models are based on the ionic double layer observed in shaley sandstones. In reality, the conductivity of the shale component is a function of the CECs of the various types and abundances of clay minerals that are present. Since the cations are exchanged primarily at broken bonds on mineral surfaces, the phenomenon tends to be surface area-dependent rather than controlled simply by the volume of clay minerals. This implies that fine-grained clay has a higher exchange capacity than a coarse-grained form of the same clay volume, and this observation is confirmed by experimental data. In fact, surface conduction studies can now benefit from electrochemical modeling of the electrical double or triple layer structures that form at mineral/fluid interfaces (see **Section 11.04.4**) and it turns out that clays have higher-surface-conductivity contributions than a silica matrix not because their surfaces are intrinsically more conductive, but because they have large internal surface areas (Revil and Leroy, 2001).

The problem with the Waxman and Smits model is that it contains parameters that cannot be obtained from borehole measurements, which give only the approximate volume of shale and the total porosity of the rock. Neither is there any estimation of grain or pore size from downhole measurements. The CEC can be measured in the laboratory (see Ross and Ketterings, 2011 for a summary of the different methods), albeit on crushed rock samples that may or may not represent the *in situ* reality. Consequently, the model equations that use cation-exchange data have been modified to variants that substitute quantities that can be measured on logs as surrogate variables. The most widely known of these is the dual-water model introduced by Clavier et al. (1977), which, when generalized, takes the form

$$S_{wt}^n-\left[S_b\left(1-\frac{a\rho_w}{\rho_b}\right)\right]S_{wt}-\frac{a\rho_w\phi_t^m}{\rho_t}=0 \qquad [45]$$

where $\rho_b=\rho_{sh}\phi_{tsh}^2$, $S_b=V_{sh}\phi_{tsh}/\phi_t$, and $\phi_t=\phi_{eff}+V_{sh}\phi_{tsh}$ and where ρ_b is bound-water resistivity, S_b is bound-water saturation, S_{wt} is total water saturation (including S_b), ϕ_{tsh} is shale porosity (some weighted average of the neutron and density porosities of shale), ϕ_{eff} is effective porosity, ϕ_t is total porosity (including the shale porosity term), and a is Winsauer et al.'s (1952) modification to Archie's law.

Although the Simandoux and dual-water equations were developed from different models, they do have a number of features in common (and with many other shaley sandstone equations):

1. At zero shale content, the equations collapse to the combined Archie's equation (although often with the saturation exponent n set to 2).
2. The equation forms can be written as polynomials and solved reiteratively.

3. The input shale properties are typically drawn from shales between the reservoir units, which may not be representative of clays within the reservoir zones.

11.04.4 Surface Conduction

11.04.4.1 The Electrical Double Layer and Surface Conduction

11.04.4.1.1 The electrical double layer (EDL)

When a freshly broken mineral surface is exposed to an aqueous pore fluid, it attracts and adsorbs positive and negative ions from the fluid (Adamson, 1976; Davis and Kent;, 1990; Dukhin and Derjaguin, 1974; Glover et al., 1994; Hunter, 1981; Sposito, 1989). In the following discussion, we consider a silica surface. However, the same approach may be taken for any mineral, for example, Revil and Leroy (2001) who applied a triple-layer model to clay minerals.

A quartz surface, such as that shown in green in Figure 11, provides two types of neutral surface group on the silica surface, a doubly coordinated siloxal $>Si_2O^o$ group, which can be considered inert and is not shown in the figure, and a singly coordinated silanol $>SiOH^o$ group (where $>$ represents the matrix) (e.g., Iler, 1979; Revil and Glover, 1997, 1998; Revil et al., 1999a). The silanol group reacts readily to give $>SiOH_2^+$ when $pH < pH_{pzc}$ and $>SiO^-$ when $pH > pH_{pzc}$. Both of these are shown in the inner Stern layer in Figure 11, noting that the negative group is surrounded by a hydration shell. The pH_{pzc} is the pH at which the surface has no net charge (i.e., $[>SiOH_2^+] = [>SiO^-]$, where the square brackets indicate concentration) and is called the point of zero charge. For quartz, $pH_{pzc} \approx 3$ (Lorne et al., 1999a,b).

These surface sites, which form the inner Stern layer, react with ionic species in the bulk fluid. If we consider a 1:1 electrolyte with single-valency anions and cations, such as NaCl,

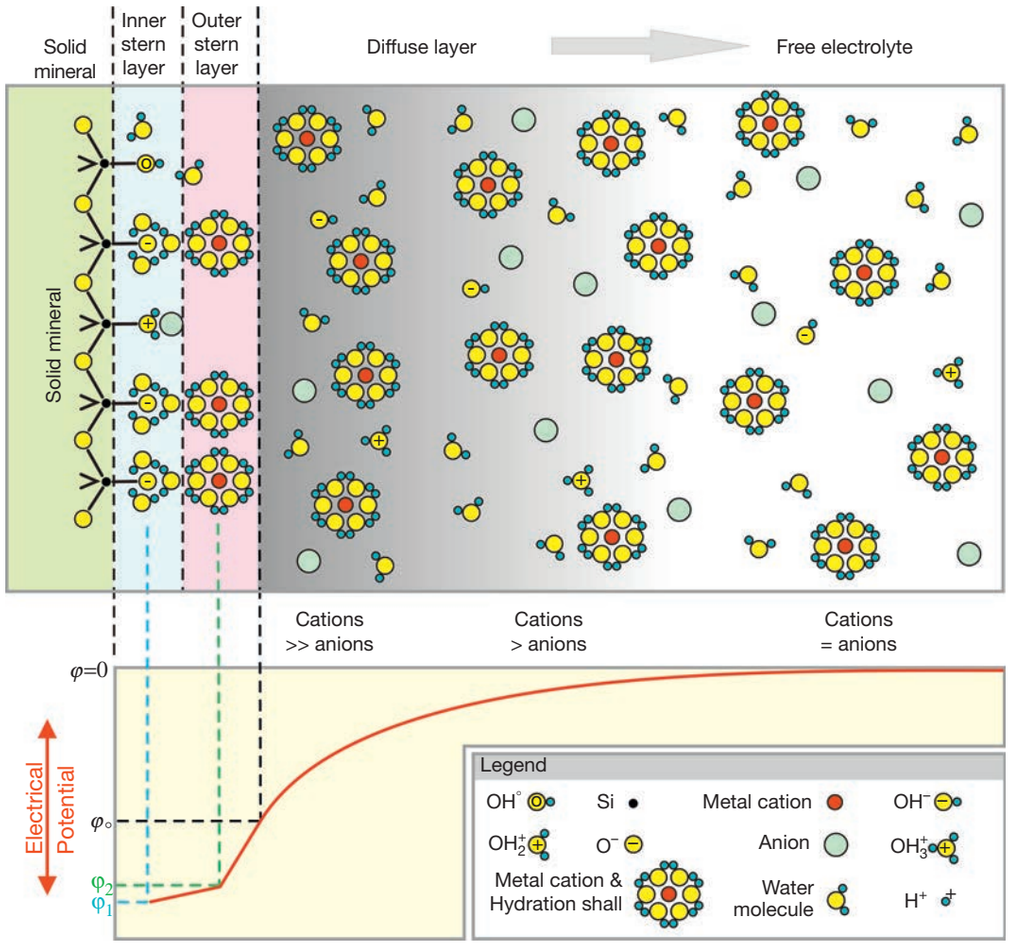

Figure 11 A schematic representation of the electrical double layer that exists at the interface between the rock matrix and the pore water. The rock is shown on the left-hand side in green. Here, it is silica, which forms three types of surface site (positive $SiOH_2^+$, neutral SiOH, and negative SiO^-). The relative concentrations of these depend upon the fluid pH. At reservoir fluid pH, the negative sites dominate. Hydrated positive ions (in red here) are adsorbed to these sites. The adsorbed positive ions cannot cancel out all of the negative surface charge, so there exists a fluid diffuse layer that has an excess positive charge (more hydrated cations than anions), which falls off exponentially until there are equal numbers of positive and negative ions (the bulk fluid). The thickness of the diffuse layer depends upon fluid concentration. At low concentrations, it may be several microns thick, which is sufficient to ensure that a rock with small pores has all of its aqueous fluid in the form of the diffuse layer rather than as bulk fluid. In this case, there is no bulk fluid conduction, only surface conduction mediated through the EDL. Modified from Glover PWJ and Jackson MD (2010) Borehole electro-kinetics. *The Leading Edge* 29: 724–728, http://dx.doi.org/10.1190/1.3447786.

and we consider a geologically reasonable pore fluid pH range of 6–8, the surface reactions can be written as (Davis et al., 1978; Revil and Glover, 1997; Revil et al., 1999a,b)

$$>\mathrm{SiOH}^{o} \overset{K_{(-)}}{\Leftrightarrow} >\mathrm{SiO}^{-} + \mathrm{H}^{+} \quad [46]$$

and

$$>\mathrm{SiOH}^{o} + \mathrm{Me}^{+} \overset{K_{Me}}{\Leftrightarrow} >\mathrm{SiOMe}^{o} + \mathrm{H}^{+} \quad [47]$$

where the metal cation is Me^+, for example, Na^+, K^+, or some other single-valence cation. The positive surface site $>SiOH_2^+$ does not occur in eqns [46] and [47] because at $pH > 6$, $[>SiOH_2^+] \approx 0$. Hence, there result three types of site, two neutral ones ($>SiOH^o$ and $>SiOMe^o$) and one negative ($>SiO^-$) (Revil and Glover, 1997; Revil et al., 1999a,b). The metal ions that take part in these surface adsorption reactions form the outer Stern layer, as shown in **Figure 11**.

The position of the equilibrium of eqn [46] is given by the disassociation constant for dehydrogenization of silanol surface sites $K_{(-)}$. If $K_{(-)}$ is large, eqn [46] has an equilibrium towards the right, giving very many more $>SiO^-$ sites than $>SiOH^o$ sites, and vice versa. The position of the equilibrium in eqn [47] is given by the binding constant for cation (sodium) adsorption on quartz K_{Me}. If K_{Me} is large, eqn [47] has an equilibrium towards the right, where there are very many more $>SiOMe^o$ sites than $>SiOH^o$ sites, and vice versa. So $K_{(-)}$ and K_{Me} describe the relative concentrations of the three surface sites. They are unitless.

The final parameter of interest is the total surface site density Γ_s^o (in m^{-2}), which is the sum of the surface site densities for each of the three types of surface site. For quartz and most geologic pore fluids (where $pH \gg pH_{pzc}$). $K_{(-)}$ is large and the inner Stern layer has an overall negative charge, which attracts cations from the bulk fluid. This is a self-limiting process because the number of negative sites is limited. However, the bulk fluid becomes depleted to some extent in cations. This depleted zone is called the diffuse layer as shown in **Figure 11**. It should be noted that the ions in the outer Stern layer are not usually considered to be mobile, while the ions that make up the diffuse layer are mobile.

The adsorbed ions of the outer Stern layer are not sufficient to balance the negative surface charge associated with inner Stern layer. Hence, the net charge of the two Stern layers remains slightly negative as shown by the bottom portion of **Figure 11**. It is this negative charge that attracts cations from the bulk solution and ultimately generates a diffuse layer that is depleted in cations.

The global requirement for electrical neutrality ensures that the depletion is greatest near the Stern plane and reduces exponentially with distance from the Stern plane until the diffuse layer blends seamlessly with the bulk fluid. During this process, the electric potential reduces exponentially until it reaches zero in the bulk fluid as shown in the bottom portion of **Figure 11**.

11.04.4.1.2 Thickness of the electrical double layer

Since the diffuse layer has no well-defined boundary towards the bulk fluid, its width is difficult to define. The traditional measure of the width of the diffuse layer is the Debye screening length that is given by

$$\chi_d = \sqrt{\frac{\varepsilon_o \varepsilon_r k_b T}{2000 N e^2 I_f}} \quad [48]$$

where $\varepsilon_o = 8.854 \times 10^{-12}\ \mathrm{F\,m^{-1}}$ is the electric permittivity *in vacuo* of the fluid (Lide, 2012), ε_r is the relative electric permittivity of the fluid (no units), T is the temperature (in K), and I_f is the ionic strength, which is given by

$$I_f = \frac{1}{2}\sum_{i}^{n} Z_i^2 C_i^f \quad [49]$$

where there are i ionic species in solution, Z_i is the valency of each ionic species, and C_i^f is the concentration of each ionic species in solution. The factor of 2000 arises due to the units for ionic strength here being $mol\,l^{-1}$. This equation is often found cited with a 2 in place of the 2000, in which case the units for I_f would be $mol\,m^{-3}$.

In most geologic fluids in the upper crust the ionic contribution to fluid conductivity from acid ions $[H_3O^+]$ and alkali ions $[OH^-]$ are much smaller than the contribution from the electrolyte, for example, $[Na^+]$ and $[Cl^-]$ and for an NaCl electrolyte. Hence, for the most common scenarios where $C_f > 10^{-5}\ mol\,l^{-1}$ and $5 < pH < 9$, we can say that $I_f \approx C_f$. In fact, recent experimental studies have shown that it is extremely difficult to have a pore fluid with $C_f < 10^{-5}\ mol\,l^{-1}$ in full chemical equilibrium with a sandstone (Walker et al., 2014) because the salinity of the fluid is raised by dissolution. It is likely that this observation is also true for many other rock types, making the approximation $I_f \approx C_f$ valid in most geologic scenarios.

The most common measure of the effective width of the diffuse layer is twice the Debye screening length (e.g., Revil and Glover, 1997). **Figure 12** shows how the Debye screening length and the effective width of the diffuse layer vary with the salinity of the bulk fluid. The diffuse layer is thicker at low salinities than at high salinities. This is simple to explain physically: A low-salinity bulk fluid has fewer cations per unit volume than a high-salinity fluid. Hence, it will take a greater volume of low-salinity fluid to provide cations to adsorb to the surface and to completely saturate all the surface sites than would be the case for a high-salinity fluid with more cations per unit volume. Since the area of the rock–fluid interface is fixed, the diffuse layer must be thicker for low-salinity fluid.

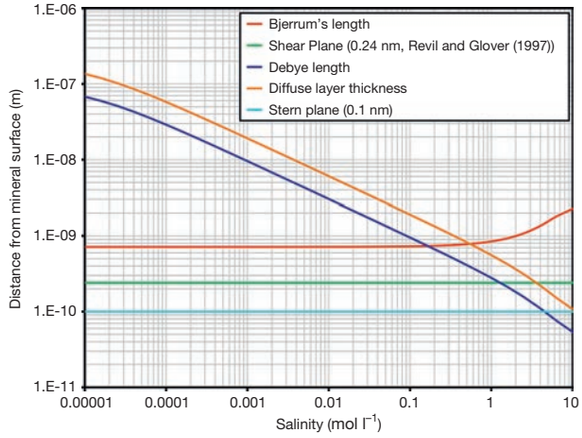

Figure 12 Characteristic length scales related to the electrical double layer in saturated porous media.

For low-salinity fluids and rocks with small pore sizes, it is possible for the width of two diffuse layers (one associated with each of two opposing grains of the rock) to be larger than the distance between the grains. In this case, there is no bulk fluid and all of the fluid between the two grains is composed of the diffuse layers of each EDL. Since the diffuse layer is charged (positively for silica geologic pHs), ions of the same charge can be excluded from entering these pores and pore throats, with the overlapping diffuse layers acting as a charge selective barrier. Such a scenario can occur in clay-rich rocks or clay concentrations within heterogeneous reservoir rocks.

For all salinities, the thickness of the diffuse layer is significantly larger than the thickness of the Stern layer (the blue line in **Figure 12**), which may be taken as being of the order of the diameter of a hydrated metal ion (viz., 10^{-10} m).

Figure 12 also shows the distance of the shear plane from the Stern plane $\chi_\zeta = 2.4 \times 10^{-10}$ m (the green line in **Figure 12**), which was calculated by Revil and Glover (1997) and the Bjerrum length (the red line in **Figure 12**). The Bjerrum length λ_b is the distance at which the electrostatic interaction between the two elementary charges is comparable in magnitude to the thermal energy scale. It is given by $\lambda_b = e^2/4\pi\varepsilon_r\varepsilon_o k_b T$. For an aqueous solution of NaCl, we find that the Bjerrum length remains constant at $\lambda_b = 7.16 \times 10^{-10}$ m for salinities less than about 0.1 mol l^{-1}, increasing substantially as salinity increases past 0.1 mol l^{-1} until it reaches a value of 13.5×10^{-10} m at 3.98 mol l^{-1}.

At length scales larger than λ_b, fluid ions are more affected by thermal agitation than the presence of the Stern layer. At length scales smaller than λ_b, fluid ions are significantly affected by the presence of the Stern layer. Indeed, the local field strength is sufficient to alter the viscosity and the permittivity of the fluid considerably. It should be noted that the Bjerrum length is greater than the EDL thickness for all salinities greater than about 0.55 mol l^{-1} (dashed line in **Figure 12**). In other words, interionic electrostatic interactions are significant for the entire EDL, including all of its mobile fraction ($\chi > \chi_\zeta = 2.4 \times 10^{-10}$ m) for salinities greater than 0.55 mol l^{-1}, and it is these electrostatic interactions that may increase the viscosity of the fluid in the double layer and decrease the local permittivity.

11.04.4.2 Basic Theory of Surface Conduction

Originally, it was thought that surface conduction was only significantly developed in clays where the presence of Al^{3+} ions in place of Si^{4+} ions led to a charge deficit that was counterbalanced by the adsorption of cations from solution that then took part in surface conduction. The description in the previous section updates this view by making the process general to all minerals. Further development stemmed from the approach taken by Waxman and Smits (1968), whose model has already been mentioned in **Sections 11.04.2.4** and **11.04.3.5**.

11.04.4.2.1 Waxman and Smits model

It became increasingly clear throughout the 1950s and 1960s that Archie's simple empirical laws could not be applied to rocks that contained substantial clay fractions because of the significant surface conduction they exhibited. One of the first, empirical, and most successful formulations to overcome this problem was proposed by Waxman and Smits (1968), who included a surface conduction term in Archie's equation:

$$\sigma_{\text{eff}} = \frac{1}{F^*}(\sigma_f + BQ_v) \qquad [50]$$

The extra surface conduction is accounted for by the term BQ_v, where B (in Sm^2 mequiv.$^{-1}$) represents the mobility of surface cations and Q_v (in mequiv. m^{-3}) is the volume concentration of clay exchange cations (mequiv. = milliequivalents). Both parameters are usually obtained by fitting the model to experimental data, but the CEC is sometimes measured independently. It is worth noting that the single value for the Waxman and Smits formation factor F^* shows that the model assumes that the pathways for conduction through the bulk fluid and via surface conductivity are the same.

The critical point in the Waxman and Smits model is that the surface conduction term is composed of the product of an element that describes the number density of charge carriers on the mineral surface, which is represented by Q_v, and an element describing the mobility of those ions, which is represented by B.

11.04.4.2.2 Ionic surface electrical conduction models

In 1994, Glover et al. (1994) recognized that a model for surface conduction would have to describe the theoretical framework behind both the number density and the mobility of surface charge carriers. Restricting themselves to the first of these challenges Glover et al. (1994) attempted to create a model to calculate the concentration of surface charge carriers, which they called ISCOM1 (ionic surface concentration model). This basic model was quickly superseded by a full model for surface conduction that grew from ISCOM1 but that took account of the full expression of the electrical double layer and included surface mobilities (Revil and Glover, 1997, 1998; Revil et al., 1999a,b). Various versions of the latter model now exist and are widely applied for expressing the surface conduction in porous media (e.g., Revil and Leroy, 2001).

11.04.4.3 Application to Clean Rocks

An application of the Revil and Glover (1997) model to clean quartz-dominated rocks can be found in the last part of that paper. The equations are developed for a quartz matrix immersed in an electrolyte. The application of the Revil and Glover approach allows the calculation of the Stern plane potential (**Figure 13**) and hence the surface charge density as a function of pH and electrolyte salinity (**Figure 14**).

The use of these parameters allows the calculation of the electrical conductivity of the rock as a function of salinity and pH once certain microstructurally defined parameters are known (**Figure 15**). These parameters are the formation factors related to electrical transport through the bulk pore fluid and via surface conduction and their respective length scales. **Figure 15** shows a comparison of the model for all the surface sites on the quartz being negative (the situation in the previous theory by Glover et al., 1994), which is shown by the dotted line, and the more sophisticated Revil and Glover (1997) model. The latter model is now used more commonly.

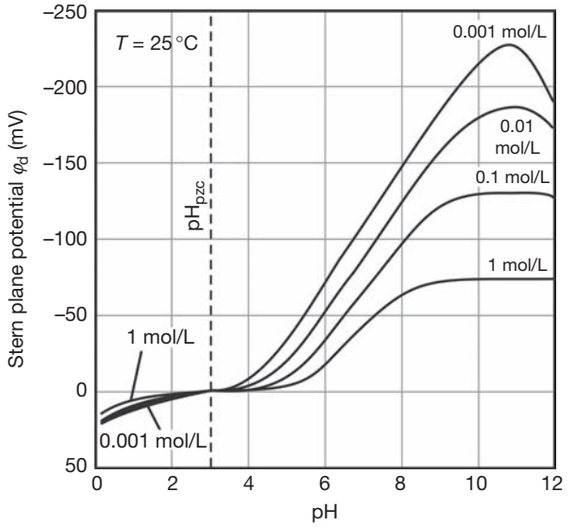

Figure 13 Stern plane potential for a quartz rock saturated with a monovalent electrolyte calculated from the Revil and Glover (1997) theory as a function of pH and electrolyte salinities at $T = 25$ °C. The dashed line marked 'pzc' is the point of zero charge; it corresponds to that pH at which there are equal densities of positive and negative sites on the quartz surface. When this is the case, the surface is neutral and no electrical double (or triple) layer is developed leading to no surface conduction.

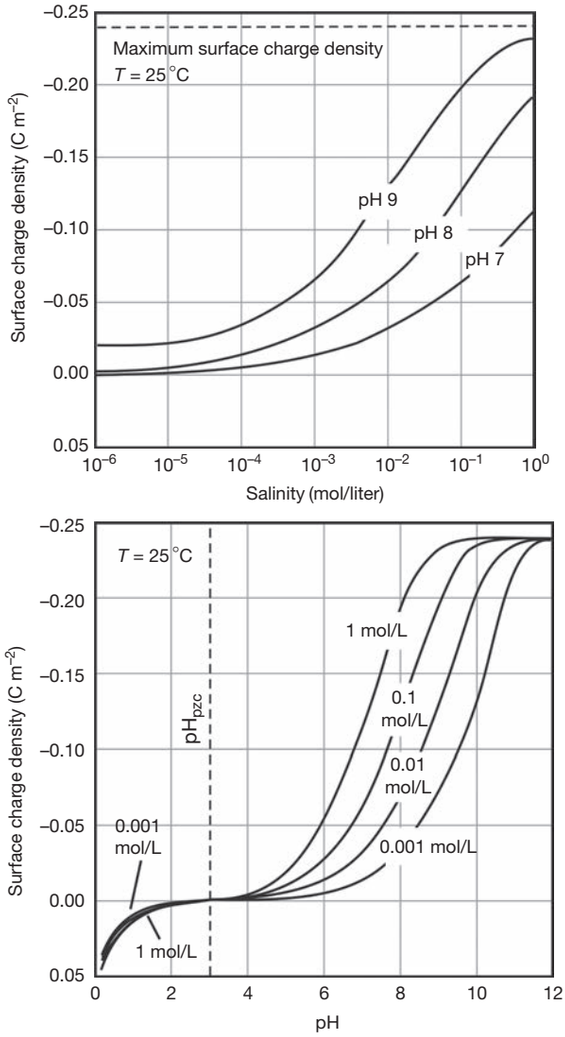

Figure 14 The surface charge density for a quartz rock saturated with a monovalent electrolyte calculated from the Revil and Glover (1997) theory as a function of salinity and pH at $T = 25$ °C. The dashed line marked 'pzc' is the point of zero charge; it corresponds to that pH at which there are equal densities of positive and negative sites on the quartz surface. When this is the case, the surface is neutral and no electrical double (or triple) layer is developed leading to no surface conduction.

11.04.4.4 Application to Clay-Rich Rocks

The electrical conductivity of clays is a far more difficult problem due to the variability of both the composition and the structure of the clay minerals. Initially, the problem was approached using a macroscopic model (Revil and Glover, 1998; Revil et al., 1998), but subsequent works by Revil and Leroy (e.g., Leroy and Revil, 2004; Revil and Leroy, 2001, 2004) have led to a full theoretical understanding of the electrochemical properties of clay minerals and ionic transport in porous shales.

11.04.5 Frequency-Dependent Electrical Properties

So far, we have only considered steady-state electrical flow, that is, when a constant potential difference is applied to a material and a constant electric current flows. Often, the applied potential will vary with time, either as a transient or with a regular repeating manner such as a harmonic pattern. This section considers such time-dependent behavior. The theoretical description of such behavior needs to take account of the fact that current flow may not keep in step with the applied potential difference due to the way that a material may store charge over short timescales or the fact that some electrochemical processes take time to occur.

There are two processes, (i) the transport of charge, which is described by the electrical conductivity of a material, and (ii) charge storage, which is described by the dielectric polarization of a material.

These two process are described fundamentally by

and
$$\vec{J} = \sigma \vec{E} \qquad [51]$$

$$\vec{D} = \varepsilon \vec{E} \qquad [52]$$

where $\vec{E}$ is the electric field strength (in V m^{-1}), $\vec{J}$ is the current density (in A m^{-2}), $\vec{D}$ is the electrical displacement (in C m^{-2}), σ is the electrical conductivity (in S m^{-1}), and ε is the dielectric permittivity (in F m^{-1}), which is often written as the product of the permittivity of free space and the dimensionless relative permittivity or dielectric constant of the material ε_r; hence, $\varepsilon = \varepsilon_o \varepsilon_r$. The electric field strength, current density, and electrical displacement are vectors, while the electrical conductivity and dielectric permittivity are frequency-dependent tensors that take account of the anisotropy of the material.

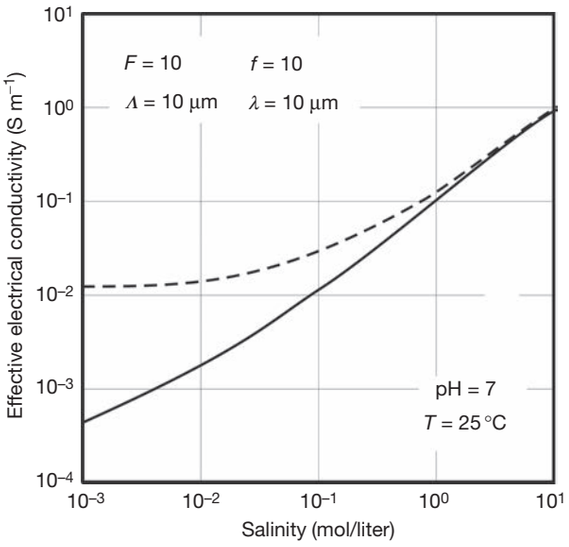

Figure 15 The effective electrical conductivity for a quartz rock saturated with a monovalent electrolyte at pH = 7 and $T = 25\ ^{\circ}C$ as a function of the electrolyte conductivity calculated from the Revil and Glover (1997) theory. The dotted line is the relationship with a quartz surface saturated with negative sites as in the Glover et al. (1994) model, and the solid line is the Revil and Glover (1997) theory. Symbols F and f are the formation factors that relate to conduction through the bulk fluid and associated with surface conduction, respectively (cf. eqn [38]). Λ and λ are the characteristic length scales associated with conduction through the bulk fluid and associated with surface conduction, respectively (cf. eqn [39]). Reproduced from Revil A and Glover PWJ (1997) Theory of ionic-surface electrical conduction in porous media. *Physical Review B - Condensed Matter and Materials Physics* 55(3): 1757–1773.

11.04.5.1 Complex Conduction

The conductive aspect of charge movement, described by [51], can be described using a complex conductivity (Guéguen and Palciauskas, 1994):

$$\tilde{\sigma} = \sigma' + i\sigma'' \qquad [53]$$

where $i = \sqrt{-1}$. We will use the convention that all complex quantities have a superscripted tilde. Hence, the complex conductivity is equal to the sum of the real (σ') part and the imaginary ($i\sigma''$) part.

Since the electrical resistivity is the inverse of the conductivity, we may also write (Guéguen and Palciauskas, 1994)

$$\tilde{\rho} = \tilde{\sigma}^{-1} = \rho' - i\rho'' \qquad [54]$$

The real part of the complex conductivity describes energy transport, while the imaginary part describes energy dissipation.

11.04.5.2 Dielectric Permittivity and Polarization

When an electric potential difference is applied to a geomaterial, charges move in response to the electric field. Mobile charges form an electric current that is described by the conductivity of the material, while bound charges also move within their ability to give a polarization of charges.

For example, the electrons that surround the atom of a molecule redistribute themselves with respect to an applied electric field, and the electron 'cloud' becomes distorted towards the positive of the applied external field. This is called electronic polarization. From a distance, the atom has been polarized with a slight excess of negative charge facing the positive of the external field and a slight excess of positive charge facing the negative pole of the applied field. Electrons have a small mass, and hence, the polarization occurs very quickly (of the order of 10^{-15} s). This is called the 'relaxation time' of the process. The relaxation time associated with electron polarization is the same order as the period of visible light. It is for this reason that the electronic contribution to permittivity is related to the refractive index, n, of a material ($\varepsilon_r = 1/n^2$). Hence, the permittivity from this source for most solid materials is in the range 1–4.

There are other sources of polarization and each operates at a different timescale. The next process, in order of increasing timescale, is atomic or ionic polarization, where atoms or ions in crystalline and amorphous solids polarize with respect to an applied electric field. As ions are heavier than electrons, the relaxation time for this process is longer (10^{-12}–10^{-13} s), but still very fast. The permittivity from this source is in the range 1–11. At microwave frequencies and below (i.e., less than 10^{12} Hz), we can say that most solid materials, including all minerals, have a relative permittivity of about 4–15 because relative permittivities from different sources add algebraically.

Dipolar polarization is another process, this time affecting materials that already have polar molecules. These polar molecules align themselves with an applied electric field. Once again, the timescale is slower (10^{-8} to 10^{-12} s), which reflects the masses of the polar molecules and the ease with which they may rotate. These polarizations can be large (5–100). The relative permittivity of water (~80) is due to electronic polarization and dipolar polarization, of which the latter is by far the largest contributor, while that of most oils is about 2 because oils contain almost no polar substances and the permittivity is controlled by electronic polarization.

Heterogeneous materials, which include all rocks, have an additional mechanism that is associated with mobile charge carriers that become stuck at or accumulate at interfaces. This occurs in porous and cracked rocks where ions in the pore fluid respond to the application of an external electric field, but solid mineral grains get in the way. Ions accumulate near the grain surface and their charge counteracts further motion of ions. The process is sometimes called the Maxwell–Wagner process, but this term was originally coined for a material consisting of one material of one relative permittivity dispersed in another of a second relative permittivity. It is also called interfacial polarization. Interfacial polarization has a relaxation time of 10^{-3} to 10^{-6} s and can be very large. Values of the order of 1000 are not unusual, which is much larger than the relative permittivity of water (~80) or mineral grains (~4–15). Hence, we can say that, as far as relative permittivity is concerned, the heterogeneity and arrangement of the materials that make up a geomaterial are much more important than the relative permittivities of its individual components. Recently, there has been an upsurge in work on dispersion mechanisms in porous media. Particular attention is now being paid to polarization processes occurring in the Stern layer of the electrical double

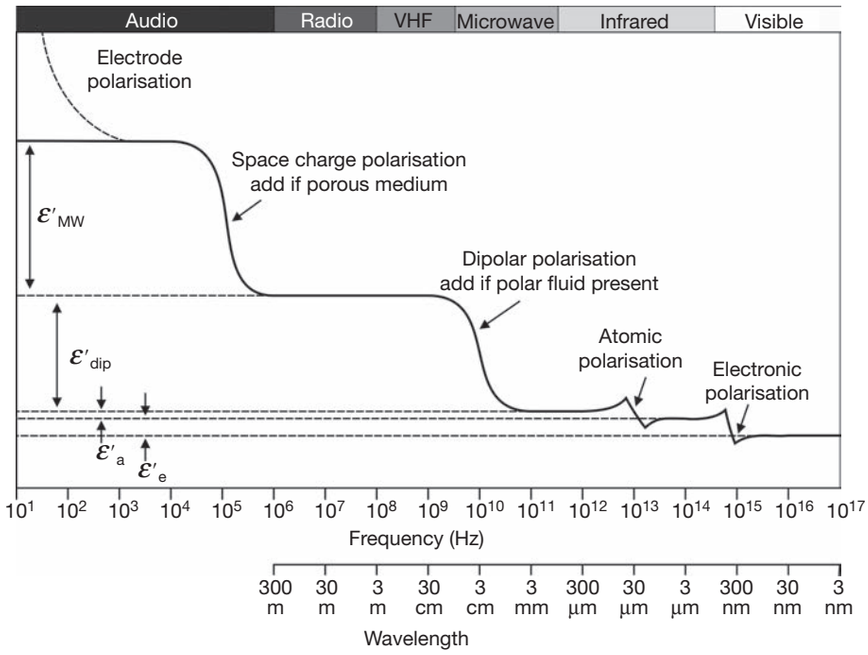

Figure 16 Dielectric polarization processes (e.g., Izgorodina et al., 2009). The dashed line shows where electrode polarization would manifest itself. This is a measurement artifact and hence shown with a dashed line.

layer or the electrical triple layer (Revil and Florsch, 2010; Revil and Skold, 2011; Schmutz et al., 2010; Skold et al., 2011).

Electron, atomic, dipolar, and interfacial dispersion mechanisms are shown in the classic diagram (Figure 16). Here, the relative size and frequency of each process are shown (e.g., Izgorodina, et al., 2009). At frequencies above about 10^{15} Hz, only electronic polarization (ε'_e) contributes to the permittivity. As frequency reduces to about 10^{12} Hz, atomic polarization (ε'_a) also contributes and is added to the electronic contribution. Further decrease in frequency to radiofrequencies sees dipolar contributions (ε'dip) added to the permittivity, and finally, at low frequencies, we see the addition of interfacial polarization (ε'_{MW}). This diagram implies that the permittivity that one must use in any application should be chosen with care, taking into account the frequency range in which one works.

Figure 16 also shows a fifth process called electrode polarization. This is not a property of the material itself, but represents a technical difficulty in making measurements of the electrical properties of geomaterials. It is shown in the figure as a broken line to indicate that it is an artifact and to show where it would manifest itself if it were present in measurements. It arises from the electrochemical reactions that occur at the surface of the electrodes that transport current into and out of the sample rather than any process in the sample itself. In an electrical measurement on a rock the current is carried by a flow of electrons in the wires of the measurement device and the electrodes, but is carried by ions in the electrolyte which occupies the pores. The transfer of charge occurs at the electrode surface through equations such as

$$e^- + Na^+ \leftrightarrow Na \qquad [55]$$

Here, the electron provided by the electrode reacts with the sodium ion from the solution that has been attracted to the electrode and neutralizes it, thus facilitating electrical flow in the pore fluid. The trouble is that these processes take time to occur causing charge to build up at the electrode surface which repels further charges and reduces current flow. The relaxation time is large compared to the processes mentioned previously. Hence, electrode polarization can be a significant problem for measurements made at frequencies lower than about 200 Hz.

There is now growing evidence that other processes exist at lower frequencies still. These are not shown in Figure 16. Electrochemical polarization can occur in the Stern layer of the electrical double or triple layer that coats the grain surfaces. Leroy et al. (2008) measured a dispersion associated with particle size occurring at about 75 mHz for a random pack of spherical grains of modal grain size 187.5 μm and another dispersion that they associated with the characteristic size of asperities on the surface of their grains (i.e., surface roughness) at about 20 Hz, to which they attributed a characteristic scale of 12 μm. A modeling study by Volkmann and Klitzsch (2010) also showed the presence of a low-frequency dispersion, but at slightly higher frequencies.

The existence of these low-frequency polarization mechanisms shows that it is extremely important to control electrode polarization. Section 11.04.5.7 discusses several methods for reducing or removing electrode polarization from measurements.

11.04.5.3 Dielectric Permittivity Models

Figure 16 only shows the real part of the permittivity. In reality, the permittivity is a complex quantity in the same way as the conductivity and resistivity. It can be written as

$$\tilde{\varepsilon} = \varepsilon' - i\varepsilon'' \qquad [56]$$

The classical model for describing the transition of permittivity due to each of the polarization processes is that of the

Nobel laureate Peter Debye (Debye, 1929), who developed a model for dipolar liquids and a single relaxation time (i.e., one polarization process with a well-defined timescale):

$$\tilde{\varepsilon}(\omega) = \varepsilon_\infty + \frac{\varepsilon_o - \varepsilon_\infty}{1 + i\omega\tau} \quad [57]$$

where ω is the angular frequency ($=2\pi f$ in rad s^{-1}), τ is the relaxation time (s), and ε_o and ε_∞ are the values of permittivity at low and high frequencies with respect to the critical frequency ($\omega_{crit}=\tau^{-1}$). While the Debye model was developed for dipolar polarization, it has also been applied to other polarization mechanisms. Equation [57] can be separated into its real and imaginary parts (Guéguen and Palciauskas, 1994):

$$\varepsilon'(\omega) = \varepsilon_\infty + \frac{\varepsilon_o - \varepsilon_\infty}{1 + \omega^2\tau^2} \quad [58]$$

and

$$\varepsilon''(\omega) = \frac{(\varepsilon_o - \varepsilon_\infty)\omega\tau}{1 + \omega^2\tau^2} \quad [59]$$

The real and imaginary parts of permittivity according to the Debye model are shown in **Figure 17**. The solid blue line shows how the normalized in-phase permittivity varies between 0 and 1. The imaginary part of the permittivity (in red), which describes energy loss, peaks at the critical frequency ($\omega_{crit}=1/\tau$), and almost all of the change occurs within one order of magnitude of the critical frequency. The frequency dependence is also shown in the form of an argand diagram, where the out-of-phase (imaginary) relative permittivity is plotted as a function of the real (in-phase) permittivity. The Debye model plots as a semicircle on an argand diagram, with the center of the circle on the *x*-axis as shown by the reference mark in the figure.

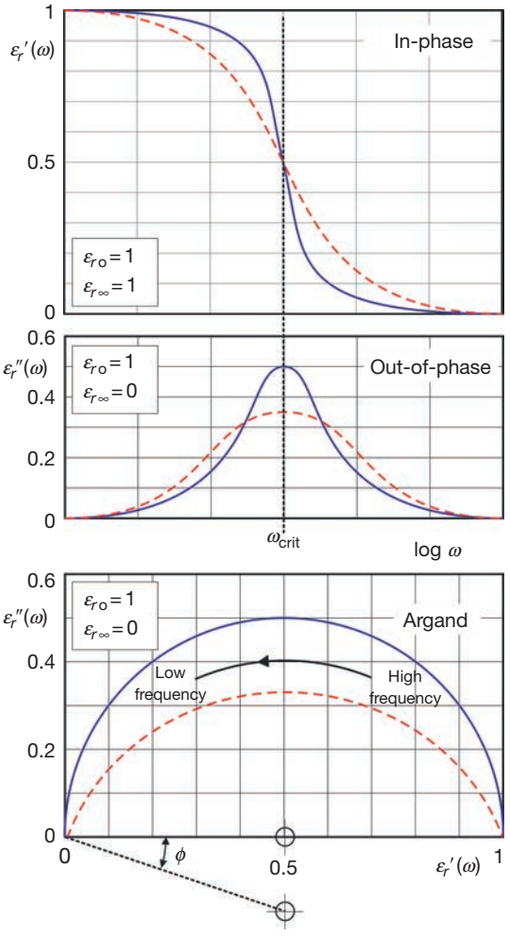

Figure 17 **The** Debye (solid blue) and Cole and Cole (dashed red) dispersion models (here, an arbitrary value of $\alpha=0.22$ has been used).

Sometimes, there is difficulty in understanding this complex model from a physical point of view. At frequencies significantly lower than the critical frequency, the polarization occurs quickly enough for it to always be fully developed. Hence, the permittivity is described fully by the real (in-phase) part of the complex permittivity, and the imaginary part is negligible. At frequencies much higher than the critical frequency for the polarization process, there is insufficient time for the polarization to occur at all. Hence, there is no contribution to permittivity from either the in-phase (real) part of the complex permittivity or the imaginary (out-of-phase) part. In between, there exist frequencies that are about the same as the critical frequency. Polarization process that occurs at these timescales is only partly completed during each cycle of the applied electric potential difference leading to polarization that is out of step with the applied field and generates a nonzero out-of-phase (imaginary) permittivity, which peaks when the applied frequency is the same as the critical frequency.

Although the Debye model has been applied to interfacial polarization, it has been recognized that there is a broader frequency dependence (Chelidze and Guéguen, 1999; Chelidze et al., 1999) for this process. The broader frequency dependence probably arises from there being a spectrum of relaxation times rather than a single relaxation time. It is easy to imagine that a pore structure that is now widely deemed to be fractal (Ruffet et al., 1991a) will have relaxation times associated with interfacial polarization occurring at the different scales of structure exhibited by the pores. A modification of the Debye model by Cole and Cole (1941) takes an ensemble of relaxation times into account:

$$\tilde{\varepsilon}(\omega) = \varepsilon_\infty + \frac{\varepsilon_o - \varepsilon_\infty}{1 + (i\omega\tau)^{1-\alpha}} \quad [60]$$

where α can take values between 0, where it is formally the same as the Debye model, and 1. The angle ϕ (in radians) in **Figure 17** and α are related by $\alpha=2\phi/\pi$ (Glover et al., 1994). The exponent in the Cole and Cole relationship has been related to the fractal dimension of the surface of the grains of the rock by several researchers (see Glover et al., 1994), but none have been sufficiently supported by experimental evidence to be regarded as credible. The fractal dimension, in some of these models, tends towards 2 as the salinity of the pore fluid decreases, which may indicate that the thickness of the EDL has a role to play.

Figure 17 shows the Cole and Cole model as dashed red lines. It can be seen that the in-phase permittivity varies between the same (normalized) endpoints more gradually. The peak in the out-of-phase permittivity is at the critical frequency, but is broader than the Debye model. The Cole and Cole model also plots as a semicircle on an argand diagram, but now, the center of the semicircle is depressed below the *x*-axis. The angle ϕ subtended by the line that joins the center to the orgin ($\varepsilon_r'=0, \varepsilon_r''=0$) is related to the Cole and Cole α parameter. Models that are based

on the approach of Dissado and Hill (1984) have been developed that relate the Cole and Cole parameter to the fractal dimension of the grain/fluid interface (Le Méhauté and Crepy, 1983; Ruffet et al., 1991a,b; Wong, 1987).

In 1951, Davidson and Cole (1951) added a third frequency dependence model, which is usually known as the Cole–Davidson model. The Cole–Davidson model is given by

$$\tilde{\varepsilon}(\omega) = \varepsilon_\infty + \frac{\varepsilon_o - \varepsilon_\infty}{(1 + i\omega\tau)^\beta} \quad [61]$$

where the parameter β varies between 0 and 1. It is rarely fitted to complex electrical rock data because it is asymmetrical, the out-of-phase component falling off more slowly at frequencies above the critical frequency (Lockner and Byerlee, 1985). However, there are some indications that it may be of use in the modeling of frequency-dependent electrokinetic measurements (see **Section 11.04.6.9**).

11.04.5.4 Integrated Conduction and Permittivity

Maxwell recognized that there exist not only electric currents which arise from the transport of charges ($\vec{J}_{\text{cond}} = \sigma\vec{E}$) but also what he called displacement currents ($\vec{J}_{\text{disp}} = \partial\vec{D}/\partial t$), which only exist when the applied electric field varies with time. The total resulting current is the sum of both of these processes:

$$\vec{J}_{\text{total}} = \sigma\vec{E} + \frac{\partial\vec{D}}{\partial t} = \sigma\vec{E} + \varepsilon\frac{\partial\vec{E}}{\partial t} \quad [62]$$

If we consider a harmonically varying field (i.e., $E = E_o e^{i\omega t}$), eqn [62] can be written as

$$\vec{J}_{\text{total}} = (\sigma + i\omega\varepsilon)\vec{E} \quad [63]$$

Then, we can define

$$\vec{J}_{\text{total}} \equiv \sigma_{\text{total}}\vec{E} \equiv \varepsilon_{\text{total}}\frac{\partial\vec{E}}{\partial t} \quad [64]$$

where σ_{total} and $\varepsilon_{\text{total}}$ are the conductivity and permittivity arising from processes involving conduction and displacement currents, and hence,

$$\sigma_{\text{total}} = i\omega\varepsilon_{\text{total}} \quad [65]$$

$$\sigma_{\text{total}} = (\sigma + \omega\varepsilon'') + i\omega\varepsilon' \quad [66]$$

and

$$\varepsilon_{\text{total}} = \varepsilon' - i\left(\frac{\omega\varepsilon'' + \sigma}{\omega}\right) \quad [67]$$

Hence, the complex electrical properties of the rock can be expressed fully either in permittivity space, in conductivity space, or as resistivity, depending upon which is easiest in the given application.

In each of [66] and [67], the term in parentheses describes the dissipation of energy by conduction currents (σ) and displacement currents ($\omega\varepsilon''$). These equations are shown graphically in **Figure 18**. Here, it can be seen that the out-of-phase permittivity that describes energy dissipation has two terms: one for the displacement currents that peaks at the critical frequency and is associated with the interplay between polarization at the critical frequency and the frequency of the applied electric field ε_r'', and one for the conduction currents that increases with decreasing frequency noting that the permittivity is higher for greater salinities ($\sigma/\omega\varepsilon o$). The contribution from the conductivity of the rock is particularly important. If the salinity is increased, the conductivity of the fluid and of the rock increases, with the $\sigma/\omega\varepsilon_o$ contribution at any given frequency increasing. By contrast, decreasing the saturation of the rock, while keeping the salinity of the saturating fluid constant, decreases the $\sigma/\omega\varepsilon_o$ contribution (Knight et al., 1985).

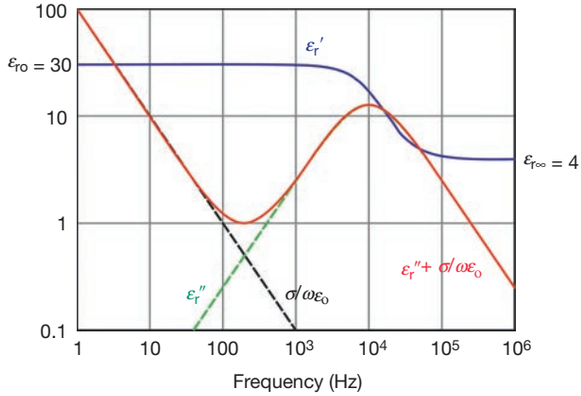

Figure 18 The behavior of the electric permittivity of geomaterials as a function of frequency. The in-phase (real) permittivity is represented by the solid blue curve. The out-of-phase (imaginary) part, which is associated with energy dissipation (solid red curve), is made up of a part related to dissipation due to displacement currents (green dashed line) and due to conduction currents (black dashed lines). In this example, we have taken $\varepsilon_{r\infty} = 4$ as typical as the permittivity for solid minerals and a value of $\varepsilon_{ro} = 30$ to represent the permittivity of a dipolar fluid.

The energy dissipation is characterized by the ratio of the imaginary part of $\varepsilon_{\text{total}}$ to its real part or, equivalently, the real part of σ_{total} to its imaginary part, and this ratio is defined as equal to tan δ, where δ is called the loss tangent. Hence,

$$\frac{\sigma + \omega\varepsilon''}{\omega\varepsilon'} \equiv \tan\delta \quad [68]$$

Large values of tan δ indicate high energy loss from the system.

Equation [68] can be written in the form

$$\tan\delta \equiv \frac{\sigma}{\omega\varepsilon'} + \frac{\varepsilon''}{\varepsilon'} \quad [69]$$

where the first term represents conductive energy loss and the second term represents energy loss associated with relaxation processes. At low frequencies, the conductive energy loss becomes significant if $\sigma/\varepsilon' \gg \omega$. For example, for water with a conductivity of 1 S m^{-1} (which is roughly that of a 0.1 mol l^{-1} solution of NaCl at 20 °C) $\sigma/\varepsilon' \approx 1.4 \times 10^9$ rads^{-1}. If the requirement for conductive losses to begin to be significant is that the parameter σ/ε' is just bigger than ω, which would occur as ω dropped lower than 1.4 Grad s^{-1} (220 MHz). However, the requirement is that the parameter σ/ε' is much greater than ω. Let us suppose that the much greater than symbol requires one parameter to be at least two orders of magnitude greater than the other. This would indicate that conductive losses will be significant for frequencies lower than 14 Mrad s^{-1} (2.2 MHz).

Electrical data may also be given as the magnitude of the complex vector together with the phase angle $\varphi = \tan^{-1}(x''/x')$, where x may be conductivity, resistivity, or permittivity.

11.04.5.5 Mixing Models for Complex Electrical Properties

The dielectric response of a geomaterial that is 100% saturated with a fluid can be considered as a two-component mixture with a matrix dielectric constant (relative permittivity) ε_{rs} and a fluid dielectric constant (relative permittivity) ε_{rf}. In general, both are complex and vary with frequency. However, at the frequencies less than 100 GHz, we can consider the dielectric constant of the matrix and that of gases ε_{rg} and oils ε_{ro} to be wholly real and independent of frequency (i.e., $\varepsilon_{rs} = \varepsilon_{rs}^{'}$, $\varepsilon_{rg} = \varepsilon_{rg}^{'}$, and $\varepsilon_{ro} = \varepsilon_{ro}^{'}$), leaving only the complex dielectric constant of water $\varepsilon_{rw}(\omega) = \varepsilon_{rw}^{'}(\omega) + i\varepsilon_{rw}^{''}(\omega)$. At frequencies below the critical frequency for dipolar relaxation (about 10^{10} Hz), it is possible to assume that the imaginary part of the complex dielectric constant of water is negligible ($\varepsilon_{rw}^{''} \approx 0$), which allows us to write

$$\varepsilon_{rw} = \varepsilon'_{rw}(1 - i\tan\delta_w) \cong \varepsilon'_{rw} - i\frac{\sigma_w}{\varepsilon_o\omega} \qquad [70]$$

Hence, from the point of view of its constituents, the dielectric response of the fully water saturated rock can be fully defined by the three parameters, $\varepsilon_{rs}^{'}$, $\varepsilon_{rw}^{'}$, and σ_w. However, from the point of view of the saturated rock as an ensemble, the dielectric constant at low frequencies can also be written as

$$\widetilde{\varepsilon}_{rr} \equiv \varepsilon'_{rr} - i\frac{\sigma_r}{\varepsilon_o\omega} \qquad [71]$$

where $\varepsilon_{rr}^{'}$ is the effective dielectric constant of the composite medium and σ_r is the effective electrical conductivity of the composite medium. Since both [70] and [71] must be true for the same composite medium, it can be inferred that $\varepsilon_{rr}^{'}$ and σ_r depend on the four parameters, ω, $\varepsilon_{rs}^{'}$, $\varepsilon_{rw}^{'}$, and σ_w.

Scaling arguments (Guéguen and Palciauskas, 1994) imply that the ratio $\widetilde{\varepsilon}_{rr}/\widetilde{\varepsilon}_{rs}$ depends only on the ratio $\widetilde{\varepsilon}_{rw}/\widetilde{\varepsilon}_{rs}$ and the volume fractions of the two phases

$$\frac{\widetilde{\varepsilon}_{rr}}{\widetilde{\varepsilon}_{rs}} = f\left(\frac{\widetilde{\varepsilon}_{rw}}{\widetilde{\varepsilon}_{rs}}, \phi\right) \qquad [72]$$

with

$$\frac{\widetilde{\varepsilon}_{rw}}{\widetilde{\varepsilon}_{rs}} = \frac{\varepsilon'_{rw}}{\varepsilon'_{rs}}(1 - i\tan\delta_w) \quad \text{and} \quad \tan\delta_w = \frac{\sigma_w}{\omega\varepsilon'_{rw}} \qquad [73]$$

The functional form of $f()$ is determined by the rock microstructure.

11.04.5.5.1 The CRIM model

One form of $f()$ was arrived at empirically and is most accurate at very high frequencies (above 100 MHz). This model is called the complete refractive index method (CRIM) and is given by

$$\widetilde{\varepsilon}_r^{1/2} = \widetilde{\varepsilon}_{rw}^{1/2}\,\phi + \widetilde{\varepsilon}_{rs}^{1/2}(1 - \phi) \qquad [74]$$

At such high frequencies, the square root of the dielectric constant is inversely proportional to the phase velocity, which makes [74] a type of time-average equation describing the transmission of an electromagnetic wave through a composite material composed of matrix $(1-\phi)L$ and pore fluid ϕL, where L is the overall length of the sample and ϕ is the porosity.

An interesting feature of the CRIM model is that in the low-frequency limit, where $\omega \to 0$ and $\delta_w \to \pi/2$, it collapses to give $\sigma = \sigma_w\phi^2$, which is Archie's first law with a cementation exponent of 2.

11.04.5.5.2 The Lichtenecker–Rother equation

A more general mixing law that can be applied to permittivities is the empirical Lichtenecker–Rother equation:

$$\widetilde{\varepsilon}_r = \left(\sum_{i=1}^{n} \widetilde{\varepsilon}_{ri}^{1/m}\phi_i\right)^m \qquad [75]$$

where $-1 \le 1/m \le 1$ and each phase has a relative permittivity $\widetilde{\varepsilon}_{ri}$ and a volume fraction ϕ_i. This equation simulates mixing of permittivities between the two extremes where the mixed phases are arranged in series $(1/m = -1)$ to parallel $(1/m = 1)$, with the CRIM model being represented by the value $1/m = 0.5$, that is, $m = 2$. When using this equation, it should be realized that the value of m may change with frequency. When used at high frequencies, in dielectric logging, a polarization factor p for the water phase is often included. In this case, the exponent $1/m$ becomes p/m, but only for the term representing the water phase; the exponents of the terms for the solid and hydrocarbon phases remain $1/m$.

11.04.5.6 Modeling the Frequency-Dependent Electrical Properties of Rocks

There is currently no theoretical model that can predict the frequency-dependent electrical properties of rocks, which contrasts with the models for steady-state conductivity (Archie, 1942; Waxman and Smits, 1968), surface conductivity (Revil and Glover, 1997), zeta potential (Revil et al., 1998), and streaming potential coefficients (Glover et al., 2012a).

The traditional approach has been to match experimental measurements to equivalent electrical circuits composed of capacitors for charge storage and resistors for energy dissipating electrical conduction (e.g., Guéguen and Palciauskas, 1994; Knight et al., 1985; Barsoukov and Macdonald, 2005). Many such equivalent circuits exist, but it is unclear whether any of them help further the understanding of the real physical process occurring in the rock.

Recent theoretical studies have concentrated on characterizing the electrical behavior of geomaterials as macroscopic multicomponent systems over a wide frequency range by combining different influencing polarization mechanisms (e.g., de Lima and Sharma, 1992; Glover et al., 2006b; Leroy and Revil, 2009; Leroy et al., 2008). Often, these models have been compared to experiments that have measured the frequency-dependent electrical properties of glass bead packs. Glover et al. (2006b) combined Debye and Cole and Cole responses for the permittivity of solid grains, pore fluid, and the fixed and diffuse layers of an electrical double layer with a conformable mapping of the Bruggeman–Hanai–Sen effective medium equation (Glover et al., 2010) to predict the frequency response of a pack of glass beads of single size with reasonable results. A much more convincing study was carried out by Leroy et al. (2008) and Leroy and Revil (2009) who used a triple-layer model, and were not only able to model the Maxwell–Wagner response of a bead pack with multiple bead diameters, but were also able to take account of the polarization due to roughness on the bead surfaces (**Figure 19**).

By contrast, Volkmann and Klitzsch (2010) had focused on the microscopic effects that cause the polarization at the scale of single grains or pores. In 1962, Schwarz (1962) studied the dielectric dispersion of spherical particles in an electrolyte

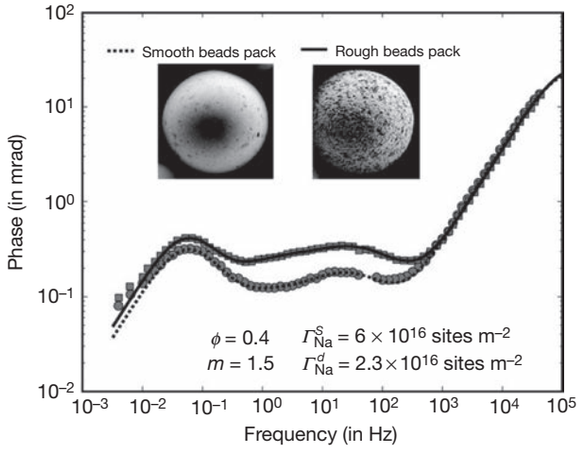

Figure 19 Phase for smooth and rough glass beads (samples 3 and 4) as a function of frequency (from Leroy et al., 2008). The phase is defined here as $\varphi = \tan^{-1}(\sigma''/\sigma')$. The measured porosity is 0.40 and the measured pH is 9.3 for an electrical conductivity of 2.6×10^{-2} S m^{-1}, assuming that $m = 1.5$, with other parameters determined from a TLM model. The modal grain size diameter was 187.5 μm. Symbols: experiment. Lines: model. The left-hand peak is defined by polarization of the triple layer and the size of the beads, the middle peak, by the surface roughness and the right-hand increase by the Maxwell–Wagner effect.

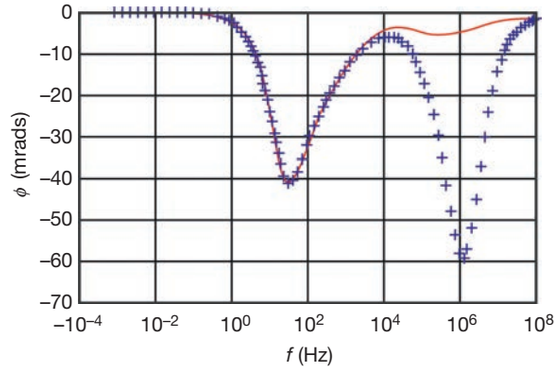

Figure 20 Phase spectrum (dependence of the resistivity phase ϕ_ρ on the frequency f) of a pore model with electrolyte concentration $C_f = 1$ mol m^{-3}, radius of large pore $R_{large} = 1.4 \times 10^{-7}$ m, radius of small pore R_{small} 1.4×10^{-8} m, length of large pore $L_{large} = 10$ μm, and length of small pore $L_{small} = 0.01$ μm; model results without space charges (red solid line) and with space charges allowed (blue crosses). Modified from Volkmann J and Klitzsch N (2010) Frequency-dependent electric properties of microscale rock models for frequencies from one millihertz to ten kilohertz. *Vadose Zone Journal* 9: 858–870, http://dx.doi.org/10.2136/vzj2009.0162.

solution and found a Debye-type electrical dispersion with a relaxation time τ that depends on the radius of the particle R:

$$\tau = \frac{R^2}{2\mu_m kT} \quad [76]$$

where μ_m is the mechanical surface mobility (in s kg^{-1}) of the counterions. If one makes an analogy with rocks, one might say that dispersion processes that occur at a small scale are associated with small relaxation times (i.e., high frequencies) because the spatial influence of a process depends upon the duration of the perturbation for any given mobility and vice versa.

In 1959, Marshall and Madden (1959) developed 'membrane polarization' as a mechanism for describing the mechanism of space charge polarization in geomaterials. Their one-dimensional model consisted of a pore system of alternating 'active' and 'passive' zones. The 'active' zones represent pore throat passages and are characterized by a reduced anion transport number. As these active zones block anions, they behave as ion-selective membranes. For small excess electrolyte concentrations and electric fields, Marshall and Madden (1959) solved the dependence of the complex impedance as a function of the angular frequency and discovered that the relaxation time is related approximately to the square of the length of the active and passive pores. An improvement in the model by Titov et al. (2002) reduced the width and length of the active zones compared to the passive pores and found that the resulting relaxation time is related to the square of the length of the short narrow active zones. Hence, all three theories suggest a quadratic dependence of relaxation time on some geometric length scale of the porous medium, such as pore throat size, grain size, or pore size. This is analogous to the case for fluid permeability (Walker and Glover, 2010) and poses the question whether there is a direct relationship between the relaxation time(s) for electrical dispersion in a geomaterial and its fluid permeability. The prediction that relaxation times are quadratically related to some geometric length scale has been confirmed qualitatively by some experimental data. For example, Kruschwitz (2007) found an exponent of 2.1 for the dependence of the Cole–Cole relaxation time τ_{cc} on the dominant pore throat diameter. Unfortunately, there are plenty of other experimental data that indicate the exponent may be as low as 1.04 (Binley et al., 2005, 2010) to about 3 (Kruschwitz et al., 2010) or even take a logarithmic form in place of a power law (Scott and Barker, 2003, 2005; Titov et al., 2010).

Volkmann and Klitzsch (2010) also noted that there is some evidence for a relationship with the conductivity of the pore fluid. In order to improve the modeling of the membrane polarization approach, Volkmann and Klitzsch (2010) implemented it in three different geometric models and included an electrical double layer. Their finite element modeling showed there are two dispersion mechanisms at work: one associated with a phase angle minimum at a high frequency (approximately 10^5–10^7 Hz) and one at lower frequencies (10^{-3}–10^4 Hz) as shown in **Figure 20**. The high-frequency minimum is associated with the charge buildup at the interface between materials with different electrical properties. This process is known as the Maxwell–Wagner polarization and is described by MWBH theory, which is named after Maxwell (1873), Wagner (1914), Bruggeman (1935), and Hanai (1960). Volkmann and Klitzsch (2010) demonstrated that the high-frequency minimum arose from separation of interfacial space charges by imposing electroneutrality in their model, which removed the space charges and which also caused the high-frequency minimum to be almost completely removed, as shown in **Figure 20**. Imposition of electroneutrality did not affect the low-frequency minimum. Volkmann and Klitzsch (2010) attributed this minimum to a 'diffusion current effect'. Its relationship, if any, to the electrochemical Stern

layer polarizations studied by Leroy et al. (2008) is not currently clear.

The results of the Volkmann and Klitzsch (2010) model are many and varied. However, the main ones are as follows:

- The only significant geometric length scale to affect the frequency of the low-frequency minimum is the size of pores that are interconnected by narrow pore throats in the direction of current flow.
- The frequency is related to that length scale by a power law with an exponent of either -1.7 or -1.8 depending on the model used (i.e., an exponent of +1.7 and +1.8 relating relaxation time to the geometric length scale).
- There is no relationship between the frequency of the minimum and any other geometric property of the model such as pore throat size and length, such that the characteristic frequency of the process is solely controlled by the size of the pores of the geomaterial in the direction of current flow.
- The phase magnitude of the characteristic frequency is inversely related to the concentration of the pore fluid.

The works of both Leroy et al. (2008) and Volkmann and Klitzsch (2010) involve measurement and modeling of electrical dispersion processes at frequencies less than 200 Hz and sometimes significantly lower. It is becoming clear, therefore, that the control or elimination of electrode polarization in experimental measurements is critical if physical processes occurring in geomaterials are not to be overwhelmed and missed.

Meanwhile, there has also been significant progress in understanding electrical dispersion in colloids, which also have an electrical double layer (Grosse, 2010, 2012). A thorough review is given in Grosse and Delgado (2010).

11.04.5.7 Measurement of Frequency-Dependent Electrical Properties

The measurement of complex conductance, admittance, or permittivity of a geomaterial is usually carried out by impedance spectroscopy. Good treatments of this measurement technique are available (e.g., Lasia, 1999; Barsoukov and Macdonald, 2005; Orazem and Tribollet, 2011; Kanoun, 2012; Macdonald and Kenan, 1987). Measurements are carried out with commercial impedance spectrometers that range from the relatively cheap to the extremely expensive depending on the required specifications, the most important of which is usually the frequency range. However, cheaper but high-quality logging boards that sit inside the logging computer are a relatively recent, attractive alternative. The measurements are complicated by a number of technical issues such as electrode polarization, ground loops, and stray capacitances.

The problem of electrode polarization (**Figure 16**) can be neglected in rocks above about 1 kHz. For frequencies lower than this, it can be removed completely by using four electrodes. In this arrangement, the measurement of the potential difference across the sample is carried out across the inner pair of electrodes. Since these electrodes carry a negligible current, they do not polarize significantly. All polarization occurs at the outer current electrodes, but since it is not necessary to measure the potential between these two electrodes, their polarization is not important. Sometimes, it can be difficult to incorporate four electrodes into a measurement setup, in a triaxial rig, for example. In this case, a two-electrode system using blacked platinum gauze electrodes has been used successfully (Glover et al., 1994). This paper also describes how blacked platinum electrodes are prepared. In this case, the platinum gauze is electrodeposited with a dendritic coating of amorphous platinum that has a surface area much larger than that of the original platinum gauze. The larger area facilitates the charge transfer equations such as [49], which reduces polarization. Another method is to use an electrode that will not polarize such as an Ag/AgCl electrode (Guichet et al., 2003; Tardif et al., 2011). These electrodes are useful for ambient measurements, but are usually too delicate to be incorporated in cells designed to work at elevated stresses or temperatures.

Careful note should be taken of how the impedance spectrometer is connected to the sample in order to ensure that there are no ground loops or stray capacitances and that electrical noise is minimized. The latter is usually carried out by ensuring that all leads are coaxial and that all coaxial leads are matched to the impedance of the measuring device.

11.04.5.8 Dielectric Properties of Pore Fluids

All gases and crude oils have very low relative permittivity values at all frequencies (less than 2.5), while air is 1.0006 (Lide, 2012). Their permittivities are defined solely by the electronic contribution to polarization.

Aqueous pore fluids, however, have a significant permittivity that is a function of frequency, temperature, and salinity. Water is an extremely polar molecule that follows a Debye frequency dependence with a relaxation time of about 10^{-10} s. At frequencies below the critical frequency, the permittivity depends significantly on temperature and salinity. Higher temperatures reduce the permittivity because thermal agitation opposes the alignment of polar molecules, while the onset of freezing also reduces the permittivity considerably again because polar molecules cannot align themselves in the solid ice. The addition of any solute also reduces the permittivity, but the effect is small. Pure water has a relative permittivity of about 80 (78.36 at 0 Hz and 25 °C (Archer and Wang, 1990)). A table of the complex relative dielectric constants for water in the frequency range 0–50 GHz and temperatures from 0 to 50 °C from Archer and Wang (1990) can also be found in the CRC Handbook of Chemistry and Physics (Lide, 2012). Ice has a typical relative permittivity of 3.1.

A useful low-frequency ($<10^8$ Hz) empirical equation for the relative permittivity of water is given by Olhoeft (Revil et al., 1999b):

$$\varepsilon_r(T, C_f) = a_0 + a_1 T + a_2 T^2 + a_3 T^3 + c_1 C_f + c_2 C_f^2 + c_3 C_f^3 \qquad [77]$$

where $a_o = 295.68$, $a_1 = -1.2283\ \mathrm{K}^{-1}$, $a_2 = 2.094 \times 10^{-3}\ \mathrm{K}^{-2}$, $a_3 = -1.41 \times 10^{-6}\ \mathrm{K}^{-3}$, $c_1 = -13.00\ \mathrm{dm^3\ mol^{-1}}$, $c_2 = 1.065\ (\mathrm{dm^3\ mol^{-1}})^2$, $c_3 = -0.03006\ (\mathrm{dm^3\ mol^{-1}})^3$, T is in kelvin and the equation is valid in the range from 273 K to 373 K, and C_f is the salinity of the bulk pore fluid in mol $\mathrm{l^{-1}}$.

Malmberg and Maryott (1956) provided another empirical equation, but for pure water. Their relationship can be written as $\varepsilon_r(T) = 87.740 - 0.40008T + 9.398 \times 10^{-4}T^2 - 1.410 \times 10^{-6}T^3$, where the temperature is in °C.

11.04.5.9 Dielectric Properties of Minerals and Near-Surface Rocks

11.04.5.9.1 Minerals

The relative dielectric permittivities of most common rock-forming minerals occupy the range 4–10. Since these values are small compared to the dielectric constant of water (about 80) at surface temperatures and pressures, and for frequencies below about 1 GHz, there is little difference in dielectric response between rocks with a quartz, calcite, or dolomite matrix. Additionally, accessory minerals do not normally affect the dielectric response of a rock unless the mineral has a particularly high relative dielectric permittivity (e.g., rutile or pyrite) and the mineral is present in a significant volume fraction. Table 5 shows the relative dielectric permittivities of some of the most common minerals.

11.04.5.9.2 Rocks

Dipolar and interfacial or Maxwell–Wagner polarizations have a much bigger effect on the complex permittivity of porous and fractured rocks than the electronic and atomic polarizations that arise from the minerals they contain. Hence, one would expect the complex electrical properties of rocks to be much more sensitive to changes in pore structure and the saturation of that pore structure with water than to changes in matrix mineralogy.

Effect of pore structure. The dielectric response of geomaterials at frequencies below 1 MHz is related to the amount of water-wetted solid surface present (Li et al., 2001). Increasing the surface area to bulk volume ratio of a geomaterial increases the dielectric response, while treatment of water-wet rock surfaces to make them hydrophobic (Knight and Abad, 1995) removes the dielectric response associated with the development of bound-water layers. In fact, the out-of-phase conductivity σ'' is only a function of the interfacial properties of the interconnected pore surface area. There now exists a substantial volume of literature demonstrating a power-law dependence of σ'' on Spor, the surface area to pore volume ratio (Börner and Schön, 1991; Börner et al., 1996; Knight and Nur, 1987b; Schön, 2004; Slater and Lesmes, 2002; Slater et al., 2006) as shown in Figure 21.

Effect of water saturation. Measurements of the dielectric constant of whole or powdered dry rocks show little frequency dependence in the range 10^{-3}–10^{6} Hz (Knight and Nur, 1984, 1987a). Lack of a polar fluid ensures that there is no dielectric polarization and no interfacial polarization can be developed. By comparison, water-saturated rocks have a strongly frequency-dependent dielectric constant that decreases with frequency. Knight and Nur (1984) identified two different frequency regions that have different power-law frequency dependencies. In the high-frequency region (above 10 kHz up to their experimental maximum frequency of 13 MHz), the dielectric constant increased very quickly at low saturations, followed by a more gradual linear increase at medium to high saturations that can be explained by the greater water fraction alone. Knight and Nur (1987a,b) ascribed the strong increases at low saturations to the roles of bound and free water, which has been confirmed by more recent work (Jones and Or, 2002). The situation is further complicated by differences between imbibition and drainage behaviors that result in different microscopic fluid distributions. Despite the apparent complexity, Knight and Endres (1990) and Endres and Knight (1992) were successful in modeling the experimental data. Ulrich and Slater (2004) carried out experimental induced polarization measurements on rocks as a function of water saturation and concluded that IP parameters are a function of saturation for fluid distribution and saturation history.

Biological processes. Recent work has shown that a range of biochemical processes such as those associated with the breakdown of ethanol (Personna et al., 2013a,b) and other organic compounds and the biomediated precipitation of metal sulfides (Placencia-Gómez et al., 2013; Zhang et al., 2013) and

Table 5 Relative dielectric permittivity of various common minerals (after a compilation by Schön (2004) of data from Dortman (1976), Keller (1989), Olhoeft (1981), and Parkhomenko (1965))

Mineral	ε_r	*Mineral*	ε_r
Quartz	4.19–5	Apatite	7.4–11.7
Forsterite, fayalite	6.8	Calcite	6.35–8.7
Olivines	6.8	Dolomite	6.3–8.2
Sillimanite	11	Aragonite	7.4–8.67
Amphiboles, hornblende	4.9–8	Anhydrite	5.7–6.7
Graphite	>81	Barite	7–12.2
Hematite	25	Gypsum	5–11.5
Magnetite	34–81	Muscovite	6.2–8
Rutile	79–173	Biotite	6.2–9.3
Pyrite	34–81	Chlorite	9
Galena	17–81	Illite	10
Sphalerite	6.9–12.1	Kaolinite	9.1–11.8
Halite	5.7–6.2	Feldspar	
Sylvite	4.4–6.2	Microcline	5.48–5.6
Fluorite	6.2–8.5	Orthoclase	4.5–6.2
Anorthite	6.9–7.24	Oligoclase	6.06
Labradorite	5.8–5.87	Albite	5.3–6.95

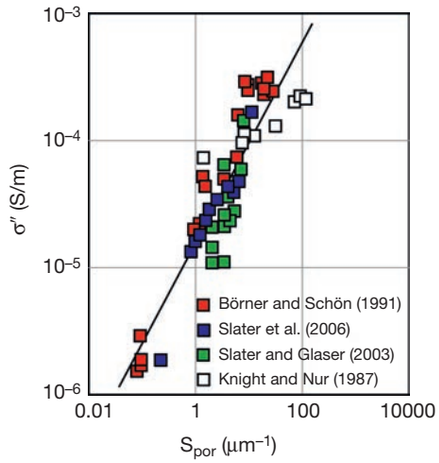

Figure 21 Observed power-law relationship between σ'' and S_{por}. Data from Knight and Nur (1987a,b) and Börner and Schön (1991) are sandstones, data from Slater and Glaser (2003) are alluvial unconsolidated sediments, and data from Slater et al. (2006) are artificial kaolinite–sand mixtures. Figure redrawn after Slater (2007). The linear regression is $\sigma''=S_{por}^{0.8}$ ($R^2=0.82$).

calcite can produce electrical dispersions with characteristic frequencies often in the low-frequency range (Personna et al., 2008; Zhang et al., 2010, 2012). This work shows the ability of impedance spectroscopy and spectral-induced polarization measurements to monitor the formation of ionic species in groundwater, during bioremediation (Kemna et al., 2012; Mewafy et al., 2013).

Effect of pH. In recent studies, Revil and his colleagues have argued for a dominating role of the Stern layer polarization below 1 kHz in sands and glass beads (Revil and Florsch, 2010; Schmutz et al., 2010; Vaudelet et al., 2011) with counterions like weakly sorbed sodium (sites >Si−O−Na+, where > represents the crystalline framework) being mobile along the mineral surface. Skold et al. (2011) studied the induced polarization as a function of pH both experimentally and by modeling. Their results showed that another polarization mechanism may exist that is associated with a hopping process of the protons along the mineral surface (a so-called Grotthuss cooperation mechanism). Consequently, low-frequency dispersion seems to have many possible contributors associated with the rock fluid interface and the rock microstructure.

Effect of pore fluid salinity and cation type. There is, as expected, a linear relationship between the conductivity of the pore fluid and the real component of electrical conductivity (σ') of the saturated rocks (e.g., Weller et al., 2011). By contrast, the imaginary component (σ'') exhibits a steeper increase at lower salinities that flattens at higher salinities. Weller et al. (2011) also found that sodium cations result in larger values of σ'' than calcium cations in solutions of equal concentration.

In 2011 Revil and Skold (2011) published the results of a combined analytical and experimental study of the salinity dependence of spectral induced polarization in sands and sandstones. They demonstrated analytically that the polarization of the inner part of the electrical triple layer coating the surface of the grains, which is usually called the Stern layer, was consistent with available data. Their model showed the both the specific surface conductivity of the Stern layer and the quadrature conductivity of the porous material depend on the conductivity of the poor water. Once again processes happening very close to the surface of the minerals, that is, in the Stern layer are extremely important to the charge storage properties, and hence frequency-dependent electrical flow in saturated rocks.

Recently, there has been a resurgence in the examination of the effects of the sorption of ions by saturated sands and the consequent effect on induced polarization (Vaudelet et al., 2011a,b). These studies recognize that polarization occurs at frequencies less than a hundred hertz, the most important of which is caused by processes occurring in the electrical double layer, and in the Stern layer in particular. These studies also show that particular cations, zinc and lead for example, can have a large effect on the induced polarization phase angle.

Effect of oil. Since the dielectric constants of gas and oil (about 1 and 2.2, respectively) are so much lower than that of water, dielectric measurements have often been used to monitor the relative saturations of hydrocarbon or water in geomaterials. For example, Vanhala (1997) used induced polarization to map oil-contaminated sand and till. However, the presence of oil in an otherwise water-wet porous rock has been found to have little effect on the frequency dependence of the dielectric response of clean water-wet sand with a relatively low internal surface area ($0.2\ m^2\ g^{-1}$) but has produced decreases as high as 50% for kaolinite, which had considerably larger internal surface area ($5–12\ m^2\ g^{-1}$) (Li et al., 2001). They concluded from their experimental study that the presence of oil leads to a detectable change in the dielectric properties of high-surface-area geomaterials. Recent studies (Schmutz et al., 2010), using the Revil and Florsch (2010) model and applying it to a partially saturated rock found that it was possible to obtain a clear peak at very low frequencies that was associated with the polarization of the Stern layer.

11.04.6 Electrokinetic Properties

Streaming potentials and electroosmosis are examples of coupled properties that link the passage of fluid and electrical flow in reservoir rocks (Jouniaux and Ishido, 2012). These phenomena occur over a wide range of spatial and temporal scales in all porous media that contain ionic fluids (e.g., Figure 2 of Guichet et al. (2003)).

11.04.6.1 Streaming Potentials

One of the fundamental electrokinetic properties is the streaming potential, which is the electric potential that develops when an aqueous fluid flows through a rock. The effect is characterized by a streaming potential coupling coefficient C_s (which is sometimes called the streaming potential coefficient). The streaming potential coefficient is the streaming potential ΔV generated (in V or mV) per difference in fluid pressure ΔP driving the flow (usually in MPa), that is, $C_s = \Delta V/\Delta P$.

Since it is the flow that separates the charge in the porous medium, it has been argued that a better measure may be the streaming potential per flow rate Q, which we call the streaming potential flow coefficient $C_{sv} = \Delta V/Q$ (and then use streaming potential pressure coefficient C_{sp} in place of streaming potential coupling coefficient). While the distinction is not very useful for steady-state conditions, it becomes important for frequency-dependent measurements where the relationship between flow rate and fluid pressure difference also depends upon frequency (see **Chapter 11.02**) and hence allows frequency-dependent processes due to the dynamic flow and the subsequent electrokinetic coupling to be separated.

The mechanism that generates streaming potential arises in the diffuse layer of the electrical double or triple layer (**Section 11.04.4.1**). When fluid flows in the pores of a geomaterial, there exists an interface between the mobile fluid in the body of the pores and that which remains linked to the surface. The interface is called the shear plane. In general, the shear plane occurs in the diffuse layer.

The electric potential on the shear plane is called the zeta potential ζ (in V), which is a parameter of fundamental importance in the theory of electrokinetics. Since, for most rocks, fluid salinities, and compositions, the diffuse layer contains more cations than anions, movement of the electrically neutral bulk pore fluid and a part of the positively charged diffuse layer will cause a positive charge to build up, and so a positive electrical streaming potential is developed in the direction of flow, that is, in the opposite direction to the fluid pressure gradient. Hence, the streaming potential coefficient is generally negative, providing the net charge on the mineral surface is negative.

The streaming potential induces a secondary current in the opposite direction, which is called the streaming current. We have seen [48] that the thickness of the double layer depends upon fluid salinity. However, salinity does not greatly affect the viscosity of the pore fluid. The result is that lower-salinity fluids have wider diffuse layers, but the position of the shear plane hardly moves, ensuring that the separation of charge is more efficient and streaming potentials are greater.

It is generally considered (Wall, 2010) that the first person to carry out experiments involving electroosmosis and electrophoresis was Reuβ (1809), which was followed in 1859 by the first measurement of a streaming potential by Georg Hermann Quincke (Quincke, 1859). Some 20 years later, in 1879, Helmholtz developed a mathematical expression for the effect (Helmholtz, 1879), which was improved by Smoluchowski in 1903 (Smoluchowski, 1903). In the following years, the phenomenon was studied by a number of researchers, including Clark in 1877, Saxen in 1892, and Bikerman in 1932.

11.04.6.2 Electroosmosis

Electroosmosis is the movement of liquid induced by an applied electric potential across a porous material, capillary tube, membrane, microchannel, or any other fluid conduit. Because electroosmotic velocities are independent of conduit size, as long as the double layer is much smaller than the characteristic length scale of the channel, electroosmotic flow is most significant when in small channels. Although the effect is only of the order of a few millimeters per second, it has been used effectively for remediation of pollutants, dewatering, and chemical separation.

The process is formally the opposite of that that gives rise to streaming potentials. The applied electric potential difference acts upon that part of the charged diffuse layer that is mobile, leading to a gross fluid volume flow. Electroosmotic flow was reported first in 1809 by the Russian imperial scientist Ferdinand Friedrich von Reuβ (Reuβ, 1809), who made water to flow through a plug of clay by applying an electric voltage. Although Reuβ studied electrokinetic properties in detail, much was lost to fire in 1812 during Napoleon's occupation of Moscow.

11.04.6.3 Seismoelectrics

Since fluid can be made to flow through rocks locally by the passage of elastic waves, we may also consider that a seismic wavelet may also create an electrical streaming potential. This effect, sometimes called the seismoelectric effect, has components that arise during the passage of the wavelet through the body of the rock and at the interface between rocks of two different properties. The heart of the seismoelectric effect is the coupling between Biot's equation and Maxwell's equations, which was made by Pride (1994) and which is key to the development of the new electroseismic exploration technique (Glover and Jackson, 2010). In this technique, a layered Earth is perturbed with a seismic pulse; then, the resulting electric signals are measured as a function of offset (e.g., Haines et al., 2007; Thompson and Gist, 1993). This method has recently been used to image the vadose zone of a sand aquifer successfully (Dupuis et al., 2007).

11.04.6.4 The Helmholtz–Smoluchowski Equation in the Steady State

The most common approach to modeling the streaming potential is called the Helmholtz–Smoluchowski (HS) equation (e.g., Overbeek, 1952; Hunter, 1981; Maineult et al., 2004; Saunders et al., 2008), which was developed for bundles of capillary tubes. In its simplest form, it is given by

$$C_{sp} = \frac{\Delta V}{\Delta P} = \frac{\varepsilon_r \varepsilon_o \zeta}{\eta_f \sigma_f^*} \quad [78]$$

where the streaming potential C_{sp} (in V m^{-1}) is the ratio of the measured streaming potential ΔV (in V) to the applied fluid pressure difference ΔP (in Pa) that drives the fluid through the capillary tube. This value depends upon the electric permittivity of the pore fluid $\varepsilon_f = \varepsilon_r \varepsilon_o$ (in F m^{-1}), where ε_r is the relative permittivity of the pore fluid (unitless), ε_o the electric permittivity of free space ($\approx 8.854 \times 10^{-12}$ F m^{-1}), η_f the dynamic viscosity of the pore fluid (in Pa s), σ_f^* the pore fluid electrical conductivity (in S m^{-1}), and ζ the zeta potential (in V). The zeta potential is the electric potential on the shear plane when a part of the diffuse layer is transported by fluid flow.

Equation [78] is commonly applied to porous media including rocks even though it has never been validated for them since there exists no independent method for measuring the zeta potential for complex porous media. The fluid conductivity in eqn [78] has contributions from the bulk fluid and surface conduction. This arises from the derivation of the HS equation. In the derivation, the current caused by ionic transport by advection (i.e., fluid movement) is balanced by a countercurrent, which is conductive. The countercurrent occurs by all conduction mechanisms, which includes conduction through the bulk pore fluid and surface conduction, and would even include conduction through the rock matrix if it were not electrically insulating. Hence, the pore fluid conductivity term in eqn [78] should include a contribution to account for conduction through the bulk fluid and a contribution to account for the surface conduction.

The surface conduction depends on both the surface conductance and the microstructural properties of the rock (porosity, cementation exponent, grain size, etc.) as discussed in detail in Glover and Déry (2010). Consequently, eqn [78] can be rewritten as (Morgan et al., 1989)

$$C_{sp} = \frac{\Delta V}{\Delta P} = \frac{\varepsilon_r \varepsilon_o \zeta}{\eta_f \left(\sigma_f + \frac{2\Sigma_s}{\Lambda} \right)} \quad [79]$$

where Σ_s is the specific surface conductance (in S) and Λ is a length scale that is characteristic of the pore microstructure (in m) that was introduced by Johnson et al. (1986). This equation implies that the streaming potential coefficient depends on pore size (and consequently grain size and pore throat size) (see **Section 11.04.6.6**). Examination of this implication has led to a model for calculating the zeta potential and streaming potential coefficient for rocks (see **Section 11.04.6.7**).

11.04.6.5 Calculating Zeta Potentials from Experimental Measurements

Equation [78] can be used to derive zeta potentials from experimentally derived streaming potential coefficient data. The pore fluid permittivity can be either measured experimentally or obtained using the empirical relationship given as eqn [77]. The pore fluid viscosity can be measured experimentally or obtained using the empirical relationship developed by Phillips et al. (1978). The pore fluid conductivity must account for any surface conduction that is present. Consequently, eqn [78] is rearranged for the zeta potential with an additional factor to convert the bulk pore fluid conductivity into that that also takes account of the surface conduction. The relevant equation is

$$\zeta = \frac{C_{sp}\eta_f}{\varepsilon_r \varepsilon_o} \frac{\sigma_f F_{HS}}{F(C_f)} \quad [80]$$

where the formation factor F is defined as the ratio of the electrical conductivity of the fluid to that of the fluid-saturated rock, F_{HS} is the formation factor of the sample at high salinity (where the surface conduction is insignificant compared to conduction through the bulk fluid), $F(C_f)$ is the formation factor of the sample of each pore fluid concentration C_f (where there may be a significant contribution of surface conduction to the total fluid conductivity), η_f is the viscosity of the pore fluid, ε_f is the permittivity of the pore fluid, σ_f is the electrical conductivity of the pore fluid, ζ is the zeta potential, and C_{sp} is the measured streaming potential coefficient. The ratio of the two formation factors is termed the Overbeek correction (Overbeek, 1952).

It has also been noted that many streaming potential coefficient data have a quasilinear relationship if the pH is constant and the salinity is not greater than about 1 mol l^{-1} (Jouniaux and Ishido, 2012; Allègre et al. 2010, 2011). A linear fitting gives $C_{sp} = -1.2 \times 10^{-8}/\sigma_f$, which implies a constant zeta potential of about -17 mV (Jouniaux and Ishido, 2012). Recent high-quality measurements where the pH of the pore fluids has been well controlled and for pore fluid salinities from 10^{-5} mol l^{-1} to 6 mol l^{-1} have, however, shown the zeta potential not to be constant, as discussed later.

11.04.6.6 Grain, Pore, and Pore Throat Sizes and Streaming Potential

Equation [79] implies that the streaming potential coefficient is not independent of pore size but diminishes as the characteristic pore scale diminishes. Characteristic pore scale, pore diameter, grain diameter and pore throat diameter are all related. Pore diameter and grain diameter are related by the theatre transformation (Glover and Walker, 2009), and the pore size is related to the pore throat size using empirical methods (Glover and Déry, 2010). This last reference uses these transformations to restate [79] in terms of pore diameter, grain diameter, and pore throat diameter for spherical grains as well as grains with arbitrary shape. For example, one relationship for spherical grains is

$$C_{sp} = \frac{\Delta V}{\Delta P} = \frac{d\varepsilon_f \zeta}{\eta_f (d\sigma_f + 6\Sigma_s(F-1))} \quad [81]$$

while another, which is applicable to grains of different geometries, is

$$C_{sp} = \frac{\Delta V}{\Delta P} = \frac{d\varepsilon_f \zeta}{\eta_f (d\sigma_f + 4\Sigma_s mF)} \quad [82]$$

Either of these equations can then be used to calculate the streaming coupling coefficient of a rock providing the grain size d (in m), formation factor F, cementation exponent m, and zeta potential (in V) are known. Figure 22 shows the comparison of this model with measurements that were made on random bead packs of different diameters. The dotted line shows the standard HS law, while the grain size models fit the data very well.

11.04.6.7 Streaming Potential and Zeta Potential Models

Equations [81] and [82] and allied equations for pore size and pore throat size may be used to calculate the streaming potential for rocks providing the specific surface conductance and zeta potential can also be modeled. Fortunately, these have been available since Revil and Glover (1997, 1998) and Revil et al. (1999a). Recently, models for all the input parameters to

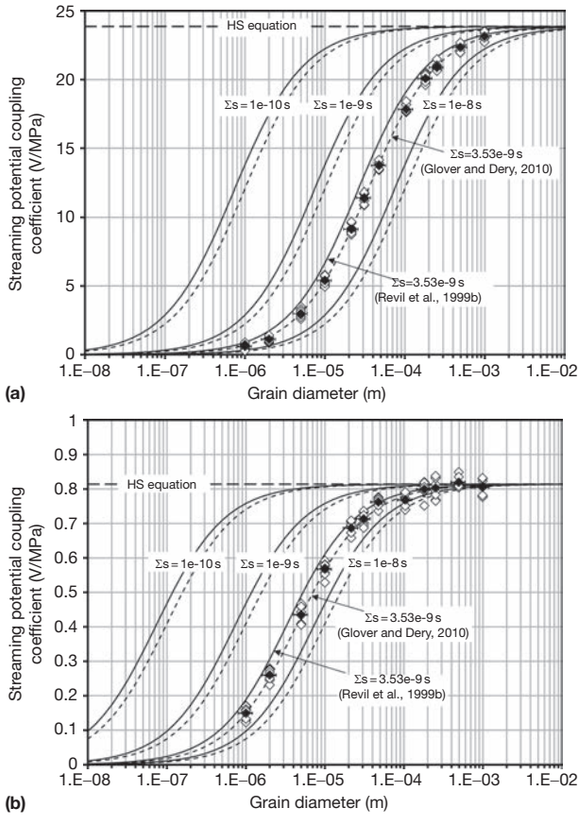

Figure 22 Streaming potential coupling coefficients of a range of quartz glass bead packs as a function of the mean diameter of the glass beads. (a) Pore fluid salinity $C_f = 2 \times 10^{-4}$ mol l^{-1}, (b) pore fluid salinity $C_f = 2 \times 10^{-3}$ mol l^{-1}. The open symbols show the streaming potential coupling coefficient measurements for individual flow rates at a given grain size, which indicates their uncertainty. The solid symbols show the mean value. The horizontal error bar shows the effective standard deviation of the laser diffraction bead size measurements. The solid line shows the model of Revil et al. (1999b) and the dashed line represents that of Glover et al. (2006a,b). Modified from Figure 5 of Glover PWJ and Déry N (2010) Dependence of streaming potential on grain diameter and pore radius for quartz glass beads. *Geophysics* 75: F225–241, http://dx.doi.org/10.1190/1.3509465.

[81] and [82] have been brought together in the first approach that is capable of modeling the streaming potential coefficient of individual rock samples and that takes account of its microstructural properties (Glover et al., 2012a).

Glover et al. (2012a) compared their model for the zeta potential and streaming potential coefficient with 269 zeta potential measurements and 290 streaming potential coefficient measurements for 17 matrix–fluid combinations that were taken from 29 experimental studies in the literature. They found a generally good agreement that became very good if accurate microstructural parameters (grain size, formation factor, and cementation factor) were known. **Figure 23** shows their modeled streaming potentials and zeta potentials when compared against the entire streaming potential coefficient and

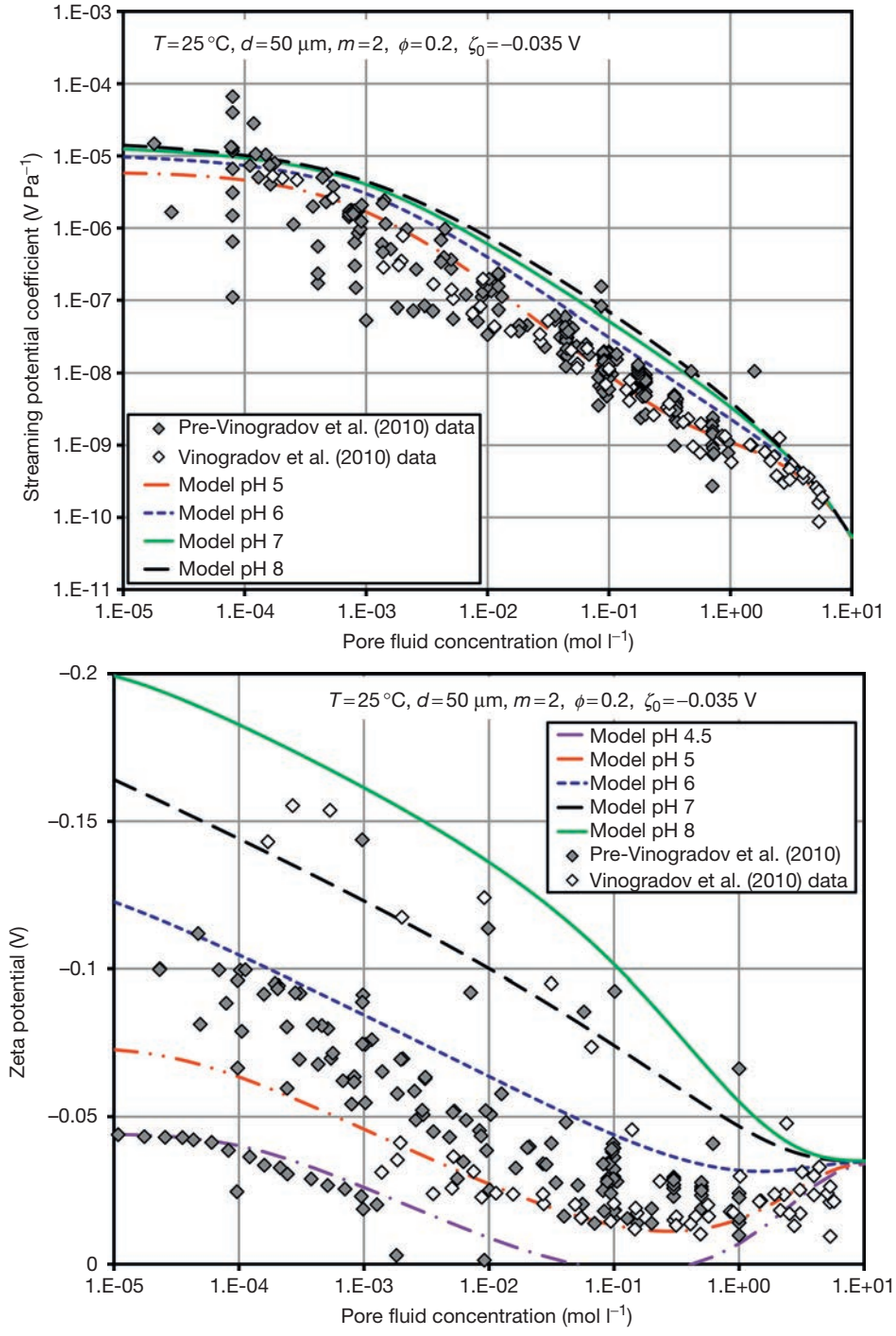

Figure 23 Comparison of the model for streaming potential coefficient (top) and zeta potential (bottom) for a generic rock (grain size = 50 μm, $m = 2$, porosity = 0.2) compared with 290 streaming potential coefficient measurements and 269 zeta potential measurements. Modified from Glover PWJ, Walker E, and Jackson MD (2012) Streaming-potential coefficient of reservoir rock. *Geophysics* 77(2): D17–D43, http://dx.doi.org/10.1190/GEO2011-0364.1.

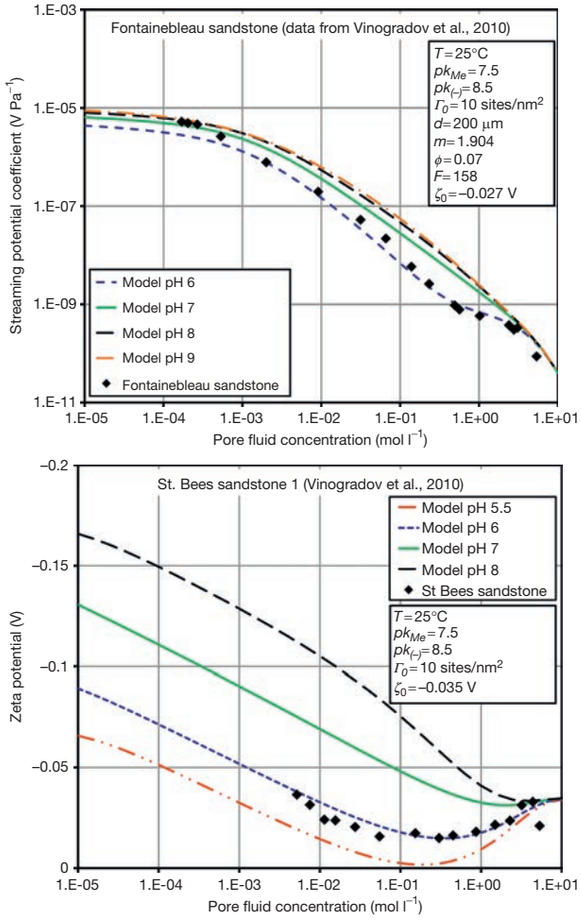

Figure 24 Top: Comparison of the model for the streaming potential coupling coefficient with data measured by Jaafar et al. (2009) for Fontainebleau sandstone (Top) and St. Bees sandstone (Bottom). Modified from Glover PWJ, Walker E, and Jackson MD (2012) Streaming-potential coefficient of reservoir rock. *Geophysics* 77(2): D17–D43, http://dx.doi.org/10.1190/GEO2011-0364.1.

zeta potential experimental datasets, while **Figure 24** shows the theoretical model compared to experimental data from two individual rock samples whose microstructural parameters were well known from independent measurements and were built into the theoretical model so that an individual modeling of each rock sample could be carried out.

It is clear that the model generally follows the trend of all the experimental data for both the streaming potential and the zeta potential, but the fit is much better when individual rock parameters are put into the model.

It is also clear that the pH of the fluid is critical, and since this may change by several points as it becomes equilibrated with the sample, researchers must not only ensure that their measurements take place only after equilibrium of the fluid has been attained but also ensure that the pH (and salinity) is measured on the fluid leaving the sample so that the streaming potential measurements may be attributed to the correct pore fluid salinity and that this salinity is used in the derivation of the zeta potential. The spread in the zeta potential data in **Figure 23** is probably due to variations in the pH of the fluid, and this is being borne out by recent measurements (Walker et al., 2014).

There is much scope for improvement in the model and certain interactions that are not understood. The most important of which is the need to include a zeta potential offset, which is not justified theoretically. However, now that a model exists for calculating the streaming potential coefficient and zeta potentials of rocks, it should be applied routinely to the analysis of all experimental measurements.

11.04.6.8 Factors Affecting the Streaming Potential of Near-Surface Rocks

The model for the steady-state streaming potential coefficient of fully saturated rocks gives us an insight into the many parameters that control electrokinetic conversion in rocks.

The major ones are

- pore fluid salinity and hence conductivity (e.g., Vinogradov et al., 2010; Walker et al., 2014);
- pore fluid pH (e.g., Ishido and Mizutani, 1981);
- grain, pore, or pore throat size (Glover and Déry, 2010);
- formation factor (e.g., Glover and Déry, 2010; Glover et al., 2012a; Walker et al., 2014);
- cementation exponent (Glover and Déry, 2010; Glover et al., 2012a; Walker et al., 2014);
- porosity (Glover and Déry, 2010; Glover et al., 2012a; Walker et al., 2014);
- the ionic mobility of each of the ions solution (Glover et al., 2012a);
- the disassociation constant of water (e.g., Glover et al., 2012a);
- the equilibrium constant for dissolution of CO_2 in water (Glover et al., 2012a; Revil et al., 1999a; Wu et al., 1991);
- the equilibrium constant for the formation of the carbonate ion in water (Glover et al., 2012a; Revil et al., 1999a; Wu et al., 1991);
- the density of sites on the mineral surface (Glover et al., 2012a; Kosmulski, 1996; Revil and Glover, 1997, 1998);
- the binding constant for cation (sodium) adsorption (Glover et al., 2012a; Kosmulski, 1996; Revil and Glover, 1997; 1998; Scales et al., 1990);
- the disassociation constant for dehydrogenization of silanol (Glover et al., 2012a; Kosmulski, 1996; Revil and Glover, 1997, 1998);
- the distance of the shear plane from the mineral surface (Glover et al., 2012a; Revil and Glover, 1997, 1998);
- the size of protonic surface conduction (Glover et al., 2012a; Revil et al., 1999a);
- the ionic stern plane mobility (Revil and Glover, 1998);
- the dielectric constant of the pore fluid (Glover et al., 2012a; Pride and Morgan, 1991; Walker et al., 2014);
- the viscosity of the pore fluid (Glover et al., 2012a; Pride and Morgan, 1991; Walker et al., 2014); and
- temperature (Reppert and Morgan, 2003a,b), which affects many of the parameters mentioned earlier.

The picture becomes even more complex if one considers a partially saturated rock (**Section 11.04.6.9.7**) or

frequency-dependent streaming potential coefficients (Section 11.04.6.10).

Many of these parameters are either well known for aqueous fluids and common minerals or can be calculated using empirical models. The microstructural parameters and surface conduction are only important for low-salinity fluids and cause the flattening that occurs in the streaming potential coefficient at low salinities (see Figures 23 and 24).

11.04.6.9 Electrokinetic Measurements under Steady-State Conditions

11.04.6.9.1 Experimental considerations

The measurement of streaming potentials, streaming currents, and electroosmotic flows is a large subject that it would be difficult to do justice to in this chapter. The most advanced proponents of these measurements include Laurence Jouniaux (e.g., Allègre et al., 2010; Guichet et al., 2006), Phil Reppert (e.g., Reppert and Morgan, 2001, 2003a,b; Sheffer et al., 2007), André Revil (e.g., Crespy et al., 2007), and Tsuneo Ishido (e.g., Jouniaux and Ishido, 2013). I would recommend that anyone who plans to start these measurements communicate with one of them. It is relatively easy to make a measurement, but it is more challenging to make accurate and well-controlled measurements. We have already discussed how the pore fluid must be in equilibrium with the rock sample so that the relevant salinity and pH are known (Walker et al., 2014), and these must be recorded with the ambient temperature for the measurement.

Analysis of the raw data is important for ensuring their accuracy. Many different ways have been tried, but most often, flow is set up at several different flow rates in one or both directions. The streaming potential coefficient is then calculated from the gradient of the resulting streaming potential/pressure difference graph (Reppert and Morgan, 2001). Flow can be induced by pumping, displacement of fluids by bottled gases, or gravity. Recently, there has been some success using a transient method where a gas bottle displacement has been turned on or a constant flow that is driven by gas displacement has been suddenly stopped (Walker et al., 2014). Logging many thousands of electrical and pressure measurements during the minute or so that the pressure takes to build up or die away allows a very accurate fit to the streaming potential/pressure difference curve to be attained. Measuring the tiny streaming potentials with high-salinity fluids (Vinogradov et al., 2010) or as the pore fluid pH approaches the isoelectric point of the mineral surface (Walker, 2012, pers. comm.) presents the greatest technical difficulties. Since the streaming potentials are steady state, the electrodes have to be nonpolarizing.

Fluid flow is not the only thing that causes electric potentials to develop; they can also arise from redox potentials, be due to temperature differences (thermoelectric effect) (Leinov et al., 2010) or chemical gradients (chemoelectric effect) (Maineult et al., 2005). All of these sources of electric potential should be reduced to a minimum within the experimental rig unless they are the subject of the study.

It is also worth pointing out that microbial activity in the pore fluids can lead to spurious potentials that may confuse electrokinetic measurements. Zhang et al. (2010) made measurements of complex conductivity, electrode potential, and self-potential on a column of sand saturated with river water in which microbial activity was altering the sulfide chemistry of the water. Changes in measured potential due to the production of the bisulfate ion HS^- by sulfate-reducing bacteria reached up to -600 mV compared to a control experiment in which there was no microbial activity. Potential changes started about 6 days after the experiment began and continued until its end, about 22 days later. The changes in potential varied with time and position in the saturated sand column. The measurements show that it is extremely important to exclude biogenic effects from electrokinetic measurements as they can critically confuse the measurements. It may be that the extremely variable potentials measured by Allègre et al. (2010, 2012) may have been affected by this biogeoelectric effect. Conversely, the measurement of this effect may, in future, allow us to monitor the production of certain ionic species in geomaterials using geoelectric measurements. Zhang et al. (2010) inverted their measurements to estimate the biogenic production of bisulfide at each point in their sand column during the whole experiment. This opens up the possibility that the progress of bioremediation of oil spills might be monitored using geoelectric measurements or that microbes might be used as oil-field probes.

For further information on the self-potential technique, please see Chapter 11.09.

11.04.6.9.2 Salinity and pore fluid conductivity

Figure 25 shows typical data for a sandstone from Walker et al. (2014), although here there are more salinities measured than is usually the case, and there are measurements at salinities greater than about 0.3 mol l^{-1}, which are difficult to make. The three samples were all fairly homogeneous and isotropic and show small offsets that are typical of data on rocks from the same lithology and are to small differences in the pH of the equilibrium fluid. The flattening of the data at low salinities is due to the effect of surface conduction on the HS law and is controlled by the specific surface conductance and the microstructural properties of the rock (grain size, formation factor, porosity and cementation exponent). Part of the discrepancy between the datasets arises because each of the three samples equilibrated with the pore fluid at slightly different pH (pH 7, 6, and 6.5, respectively), but all were well modeled using the approach described in Section 11.04.6.7 when the experimental pH had been taken into account. It should be noted that the derived zeta potentials (Figure 25, bottom panel) are certainly not constant with salinity and equal to 17 mV as suggested by Jouniaux and Ishido (2012).

11.04.6.9.3 Pore fluid pH

Measurements as a function of pH are rare because it is difficult to stabilize a solution with a given pH with the rock. Figure 26 shows typical data for silica-based rocks. Here, the data made by Ishido and Mizutani (1981) have been augmented by some very recent data (Walker, 2012, pers. comm.). The pH has a significant effect on the measured streaming potential coefficient and zeta potential, with both approaching to zero near the isoelectric point for silica, $pH_{iso} = 3$ where the electrical double layer collapses because the surface has no net charge.

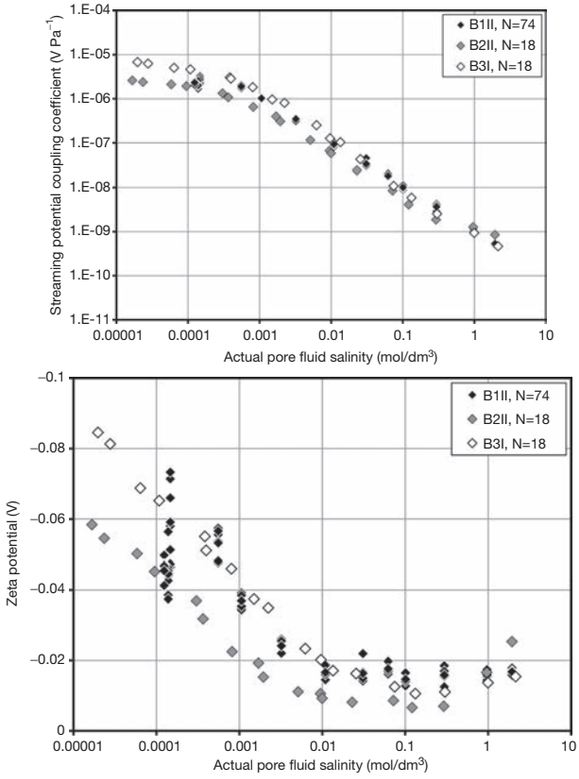

Figure 25 The measured streaming potential coefficient (top) and zeta potential (bottom) for three samples of Boise sandstone as a function of the actual salinity of the aqueous NaCl solution in the pores (B1II, pH = 7.2, T = 26 °C; B2II, pH = 5.94, T = 26 °C; B3I, pH = 6.61, T = 26 °C). Reproduced from Walker E, Glover PWJ, and Ruel J (2014) A transient method for measuring the DC streaming potential coefficient of porous and fractured rocks. *Journal of Geophysical Research: Solid Earth* 119: http://dx.doi.org/10.1002/2013JB010579.

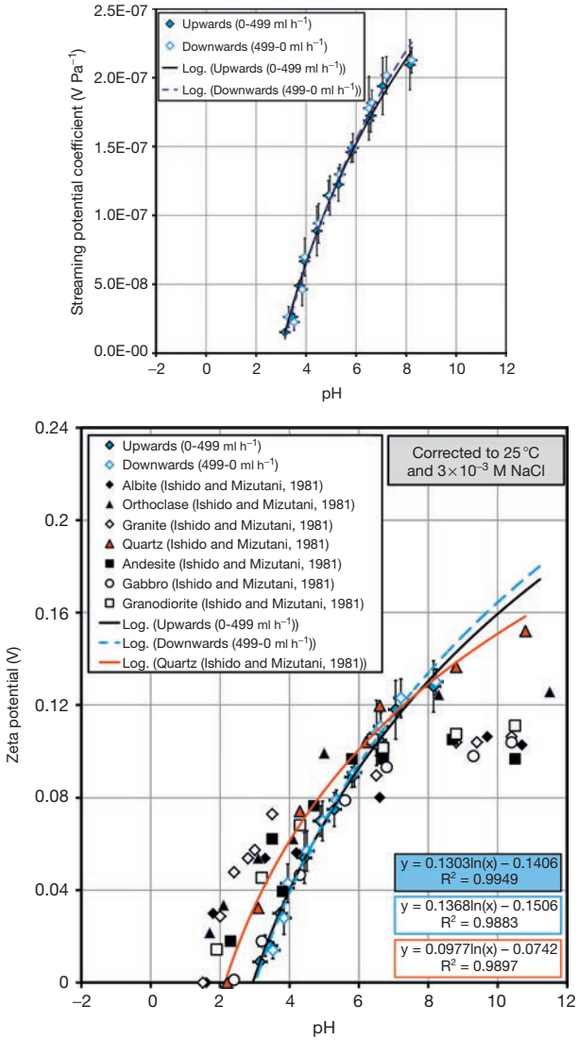

Figure 26 The measured streaming potential coefficient (top) and zeta potential (bottom) as a function of pH for a sample of Berea sandstone saturated with an aqueous NaCl solution ($C_f = 3 \times 10^{-3}$ mol l^{-1}, T = 25 °C) compared against data from Ishido and Mizutani (1981) corrected to the same conditions (Walker, 2012, pers. comm.).

11.04.6.9.4 Pore fluid composition

The streaming potential coupling coefficient also depends upon the ionic composition of the pore fluid, and in particular upon the valency of the dominant cation. For silica-based rocks, both Morgan et al. (1989) and Lorne et al. (1999a,b) have shown that fluids whose dominant cation is calcium provide a streaming potential approximately half that of monovalent cations irrespective of salinity. Morgan et al. (1989) tested KOH, KCl, NaCl, HCl, and $CaCl_2$, as a function of salinity, and although there is a clear difference in the streaming potential coefficient decreasing in the order listed, the first four fluids are fairly well grouped, while the divalent cation is significantly less than the others. Lorne tested KCl, K_2SO_4, $CaSO_4$, and $CaCl_2$ in order to examine whether the effect was controlled by divalent cations or anions or both (Lorne et al., 1999a,b). They found that KCl and K_2SO_4 provided the same high values of the coupling coefficient, showing no functional difference between the monovalent Cl^- and the divalent SO_4^{2-}. This is not surprising because for silica-based rocks at their pH (pH = 5.7), the surface is negative and it is the cation that forms the adsorbed layer and is dominant in the diffuse layer. Their divalent cation fluids provided coupling coefficients that were about half as large and once again followed a very similar trend.

11.04.6.9.5 Mineralogy

The great majority of the theoretical and experimental research into the electrokinetic properties of geomaterials has been carried out on silica-dominated rocks. However, some data exist for carbonates (Li et al., 1995; Pengra et al., 1999; Revil and Cerepi, 2004; Sprunt et al., 1994), zeolites, and shales (Revil and Leroy, 2001). Ishido and Mizutani (1981) published zeta potential data for quartz, orthoclase, albite, and granite as a function of pH (Figure 26) and found that all the samples behaved in a similar manner to their Inada granite (37% quartz, 24% alkali feldspar, 33% plagioclase, and 6% biotite (Oda et al., 2002)), occupying values between the highest values that were given by quartz and the lowest, provided by the albite. As always, the study of shales is complicated by the clays, which have slightly lower zeta potentials than quartz.

The clay zeta potential is the result of lower surface site densities but larger specific surface areas. The streaming potential of clay-rich rocks is also fairly low compared to quartz because they have augmented surface conduction that increases the denominator of the HS equation.

11.04.6.9.6 Rock microstructure

There have been no experiments dedicated to examining the effect of rock microstructure upon the streaming potential except grain size, pore size, and pore throat size (Glover and Déry, 2010). The rock microstructure should have no effect upon the zeta potential because the zeta potential is a property of the mineral/fluid interface. However, the theoretical model (**Section 11.04.6.7**) indicates that the grain size, pore size, pore throat size, formation factor, porosity, and cementation exponent should all control the size of the streaming potential coupling coefficient at low salinities, and that variations in these properties between samples are the cause of the divergence in experimental measurements recorded at low salinities which can be seen in **Figure 23**. Small grain, pore, and pore throat sizes all reduce the streaming potential coefficient, as do larger formation factors, and hence, smaller porosities and/or larger cementation exponents. These effects can be understood through [72] and [73], amplifying the effect of surface conduction in the rock. If the surface conductance increases, as in the case of clays, the coupling coefficient is also reduced.

11.04.6.9.7 Saturation

What little experimental evidence exists shows that the streaming potential coefficient is highly sensitive to water saturation, with the size of the coefficient decreasing as the water saturation decreases (Allègre et al., 2010, 2012; Guichet et al., 2003; Revil and Cerepi, 2004; Revil et al., 2007). The coefficient approaches zero at approximately the irreducible water saturation S_{wi}. This observation is important in the application of electrokinetics to oil and gas reservoirs, where the water saturation is generally not 100%. The form of the relative streaming potential coefficient curve as a function of water saturation becomes important in the interpretation of the size of the electrokinetic signal in the reservoir.

When a second fluid phase is present in the pore space, the magnitude of the streaming potential coupling coefficient becomes dependent on a number of factors including the wettability of the rock, the composition of the pore fluids, and the saturation of each phase (Jackson, et al., 2010; Saunders et al., 2012). According to Saunders et al. (2012), in the simplest case, the nonwetting phase is nonpolar and its flux causes no streaming current. The streaming potential coupling coefficient then depends on the saturation of the wetting phase (which we assume to be aqueous) and may be expressed in the form

$$\frac{\Delta V}{\Delta P} = C_i C_{sp} \qquad [83]$$

where the ratio of the streaming potential to the pressure difference that causes fluid flow is equal to the streaming potential coefficient for a fully saturated rock, C_{sp}, multiplied by a relative streaming potential coefficient function, C_i, that accounts for the variation of the streaming potential with water saturation, S_w.

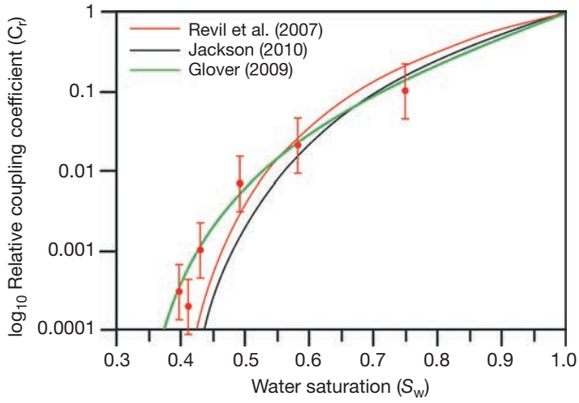

Figure 27 Streaming potential coefficient as a function of water saturation with models (Jackson, 2010; Revil et al., 2007; Glover, 2009, pers. comm.). This diagram uses the values $n = 2.7$, $S_{wi} = 0.36$, and $\lambda = 0.87$ from Revil et al. (2007) and applies them to all the models.

A number of relative streaming potential coefficient functions C_i have been proposed (Revil et al., 2007; Saunders et al., 2012), three of which are given in **Figure 27**.

Revil et al. (2007) suggested that

$$C_i = \frac{1}{S_w^{n+1}}\left(\frac{S_w - S_{wi}}{1 - S_{wi}}\right)^{(2+3\lambda)/\lambda} = \frac{k_{rw}}{S_w^{n+1}} \qquad [84]$$

where k_{rw} is water relative permeability, λ is the Brooks and Corey parameter (Brooks and Corey, 1966), S_w is the water saturation, S_{wi} is the residual water saturation, and n is an exponent.

By contrast, Jackson (2010) used a much simpler approach involving bundles of capillary tubes to obtain

$$C_i = \frac{k_{rw}(S_w)}{\sigma_{rr}(S_w)} = \frac{k_{rw}}{S_w^n} \qquad [85]$$

where the S_w is the volume fraction of water, k_{rw} is the relative permeability of water, and σ_r is the relative electrical conductivity, which is given by Archie's second law as $\sigma_{rr} = S_w^{\,n}$ (i.e., the inverse of the resistivity index [29]).

Glover (2009, pers.comm.) had also proposed that

$$C_i = S_w^{n+1}\left(\frac{S_w - S_{wi}}{1 - S_{wi}}\right)^{1/\lambda} \qquad [86]$$

using an empirical approach, which seems to fit the sparse data currently available, but is not based on sound theoretical roots. Other forms of the function exist but much more experimental data are needed in order to discriminate between the models.

The only currently available measurements of the streaming potential coefficient during multiphase flow (Vinogradov and Jackson, 2011) have indicated that there may be a slight hysteresis in the behavior between drainage and imbibition that appears whether the water is replaced by oil (undecane) or gas (moistened nitrogen). In the case of the oil/brine displacement, the streaming potential coefficient relative to that at 100% brine saturation decreased to values between 0.2 and 0.4, but decreased to almost zero for some brine/gas

displacements. However, these data are for measurements with saturations at unsteady state and hence need care in their interpretation.

11.04.6.9.8 Temperature

There have been few studies of the dependence of the streaming potential coefficient upon temperature. Those which exist are difficult to interpret because it is often unclear how much of a role is played by thermoelectric effects. Ishido and Mizutani (1981) observed an increase in the streaming potential coefficient with temperature for silica, while Morgan et al. (1989) observed a decrease for Westerly granite.

The variation of streaming potentials and zeta potential with temperature was studied theoretically and experimentally by Reppert and Morgan (2003a,b). They concluded that the variation of streaming potential with temperature cannot be explained solely by the known temperature dependence of water viscosity, permittivity, and conductivity, and that change of zeta potential with temperature must also be taken into account.

Reppert and Morgan (2003a) compiled previous experimental studies, most of which showed that the magnitude of the zeta potential increases with temperature. It was found that this increase is controlled primarily by the surface charge density, which is related to the absorption properties of the surface, the Stern layer charge, and properties of the electrical double layer according to the theory of Revil and Glover (1997).

Reppert and Morgan (2003a) found that the slope of the temperature versus zeta potential curve is controlled by the change in enthalpy of the surface reactions. Overall, the temperature dependence of the zeta potential was found to be determined by the following factors:

- The temperature-dependent behavior of the Debye–Hückel parameter, 4%.
- The temperature-dependent behavior of the diffuse layer of electrical double layer (EDL), 6%.
- The temperature dependence of the surface charge, 90%.

Clearly, it is the surface charge that has the greatest effect.

The streaming potential coefficient also depends upon temperature. The most dominant term controlling the temperature dependence of the streaming potential coefficient is the fluid viscosity.

Reppert and Morgan (2003b) have measured the streaming potential and zeta potential at temperatures between 23 °C and 200 °C and pressures of 20 MPa on samples of Fontainebleau sandstone, Berea sandstone, and Westerly granite. They found that the streaming potential coefficient and zeta potential behaved in a complex fashion that is not completely understood, but probably controlled by multiple mechanisms.

More recently, theoretical modeling (described in Section 11.04.6.7) predicts only a small temperature effect that leads to an increase in the magnitude of the streaming potential coefficient and zeta potential up to 120 °C.

11.04.6.10 Streaming Potential as a Function of Frequency

There are surprisingly few measurements of streaming potential for flow that varies in time. This is probably because such measurements have been considered very difficult to carry out. However, such measurements are likely to be of great importance in a number of fields, not least in the understanding and development of the seismoelectric exploration method (Dupuis et al., 2007; Jouniaux and Bordes, 2012).

The few previous measurements can be classified into two groups: (i) transient measurements with a percussive source and (ii) harmonic measurements with a vibrating source (Glover et al., 2012c). The first of these approaches mimics many of the possible applications more closely, while the latter is capable of providing higher-quality frequency-specific data. Glover et al. (2012b) have examined the methods for making frequency-dependent streaming potential measurements, while Reppert and Morgan (2001) have discussed the analysis of the resulting data.

Percussive source studies measure transient electrokinetic processes in sand columns that arise when a controlled impact is made on a column of saturated sand (Bordes et al., 2006, 2008; Chandler, 1981). These are difficult studies that require the impact to be repeatable and the seismoelectric and/or seismomagnetic conversion to be measured. Such transient measurements have confirmed the presence of seismoelectrokinetic and seismoelectromagnetic phenomena at high frequencies. However, the percussive seismic source does not produce a single frequency, so it cannot be used to measure the coupling coefficients as a function of frequency directly. However, it should be possible to examine the Fourier components of the seismic impact and the measured electric and magnetic signals in order to extract more specific information about the frequency dependence of the coupling coefficients (Reppert and Morgan, 2001). Reppert and Morgan carried out this procedure on a sample that they had already measured under steady-state conditions, and by using well-defined single frequencies, producing accurate results from 10 to about 120 Hz in the noninertial flow region. They could not, however, reproduce the decrease in the magnitude of the streaming potential coefficient at frequencies greater than 120 Hz that was measureable using the single-frequency approach.

A better approach is to arrange a harmonically varying fluid flow at a specific frequency and then to measure the time-varying streaming potential and fluid pressure difference, from which a streaming potential coefficient can be calculated. Repeating the experiment at different, well-defined frequencies then allows the variation of the streaming potential coefficient as a function of frequency to be obtained.

There are five ways that such data can be analyzed, and each is described with their advantages and disadvantages by Reppert and Morgan (2001). Briefly, the five approaches are as follows:

- To take the ratio of the RMS (root mean squared) streaming potential to the RMS pressure difference for a train of waves at a given frequency.
- To calculate the ratio of the instantaneous streaming potential to the instantaneous pressure difference for a train of waves at a given frequency and then calculate the mean and standard deviation of the result.
- To plot the instantaneous streaming potential against the instantaneous pressure difference for a train of waves at a given frequency and take the gradient and fitting

parameters of the best straight line through the data. This method is extremely simple but may be complicated if the data are noisy or there is hysteresis (Tardif et al., 2011).

- To cross-correlate both the streaming potential signal and the differential pressure signal, and then to calculate the ratio of the cross-correlated signals. This method works well with noisy data.
- To calculate the amplitude spectrum of both the streaming potential and the differential pressure signals. The streaming potential coefficient is then obtained by taking the ratio of the streaming potential amplitude spectrum to the differential pressure amplitude spectrum at the measured frequency. Other frequencies show the strength of the noise.

There have only been a few AC electrokinetic experiments published in the literature, amounting to measurements on several glass capillaries, one fritted glass filter, and two ceramic filters (Cooke, 1955; Packard, 1953; Reppert, 2000; Reppert and Morgan, 2001; Sears and Groves, 1978). Only one rock has ever been measured at frequencies greater than 100 Hz – a Boise sandstone with 35% porosity (Reppert, 2000). However, recent laboratory developments (Glover et al., 2012b) have provided new apparatuses that have produced high-quality data on Ottawa sand (Tardif et al., 2011) and several grades of glass beads (Glover et al., 2012c) up to 600 Hz, which holds hope for the measurement of rocks in the near future.

Figure 28 shows some recent data for the frequency-dependent streaming potential coefficient made on Ottawa sand together with several models. The top part of this figure shows the magnitude of the complex streaming potential coefficient as a function of frequency, while the bottom two parts show the in-phase (real) and out-of-phase (imaginary) components. All three parts are given because it is important that any model fits the complete complex response. There are a number of models that one can use to fit the data. It is worth noting that none of the models are of the Debye or Cole and Cole type, but all of them are dispersive, with a well-defined critical frequency f_{crit} and a slower roll-off for frequencies greater than the critical frequency, $f > f_{crit}$, than below it, $f < f_{crit}$.

Generic vibrational mechanics models are not normally useful. Sometimes, critically damped or underdamped second-order models are used; but not only do these perform worse than other models, the parameters they provide give no information about the rock. There is some indication that the frequency-dependent behavior of the streaming potential may follow a Cole–Davidson frequency dependence (Davidson and Cole, 1951). Packard (1953) introduced a model based on bundles of capillary tubes that was subsequently simplified (Reppert et al., 2001), noting that Glover et al. (2012c) contains an important correction to a misprint in the Reppert et al. (2001) paper. The best model, however, is

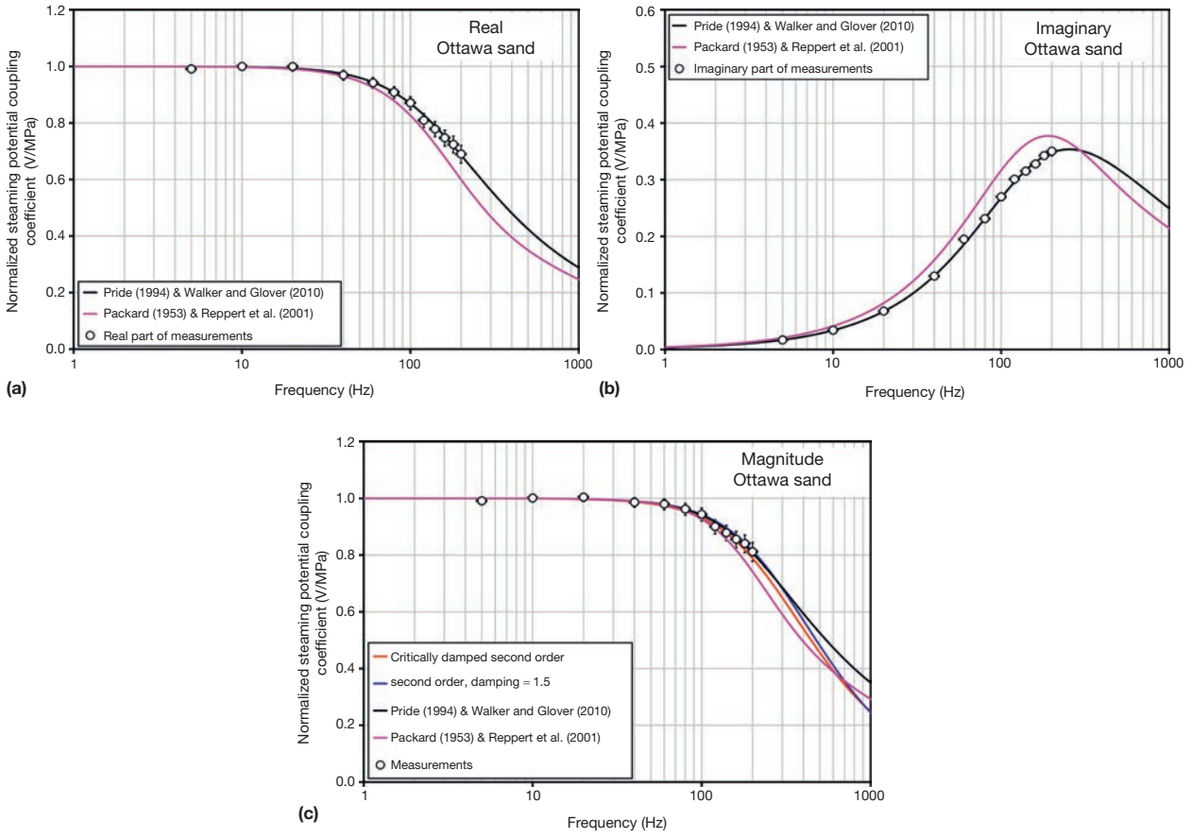

Figure 28 The calculated streaming potential coupling coefficient (normalized to the value at 5 Hz, which was 0.518 V MPa^{-1}) as a function of frequency for Ottawa sand saturated with 10^{-3} mol l^{-1} NaCl solution at 24 °C (porosity = 0.325, $\kappa_{10} = 1.19 \times 10^{-10}$ m^2). (c) Magnitude with six models shown fitting the data, (a) real component with four models, and (b) imaginary component with four models (Packard, 1953; Pride, 1994; Reppert et al., 2001; Thomson and Dahleh, 1998; Walker and Glover, 2010).

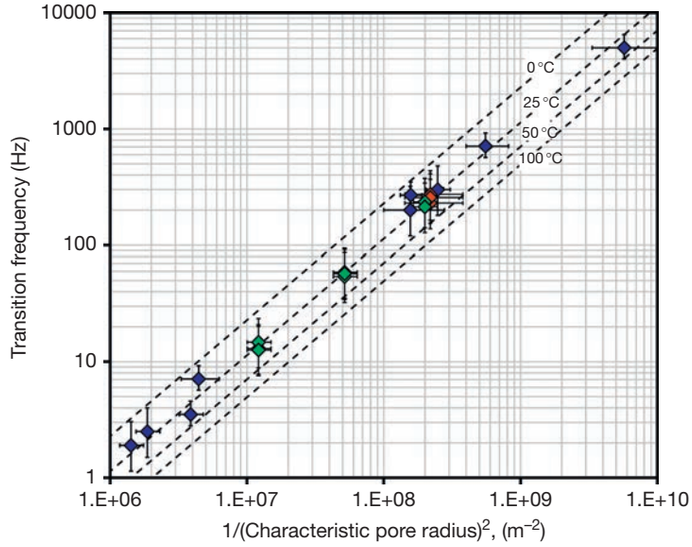

Figure 29 The electrokinetic transition frequency as a function of the inverse square characteristic pore size. Blue symbols, previous data for capillary tubes, filters, frits, and rocks (sources in Walker and Glover, 2010); red symbols, Ottawa sand measured at 24.0 °C ± 0.8 °C (Glover et al., 2012b); green symbols, glass bead packs (Glover et al., 2012b). The dashed lines represent the theoretical result [87] at four different temperatures to take account of the temperature dependence of both the fluid viscosity and the density.

that of Pride (1994), whose model was derived for a porous medium. While this model is complex, Walker and Glover (2010) provided a simplified version.

The critical angular frequency ω_{crit} ($=2\pi f_{crit}$) is related to the inverse square of the effective pore radius of the rock r_{eff} (Pride, 1994; Walker and Glover, 2010):

$$\omega_{crit} = \frac{8}{r_{eff}^2} \frac{\eta_f}{\rho_f} \qquad [87]$$

where η_f and ρ_f are the viscosity and density of the saturating fluid, respectively. Figure 29 shows this relationship for all the data currently in the public domain. Since the effective pore radius of the rock can be related to the permeability of the rock, we may use the critical frequency as a proxy for rock permeability or to predict permeability (Glover et al., 2012a,c).

11.04.7 Summary

11.04.7.1 History and Progress

Twenty years ago the electrical properties of porous and cracked rocks were described using a set of empirical relationships of which those by Archie were preeminent. They were sufficiently successful in the majority of cases that they were used in almost every assessment of oil and gas reserves for the previous 50 years.

In the last two decades, there have been large advances in the theory of the electrical properties of rocks; advances thanks to researchers such as André Revil, Steve Pride, and David Lockner. We now have theoretical tools to predict the electrical behavior of a rock in the DC regime, and at last, progress is being made in the development of theory in the AC regime. We have methods that enable the surface charge on minerals and the resulting surface conduction to be calculated, as well as a theoretical method for calculating the zeta potential. Progress in electrokinetics in both the steady-state and the frequency-dependent regimes allows us to measure and to predict the streaming potential coefficient.

Applications of the electrical and electrokinetic properties of rocks are to be found in many areas of geophysics well outside the traditional application in hydrocarbon exploration. Within the oil and gas industry, the era of large simple reservoirs is long over. Now, reserves are to be found in many, small, heterogeneous, anisotropic, difficult, and unconventional reservoirs. The analysis of these reservoirs will require the new sophisticated theoretical methods as well as the fully trained petrophysicists to use them.

11.04.7.2 Current Challenges and Future Directions

Two competing ideas can be applied to most natural sciences. The first is that any deep scientific truth will be simple and elegant. That may work well in particle physics, but such profound patterns and symmetries are difficult to see in the application of physics to natural materials. It is as if the nice bright shiny theories of Faraday and Maxwell are stained, dirtied, and rather well camouflaged by Mother Nature.

The second idea stems from this realization. It is that the Earth and its constituents are complex, and hence, their physics will be complex. It is worth realizing that the biggest challenge involving geomaterials is the complexity of their microstructure. This microstructure defines the physical properties of the material by acting as incredibly convoluted boundary conditions to the solution of constituent relationships, whether they are electrical, elastic wave, or thermal.

Advances in the speed of computers and the efficacy of programs designed to handle large datasets have started to enable us to untangle the complicated responses of complex

geomaterials and will continue to do so. The untangling of the effects of microstructure may not have the appeal of other research challenges, yet I believe that it is the biggest challenge in petrophysics.

Plenty of challenges remain. Most are related to microstructure. The most pressing challenges are as follows:

(i) To set up a fundamental theoretical framework for the frequency-dependent electrical properties of rocks that does not depend upon standard dispersion mechanisms and that is compatible with a zero frequency solution.
(ii) To ensure that all rock physical properties are viewed in terms of the way that they couple to other properties. Electrical properties couple to hydraulic, elastic wave, chemical, thermal, and magnetic properties, among others.
(iii) To improve the ability to make high-quality measurements, especially the extension of the ranges of frequency for which measurements can usefully be made.
(iv) To combine new experimental techniques with high resolutions, such as combining x-ray computed microtomography (μCT) with advanced modeling techniques to solve locally valid equations for the electrical properties of rocks, and to compare the results with existing empirical, quasiempirical, and effective medium models that are currently used.
(v) To ensure that all theory, measurements, and modeling are immediately and effectively applied to practical challenges with socioeconomic impact.
(vi) In the future, hydrocarbon reservoirs will be increasingly heterogeneous and anisotropic and smaller. The challenge will be to develop simple and effective methods for characterizing and managing production from these smaller more complex reservoirs while increasing the automation of the process. Geoelectric properties will have a part to play.

References

Adamson AW (1976) *Physical Chemistry of Surfaces*. New York: John Wiley and Sons.

Allègre V, Jouniaux L, Lehmann F, and Sailhac P (2010) Streaming potential dependence on water-content in Fontainebleau sand. *Geophysical Journal International* 182(3): 1248–1266. http://dx.doi.org/10.1111/j.1365-246X.2010.04716.x.

Allègre V, Jouniaux L, Lehmann F, and Sailhac P (2011) Reply to comment by A. Revil and N. Linde on 'Streaming potential dependence on water-content in Fontainebleau sand'. *Geophysical Journal International* 186(1): 115–117. http://dx.doi.org/10.1111/j.1365-246X.2011.05038.x.

Allègre V, Lehmann F, Ackerer P, Jouniaux L, and Sailhac P (2012) A 1-D modelling of streaming potential dependence on water content during drainage experiment in sand. *Geophysical Journal International* 189(1): 285–295. http://dx.doi.org/10.1111/j.1365-246X.2012.05371.x.

Archer DG and Wang P (1990) The dielectric constant of water and Debye-Hückel limiting law slopes. *Journal of Physical and Chemical Reference Data* 19(2): 371.

Archie GE (1942) The electrical resistivity log as an aid in determining some reservoir characteristics. *Transactions of AIME* 146(1): 54–62. http://dx.doi.org/10.2118/942054-G.

Baba K (2005) Electrical structure in marine tectonic settings. *Surveys in Geophysics* 26(6): 701–731.

Banton O, Seguin M, and Cimon M (1997) Mapping field-scale physical properties of soil with electrical resistivity. *Soil Science Society of America Journal* 61(4): 1010–1017.

Bardon C and Pied B (1969) Formation water saturation in shaly sands. In: *Society of Professional Well Log Analysts10th Annual Logging Symposium Transactions, Paper Z*, 19 pp.

Barsoukov E and Macdonald JR (2005) *Impedance Spectroscopy: Theory, Experiment, and Applications*. John Wiley, ISBN: 0471647497, 608 pp.

Beekmans NM and Heyne L (1976) Correlation between impedance, microstructure and compositions of calcia-stabilised zirconia. *Electrochimica Acta* 21: 303–310.

Bentley RW (2002) Global oil and gas depletion: An overview. *Energy Policy* 30(3): 189–205. http://dx.doi.org/10.1016/S0301-4215(01)00144-6.

Bernabé Y and Bruderer C (1998) Effect of the variance of pore size distribution on the transport properties of heterogeneous networks. *Journal of Geophysical Research* 103: 513–526.

Binley A, Slater LD, Fukes M, and Cassiani G (2005) Relationship between spectral induced polarization and hydraulic properties of saturated and unsaturated sandstone. *Water Resources Research* 41: W12417. http://dx.doi.org/10.1029/2005WR004202.

Binley A, Kruschwitz S, Lesmes D, and Kettridge N (2010) Exploiting the temperature effects on low frequency electrical spectra of sandstone: A comparison of effective diffusion path lengths. *Geophysics* 75(6): A43–A46.

Bordes C, Jouniaux L, Dietrich M Pozzi, Pozzi J-P, and Garambois S (2006) First laboratory measurements of seismo-magnetic conversions in fluid-filled Fontainebleau sand. *Geophysical Research Letters* 33: L01302. http://dx.doi.org/10.1029/2005GL024582.

Bordes C, Jouniaux L, Garambois S, Dietrich M Pozzi, Pozzi J-P, and Gaffet S (2008) Evidence of the theoretically predicted seismo-magnetic conversion. *Geophysical Journal International* 174: 489–504. http://dx.doi.org/10.1111/j.1365-246X.2008.03828.x.

Börner FD and Schön JH (1991) A relation between the quadrature component of electrical conductivity and the specific surface area of sedimentary rocks. *The Log Analyst* 32: 612–613.

Börner FD, Schopper JR, and Weller A (1996) Evaluation of transport and storage properties in the soil and groundwater zone from induced polarization measurements. *Geophysical Prospecting* 44: 583–602.

Brooks RH and Corey AT (1966) Properties of porous media affecting fluid flow. *Journal of the Irrigation and Drainage Division of the American Society of Civil Engineering* 92(IR2): 61–88.

Bruggeman DAG (1935) Berechnung verschiedener physikalischer Konstanten von heterogenen Substanzen. I. Dielektrizitätskonstanten und Leitigähigkeiten der Mischkörper aus isotropen Substanzen. *Annalen der Physik* 5: 636–664.

Bussian AE (1983) Electrical conductance in a porous medium. *Geophysics* 1983(48): 1258–1268. http://dx.doi.org/10.1190/1.1441549.

Carter LM, Campbell BA, Holt JW, et al. (2009) Dielectric properties of lava flows west of Ascraeus Mons, Mars. *Geophysical Research Letters* 36(23).

Chandler R (1981) Transient streaming potential measurements on fluid-saturated porous structures: An experimental verification of Biot's slow wave in the quasi-static limit. *Journal of the Acoustical Society of America* 70: 116–121.

Chelidze TL and Guéguen Y (1999) Electrical spectroscopy of porous rocks: A review—I. Theoretical models. *Geophysical Journal International* 137(1): 1–15. http://dx.doi.org/10.1046/j.1365-246X.1999.00799.x.

Chelidze TL, Guéguen Y, and Ruffet C (1999) Electrical spectroscopy of porous rocks: A review—II. Experimental results and interpretation. *Geophysical Journal International* 137(1): 16–34. http://dx.doi.org/10.1046/j.1365-246X.1999.00800.x.

Chelidze T, Varamashvili N, Devidze M, Tchelidze Z, Chikhladze V, and Matcharashvili T (2003) Laboratory study of electromagnetic initiation of slip. *Annali di Geofisica* 45(5): 587–598.

Clavier C, Coates G, and Dumanoir L (1977) The theoretical and experimental bases for the Dual Water Model for the interpretation of shaly sands. In: *Paper SPE 6859 presented at the 1977 SPE Annual Technical Conference and Exhibition, Denver, October 9–12*. http://dx.doi.org/10.2118/6859-PA.

Clennell MB (1997) *Tortuosity: A Guide Through the Maze*. Vol. 122. London: Geological Society, Special Publications, January, pp. 299–344. http://dx.doi.org/10.1144/GSL.SP.1997.122.01.18.

Coates GR, Boutemy Y, and Clavier C (1983) A study of the dual-water model based on log data. *Journal of Petroleum Technology* 35(1): 158–166. http://dx.doi.org/10.2118/10104-PA.

Cole KS and Cole RH (1941) Dispersion and absorption in dielectrics I: Alternating current characteristics. *Journal of Chemical Physics* 9: 341–351. http://dx.doi.org/10.1063/1.1750906.

Cooke CE (1955) Study of electrokinetic effects using sinusoidal pressure and voltage. *Journal of Chemical Physics* 23: 2299–2303. http://dx.doi.org/10.1063/1.1740742.

Crespy A, Bolève A, and Revil A (2007) Influence of the Dukhin and Reynolds numbers on the apparent zeta potential of granular porous media. *Journal of Colloid and Interface Science* 305(1): 188–194. http://dx.doi.org/10.1016/j.jcis.2006.09.038.

Cyr G, Glover PWJ, and Novikov V (2010) Can an electro-kinetic mechanism explain artificial earthquakes? In: *EGU2010, EGU2010-2526, Vienna, 2–7 May 2010*.
Dai L and Karato S (2009) Electrical conductivity of pyrope-rich garnet at high temperature and pressure. *Physics of the Earth and Planetary Interiors* 176: 83–88.
David C (1993) Geometry of flow paths for fluid transport in rocks. *Journal of Geophysical Research* 98: 12267–12278.
Davidson DW and Cole RH (1951) Dielectric relaxation in glycerol, propylene glycol, and n-propanol. *Journal of Chemical Physics* 29: 1484–1490.
Davis J and Kent D (1990) Surface complexation modeling in aqueous geochemistry. In: Hochella MF and White AF (eds.) *Mineral Water Interface Geochemistry*. Mineralogical Society of America.
Davis JA, James RO, and Leckie JO (1978) Surface ionization and complexation at the oxide/water interface. I. Computation of electrical double layer properties in simple electrolytes. *Journal of Colloid and Interface Science* 63(3): 480–499. http://dx.doi.org/10.1016/S0021-9797(78)80009-5.
de Lima OAL and Sharma MM (1992) A generalized Maxwell–Wagner theory for membrane polarization in shaly sands. *Geophysics* 57: 431–440.
Debye PJW (1929) *Polar Molecules*. New York: Initially Chemical Catalogue Co., subsequently Dover Press, pp. 77–108, Chapter 5.
Di Maio R and Patella D (1991) Basic theory of electrokinetic effects associated with earthquakes. *Bollettino di Geofisica Teorica ed Applicata* 33(130–131): 145–154.
Di Maio R and Patella D (1994) Self-potential anomaly generation in volcanic areas. The Mt. Etna case-history. *Acta Vulcanologica* 4: 119–124.
Dissado LA and Hill RM (1984) Anomalous low-frequency dispersion. *Journal of the Chemical Society, Faraday Transactions* 2: 291–319. http://dx.doi.org/10.1039/F29848000291.
Dortman NB (1976) *Fiziceskie svoistva gornich porod I polesnich iskopamych*. Nedra, Moscow: Izdat.
Doveton JH (2001) All models are wrong, but some models are useful: "Solving" the Simandoux equation. In: *Annual Conference of the International Association of Mathematical Geology, Section J, Cancun, Mexico*. http://www.kgs.ku.edu/Conferences/IAMG/Sessions/J/Papers/doveton.pdf.
Duba A, Heikamp S, Meurer W, Mover G, and Will G (1994) Evidence from borehole samples for the role of accessory minerals in lower-crustal conductivity. *Nature* 367: 59–61. http://dx.doi.org/10.1038/367059a0.
Dukhin SS and Derjaguin BV (1974) In: Matijevic E (ed.) *Surface and Colloid Science*. New York: John Wiley and Sons.
Dunlap HF and Hawthorne RR (1951) The calculation of water resistivities from chemical analyses. *Journal of Petroleum Technology* 3(3): 373–375.
Dupuis JC, Butler KE, and Kepic AW (2007) Seismoelectric imaging of the vadose zone of a sand aquifer. *Geophysics* 72(6): A81–A85. http://dx.doi.org/10.1190/1.2773780.
Einaudi F, Pezard PA, Ildefonse B, and Glover P (2005) *Electrical Properties of Slow-Spreading Ridge Gabbros from ODP Hole 1105A, SW Indian Ridge*, vol. 240, pp. 179–193, Geological Society Special Publication. http://dx.doi.org/10.1144/GSL.SP.2005.240.01.14.
Ellis DV and Singer JM (2007) *Well Logging for Earth Scientists*, 2nd ed. Dordrecht, The Netherlands: Springer, ISBN: 9781402037382.
Endres AL and Knight R (1992) A theoretical treatment of the effect of microscopic fluid distribution on the dielectric properties of partially saturated rocks. *Geophysical Prospecting* 40(3): 307–324.
Ewing RP and Hunt AG (2006) Dependence of the electrical conductivity on saturation in real. Porous media. *Vadose Zone Journal* 5(2): 731–741. http://dx.doi.org/10.2136/vzj2005.0107.
Focke JW and Munn D (1987) Cementation exponents in middle eastern carbonate reservoirs. *SPE Formation Evaluation* 2(2): 155–167.
Friedrichs B, Matzander U, Large D, and Davies M (1999) Controlled source electro-magnetic mapping-development and evaluation of its application to mineral exploration. *Transactions of the Institutions of Mining and Metallurgy, Section B: Applied Earth Science* 108(Sept–Dec): B178–B182.
Fujinawa Y, Kumagai T, and Takahashi K (1992) A study of anomalous underground electric field variations associated with a volcanic eruption. *Geophysical Research Letters* 19(1): 9–12.
Gaffney C (2008) Detecting trends in the prediction of the buried past: A review of geophysical techniques in archaeology. *Archaeometry* 50(2): 313–336.
Glover PWJ (1996) Graphite and electrical conductivity in the lower continental crust: A review. *Physics and Chemistry of the Earth* 21(4): 279–287.
Glover PWJ (2009) What is the cementation exponent? A new interpretation. *The Leading Edge:* 82–85. http://dx.doi.org/10.1190/1.3064150.
Glover PWJ (2010a) The discovery of an Anglo-Saxon grubenhaus at New Bewick, Northern UK using electrical surveying and predictive deconvolution. *Archaeometry* 52(2): 320–342.
Glover PWJ (2010b) A generalized Archie's law for *n* phases. *Geophysics* 75(6): E247–E265. http://dx.doi.org/10.1190/1.3509781.
Glover PWJ and Adám A (2008) Correlation between crustal high conductivity zones and seismic activity and the role of carbon during shear deformation. *Journal of Geophysical Research* 113: B12210. http://dx.doi.org/10.1029/2008JB005804.
Glover PWJ and Déry N (2010) Dependence of streaming potential on grain diameter and pore radius for quartz glass beads. *Geophysics* 75: F225–F241. http://dx.doi.org/10.1190/1.3509465.
Glover PWJ and Jackson MD (2010) Borehole electro-kinetics. *The Leading Edge* 29: 724–728. http://dx.doi.org/10.1190/1.3447786.
Glover PWJ and Vine FJ (1992) Electrical conductivity of carbon-bearing granulite at raised temperatures and pressures. *Nature* 360(6406): 723–726.
Glover PWJ and Vine FJ (1994) Electrical conductivity of the continental crust. *Geophysical Research Letters* 21(22): 2357–2360.
Glover PWJ and Vine FJ (1995) Beyond KTB – electrical conductivity of the deep continental crust. *Surveys in Geophysics* 16(1): 5–36.
Glover PWJ, Meredith PG, Sammonds PR, and Murrell SAF (1994) Ionic surface electrical conductivity in sandstone. *Journal of Geophysical Research* 99: 21635–21650. http://dx.doi.org/10.1029/94JB01474.
Glover PWJ, Gomez JB, Meredith PG, Hayashi K, Sammonds PR, and Murrell SAF (1997) Damage of saturated rocks undergoing triaxial deformation using complex electrical conductivity measurements: Experimental results. *Physics and Chemistry of the Earth* 22: 57–61. http://dx.doi.org/10.1016/S0079-1946(97)00078-5.
Glover PWJ, Hole MJ, and Pous J (2000a) A modified Archie's Law for two conducting phases. *Earth and Planetary Science Letters* 180: 369–383. http://dx.doi.org/10.1016/S0012-821X(00)00168-0.
Glover PWJ, Pous J, Queralt P, Muñoz J-A, Liesa M, and Hole MJ (2000b) Integrated two dimensional lithospheric conductivity modelling in the Pyrenees using field-scale and laboratory measurements. *Earth and Planetary Science Letters* 178(1–2): 59–72.
Glover PWJ, Gómez JB, and Meredith PG (2000c) Fracturing in saturated rocks undergoing triaxial deformation using complex electrical conductivity measurements: Experimental study. *Earth and Planetary Science Letters* 183: 201–213. http://dx.doi.org/10.1016/S0012-821X(00)00267-3.
Glover PWJ, Zadjali I, and Frew K (2006a) Permeability prediction from MICP and NMR data using an electro-kinetic approach. *Geophysics* 71: F49.
Glover PWJ, Déry N, and Ransford TJ (2006b) The complex electrical properties of rocks and bead-packs as a function of frequency: Experiment and modelling. In: *Ann. Gen. Ass. EGU 2006, EGU06-A-10732, Vienna*.
Glover PWJ, Ransford TJ, and Auger G (2010) A simple method for solving the Bussian equation for electrical conduction in rocks. *Solid Earth* 1: 85–91. http://dx.doi.org/10.5194/se-1-85-2010.
Glover PWJ and Walker E (2009) Grain-size to effective pore-size transformation derived from electrokinetic theory. *Geophysics* 74(1): E17–E29. http://dx.doi.org/10.1190/1.3033217.
Glover PWJ, Walker E, and Jackson MD (2012a) Streaming-potential coefficient of reservoir rock. *Geophysics* 77(2): D17–D43. http://dx.doi.org/10.1190/GEO2011-0364.1.
Glover PWJ, Ruel J, Tardif E, and Walker E (2012b) Frequency-dependent streaming potential of porous media—Part 1: Experimental approaches and apparatus design. *International Journal of Geophysics* 2012: 846204. http://dx.doi.org/10.1155/2012/846204.
Glover PWJ, Walker E, Ruel J, and Tardif E (2012c) Frequency-dependent streaming potential of porous media—Part 2: Experimental measurement of unconsolidated materials. *International Journal of Geophysics* 2012: 728495. http://dx.doi.org/10.1155/2012/728495.
Green AD (1997) Measurements of the dielectric properties of cheddar cheese. *Journal of Microwave Power and Electromagnetic Energy* 32(1): 16–27.
Grosse C (2010) Extension of a classic theory of the low frequency dielectric dispersion of colloidal suspensions to the high frequency domain. *Journal of Physical Chemistry B* 114(39): 12520–12527.
Grosse C (2012) Extension of a classic low frequency dielectric dispersion theory of colloidal suspensions to include different counterion and co-ion valences, a broad frequency range, and the stagnant layer conductivity. *Journal of Physical Chemistry B* 116(45): 13538–13553.
Grosse C and Delgado AV (2010) Dielectric dispersion in aqueous colloidal systems. *Current Opinion in Colloid and Interface Science* 15(3): 145–159.
Guéguen Y and Palciauskas V (1994) *Introduction to the Physics of Rocks*. Princeton, NJ: Princeton University Press, ISBN: 9780691034522.
Guichet X, Jouniaux L, and Pozzi J-P (2003) Streaming potential of a sand column in partial saturation conditions. *Journal of Geophysical Research, B: Solid Earth* 108(3): ECV 2-1–2-12. http://dx.doi.org/10.1029/2001JB001517.

Guichet X, Jouniaux L, and Catel N (2006) Modification of streaming potential by precipitation of calcite in a sand-water system: Laboratory measurements in the pH range from 4 to 12. *Geophysical Journal International* 166(1): 445–460. http://dx.doi.org/10.1111/j.1365-246X.2006.02922.x.

Gung Y, Panning M, and Romanowicz B (2003) Global anisotropy and the thickness of continents. *Nature* 422(6933): 707–711.

Haines SS, Pride SR, Klemperer SL, and Biondi B (2007) Seismoelectric imaging of shallow targets. *Geophysics* 72(2): G9–G20. http://dx.doi.org/10.1190/1.2428267.

Hanai T (1960) Theory of the dielectric dispersion due to the interfacial polarization and its application to emulsions. *Kolloid-Z*. 171: 23–31.

Hashin Z and Shtrikman S (1962) A variational approach to the theory of effective magnetic permeability of multiphase materials. *Journal of Applied Physics* 33: 3125–3131.

Helmholtz H (1879) Studien über electrische Grenzschichten. *Annalen der Physik* 7: 337–382.

Hilchie DW (1984) A new water resistivity versus temperature equation. *The Log Analyst* 25(4): 20–21.

Hossin A (1960) Calcul des saturations en eau par la methode du ciment argileux (formule d'Archie generalisee). *Bulletin Association Francaise des Techniciens du Petrole* 140.

Hunt AG (2004) Continuum percolation theory and Archie's law. *Geophysical Research Letters* 31(L19503): 1–4.

Hunter RJ (1981) *Zeta Potential in Colloid Science*. New York: Academic Press.

Iler RK (1979) *The Chemistry of Silica*. New York: Wiley.

Ishido T and Mizutani H (1981) Experimental and theoretical basis of electro-kinetic phenomena in rock-water systems and its applications to geophysics. *Journal of Geophysical Research* 86: 1763–1775.

Izgorodina EI, Forsyth M, and MacFarlane DR (2009) On the components of the dielectric constants of ionic liquids: Ionic polarization? *Physical Chemistry Chemical Physics* 11: 2452–2458. http://dx.doi.org/10.1039/B815835E.

Jaafar MZ, Vinogradov J, and Jackson MD (2009) Measurement of streaming potential coupling coefficient in sandstones saturated with high salinity NaCl brine. *Geophysical Research Letters* 36(21).

Jackson MD (2010) Multiphase electrokinetic coupling: Insights into the impact of fluid and charge distribution at the pore scale from a bundle of capillary tubes model. *Journal of Geophysical Research* 115: B07206. http://dx.doi.org/10.1029/2009JB007092.

Jackson MD, Gulamali MY, Leinov E, Saunders JH, and Vinogradov J (2010) Real-time measurements of spontaneous potential for inflow monitoring in intelligent wells. *Proceedings – SPE Annual Technical Conference and Exhibition* 2010, pp. 4133–4150.

Jackson PD, Northmore KJ, Meldrum PI, et al. (2002) Non-invasive moisture monitoring within an earth embankment – A precursor to failure. *NDT and E International* 35(2): 107–115.

Jha SN, Narsaiah K, Basediya AL, et al. (2011) Measurement techniques and application of electrical properties for nondestructive quality evaluation of foods—A review. *Journal of Food Science and Technology* 48(4): 387–411.

Jindal M, Kumar V, Rana V, and Tiwary AK (2013) Physico-chemical, mechanical and electrical performance of bael fruit gum-chitosan IPN films. *Food Hydrocolloids* 30(1): 192–199.

Johnson DL, Koplik J, and Schwartz LM (1986) New pore-size parameter characterizing transport in porous media. *Physical Review Letters* 57(20): 2564–2567. http://dx.doi.org/10.1103/PhysRevLett.57.2564.

Jones SB and Or D (2002) Surface area, geometrical and configurational effects on permittivity of porous media. *Journal of Non-Crystalline Solids* 305(1–3): 247–254. http://dx.doi.org/10.1016/S0022-3093(02)01098-0.

Jouniaux L and Bordes C (2012) Frequency-dependent streaming potentials: A review. *International Journal of Geophysics* 11. http://dx.doi.org/10.1155/2012/648781, Article ID 648781.

Jouniaux L and Ishido T (2012) Electrokinetics in earth sciences: A tutorial. *International Journal of Geophysics* http://dx.doi.org/10.1155/2012/286107. 16 pp., Article ID: 286107.

Juhasz I (1981) Normalised Qv-the key to shaly sand evaluation using the Waxman-Smits equation in the absence of core data. In: *Society of Professional Well Log Analysts 22nd Annual Logging Symposium Transactions, Paper Z*, 36 pp.

Kanoun O (2012) *Lecture Notes on Impedance Spectroscopy: Measurement, Modeling and Application*. CRC Press, 112 pp.

Keller GV (1989) Electrical properties. In: Carmichael RS (ed.) *Practical Handbook of Physical Properties of Rocks*. Boca Raton: CRC Press, ISBN: 9780849337031.

Keller GV and Frischknecht FC (1966) *Electrical Methods in Geophysical Prospecting*. Pergamon Press, 517 pp.

Kemna A, Binley A, Cassiani G, et al. (2012) An overview of the spectral induced polarization method for near-surface applications. *Near Surface Geophysics* 10(6): 453–468. http://dx.doi.org/10.3997/1873-0604.2012027.

Key K, Constable S, LIU L, and Pommier A (2013) Electrical image of passive mantle upwelling beneath the northern East Pacific Rise. *Nature* 495(7442): 499–502.

Kirkpatrick S (1973) Hopping conduction: Experiment versus theory. In: Stuke J and Brenig W (eds.) *5th Annual Conference on Amorphous and Liquid Semiconductors: Proceedings*, pp. 103–107. Philadelphia, PA: Taylor and Francis.

Knight R and Abad A (1995) Rock/water interaction in dielectric properties: Experiments with hydrophobic sandstones. *Geophysics* 60(2): 431–436.

Knight R and Endres A (1990) A new concept in modeling the dielectric response of sandstones: Defining a wetted rock and bulk water system. *Geophysics* 55(5): 586–594.

Knight R and Nur A (1984) Effect of level of water saturation on the dielectric constant of sandstones. In: *Transactions of the SPWLA Annual Logging Symposium (Society of Professional Well Log Analysts)*.

Knight RJ and Nur A (1987a) Geometrical effects in the dielectric response of partially saturated sandstones. *The Log Analyst* 28(6): 513–519.

Knight RJ and Nur A (1987b) Dielectric constant of sandstones, 60 kHz to 4 MHz. *Geophysics* 52(5): 644–654.

Knight RJ, Nur A, and Raistrick ID (1985) Modelling the electrical response of sandstones with an equivalent circuit. In: *Transactions of the SPWLA Annual Logging Symposium (Society of Professional Well Log Analysts)*.

Korvin G (1982) Axiomatic characterization of the general mixture rule. *Geoexploration* 19(4): 267–276. http://dx.doi.org/10.1016/0016-7142(82)90031-X.

Kosmulski M (1996) Adsorption of cadmium on alumina and silica: Analysis of the values of stability constants of surface complexes calculated for different parameters of triple layer model. *Colloids and Surfaces A: Physicochemical and Engineering Aspects* 117: 201–214. http://dx.doi.org/10.1016/0927-7757(96)03706-5.

Kruschwitz S (2007) *Assessment of the complex resistivity behavior of salt affected building materials*. Diss. Fakultät VI, Planen Bauen Umwelt. Technischen Univ. Berlin, Berlin.

Kruschwitz S, Binley A, Lesmes D, and Elshenawy A (2010) Textural controls on low frequency electrical spectra of porous media. *Geophysics* 75(4): WA113–WA123. http://dx.doi.org/10.1190/1.3479835.

Lasia A (1999) In: Conway BE, Bockris J, and White RE (eds.) *Electrochemical Impedance Spectroscopy and Its Applications, Modern Aspects of Electrochemistry*, vol. 32, pp. 143–248. New York: Kluwer Academic/Plenum Publishers.

Le Méhauté A and Crepy G (1983) Introduction to transfer and transport in fractal media. *Solid State Ionics* 9&10: 17–30.

Leinov E, Vinogradov J, and Jackson MD (2010) Salinity dependence of the thermoelectric coupling coefficient in brine-saturated sandstones. *Geophysical Research Letters* 37(23).

Leroy P and Revil A (2004) A triple-layer model of the surface electrochemical properties of clay minerals. *Journal of Colloid and Interface Science* 270: 371–380. http://dx.doi.org/10.1016/j.jcis.2003.08.007.

Leroy P and Revil A (2009) A mechanistic model for the spectral induced polarization of clay materials. *Journal of Geophysical Research* 114: B10202. http://dx.doi.org/10.1029/2008JB006114.

Leroy P, Revil A, Kemna A, Cozensa P, and Ghorbani A (2008) Complex conductivity of water-saturated packs of glass beads. *Journal of Colloid and Interface Science* 321: 103–117. http://dx.doi.org/10.1016/j.jcis.2007.12.031.

Lesparre N, Gibert D, Nicollin F, Nussbaum C, and Adler A (2013) Monitoring the excavation damaged zone by three-dimensional reconstruction of electrical resistivity. *Geophysical Journal International* 195(2): 972–984.

Li D, Jiang J, Wu J, Zhang D, and Zhang X (2005) Experimental research and statistical analysis on the dielectric properties of lunar soil simulators. *Chinese Science Bulletin* 50(10): 1034–1043.

Li SX, Pengra DB, and Wong PZ (1995) Onsager's reciprocal relation and the hydraulic permeability of porous media. *Physical Review E* 51: 5748–5751. http://dx.doi.org/10.1103/PhysRevE.51.5748.

Li C, Tercier P, and Knight R (2001) Effect of sorbed oil on the dielectric properties of sand and clay. *Water Resources Research* 37(6): 1783–1793. http://dx.doi.org/10.1029/2001WR900006.

Lichtenecker K and Rother K (1931) 'Die Herleitung des logarithmischen Mischungs-gesetzes aus allegemeinen Prinzipien der stationaren Stromung. *Physikalishce Zeitschrift* 32: 255–260.

Lide DR (2012) *Handbook of Chemistry and Physics*, 93rd edn. Taylor Francis, ISBN: 1439880492.

Liu LP (2010) Hashin-Shtrikman bounds and their attainability for multi-phase composites. *Proceedings of the Royal Society A* 466: 3693–3713.

Lockner DA and Byerlee JD (1985) Complex resistivity measurements of confined rocks. *Journal of Geophysical Research* 90: 78377847.

Lorne B, Perrier F, and Avouac J-P (1999a) Streaming potential measurements: 1. Properties of the electrical double layer from crushed rock samples. *Journal of Geophysical Research, B: Solid Earth* 104(B8): 17857–17877.

Lorne B, Perrier F, and Avouac J-P (1999b) Streaming potential measurements 2. Relationship between electrical and hydraulic flow patterns from rock samples during deformation. *Journal of Geophysical Research, B: Solid Earth* 104(8): 17879–17896.

Luo M, Wood JR, and Cathles LM (1994) Prediction of thermal conductivity in reservoir rocks using fabric theory. *Journal of Applied Geophysics* 32(4): 321–334. http://dx.doi.org/10.1016/0926-9851_94_90031-0.

Macdonald JR and Kenan WR (1987) *Impedance Spectroscopy: Emphasizing Solid Materials and Systems*. John Wiley & Sons, 368 pp.

Maineult A, Bernabé Y, and Ackerer P (2004) Electrical response of flow, diffusion, and advection in a laboratory sand box. *Vadose Zone Journal* 3(4): 1180–1192.

Maineult A, Bernabé Y, and Ackerer P (2005) Detection of advected concentration and pH fronts from self-potential measurements. *Journal of Geophysical Research, B: Solid Earth* 110(11): 1–14.

Malmberg C and Maryott A (1956) Dielectric constant of water from 0 °C to 100 °C. *Journal of Research of the National Bureau of Standards* 56(1): 1–8, Paper 2641.

Marshall DJ and Madden TK (1959) Induced polarization, a study of its causes. *Geophysics* 24: 790–816.

Maurício AM, Pacheco AMG, Brito PSD, Castro B, Figueiredo C, and Aires-Barros L (2005) An ionic conductivity-based methodology for monitoring salt system in monument stones. *Journal of Cultural Heritage* 6(4): 287–293.

Maxwell JC (1873) *A Treatise on Electricity and Magnetism*. vol. 1. Oxford, UK: Clarendon Press.

Mendelson KS and Cohen MH (1982) The effect of grain anisotropy on the electrical properties of sedimentary rocks. *Geophysics* 47(2): 257–263.

Mewafy FM, Werkema DD, Atekwana EA, et al. (2013) Evidence that bio-metallic mineral precipitation enhances the complex conductivity response at a hydrocarbon contaminated site. *Journal of Applied Geophysics* 98: 113–123. http://dx.doi.org/10.1016/j.jappgeo.2013.08.011.

Mizutani H, Ishido T, Yokokura T, and Ohnishi S (1976) Electrokinetic phenomena associated with earthquakes. *Geophysical Research Letters* 3(7): 365–368.

Montaron B (2009) Connectivity theory – A new approach to modelling non-Archie rocks. *Petrophysics* 50: 102–115.

Montaron B and Han M (2009) A connectivity model for the electrical conductivity of sandstone rocks. In: *SPWLA 50th Annual Logging Symposium, June 21–24*, pp. 1–11.

Morgan FD, Williams ER, and Madden TR (1989) Streaming potential properties of westerly granite with applications. *Journal of Geophysical Research* 94: 12449–12461. http://dx.doi.org/10.1029/JB094iB09p12449.

Nugent WH, Coates GR, and Peebler RP (1978) New approach to carbonate analysis. In: *O-SPWLA Conference Paper*.

Nurmi RD and Frisinger MR (1983) *Synergy of core petrophysical measurements, log data, and rock examination in carbonate reservoir*. Society of Petroleum Engineers of AIME, (Paper) SPE 1983.

Oda M, Katsube T, and Takemura T (2002) Microcrack evolution and brittle failure of Inada granite in triaxial compression tests at 140 MPa. *Journal of Geophysical Research* 107(B10): 2233. http://dx.doi.org/10.1029/2001JB000272.

Olhoeft GR (1981) Electrical properties of rocks. In: Touloukian YS, Judd WR, and Roy RF (eds.) *Physical Properties of Rocks and Minerals*. New York: McGraw Hill.

Oliver DP, Bramley RGV, Riches D, Porter I, and Edwards J (2013) Review: Soil physical and chemical properties as indicators of soil quality in Australian viticulture. *Australian Journal of Grape and Wine Research* 19(2): 129–139.

Orazem ME and Tribollet B (2011) *Electrochemical Impedance Spectroscopy*. John Wiley & Sons, 560 pp.

Overbeek JTG (1952) Electrochemistry of the double layer. In: Kruyt HR (ed.) *Colloid Science 1, Irreversible Systems*, pp. 115–193. Elsevier.

Packard RG (1953) Streaming potentials across glass capillaries for sinusoidal pressure. *Journal of Chemical Physics* 21: 303–307.

Palacky GV (1987) Resistivity characteristics of geologic targets. *Electromagnetic Methods in Applied Geophysics, 1. Theory*, vol. 1351.

Parkhomenko EJ (1965) *Elektriceskie Svoitsva Gornich Porod*. Nauka, Moskva: Izdat.

Parks G (1965) The isoelectric points of solid oxides, solid hydroxides, and aqueous hydroxocomplex. *Chemical Reviews* 65: 177–198.

Partzsch GM, Schilling FR, and Arndt J (2000) The influence of partial melting on the electrical behavior of crustal rocks: Laboratory examinations, model calculations and geological interpretations. *Tectonophysics* 317(3–4): 189–203. http://dx.doi.org/10.1016/S0040-1951(99)00320-0.

Patchett JG (1975) An investigation of shale conductivity. In: *Paper Presented at SPWLA 16th Annual Logging Symposium, Paper V, SPWLA, New Orleans, LA, 4–7 June*, 40 pp.

Pearce JA and Zuluaga A (2004) Electrical properties of soils at ISM radio frequencies, from 1 to 40 MHz. *Journal of Microwave Power and Electromagnetic Energy* 39(3–4): 179–190.

Pengra DB, Li SX, and Wong PZ (1999) Determination of rock properties by low-frequency AC electrokinetics. *Journal of Geophysical Research* 104: 29485–29508. http://dx.doi.org/10.1029/1999JB900277.

Peplinski NR, Ulaby FT, and Dobson MC (1995) Dielectric properties of soils in the 0.3–1.3-GHz range. *IEEE Transactions on Geoscience and Remote Sensing* 33(3).

Personna YR, Ntarlagiannis D, Slater L, Yee N, O'Brien M, and Hubbard S (2008) Spectral induced polarization and electrodic potential monitoring of microbially mediated iron sulfide transformations. *Journal of Geophysical Research: Biogeosciences* 113(2): G02020. http://dx.doi.org/10.1029/2007JG000614.

Personna YR, Slater L, Ntarlagiannis D, Werkema D, and Szabo Z (2013a) Complex resistivity signatures of ethanol in sand-clay mixtures. *Journal of Contaminant Hydrology* 149: 76–87. http://dx.doi.org/10.1016/j.jconhyd.2013.07.005.

Personna YR, Slater L, Ntarlagiannis D, Werkema D, and Szabo Z (2013b) Electrical signatures of ethanol–liquid mixtures: Implications for monitoring biofuels migration in the subsurface. *Journal of Contaminant Hydrology* 144: 99–107. http://dx.doi.org/10.1016/j.jconhyd.2012.10.011.

Phillips SL, Ozbek H, and Otto RJ (1978) Basic energy properties of electrolytic solutions database. In: *Sixth International CODATA Conference Santa Flavia (Palermo), Sicily, Italy, May 22–25*. http://www.osti.gov/bridge/purl.cover.jsp;jsessionid=3954E775156A8BC0FA35DB5CE5B402D4?purl=/6269880-iPJPhB/ accessed 10 June 2010.

Pierson HO (2004) *Handbook of Carbon, Graphite, Diamond and Fullerenes – Properties, Processing and Applications*. William Andrew Publishing/Noyes.

Placencia-Gómez E, Slater L, Ntarlagiannis D, and Binley A (2013) Laboratory SIP signatures associated with oxidation of disseminated metal sulfides. *Journal of Contaminant Hydrology* 148: 25–38. http://dx.doi.org/10.1016/j.jconhyd.2013.02.007.

Poirier J-P (2000) *Introduction to the Physics of the Earth's Interior*, 2nd edn Cambridge University Press, ISBN: 9780521663922, 328 pp.

Poupon A and Leveaux J (1971) Evaluation of water saturation in shaly formations. In: *Society of Professional Well Log Analysts 12th Annual Logging Symposium Transactions, Paper O*, 2 pp.

Poupon A, Loy ME, and Tixier MP (1954) A contribution to electric log interpretation in shaly sands. *Transactions of the American Institute of Mechanical Engineers* 201: 138–145.

Pride S (1994) Governing equations for the coupled electromagnetics and acoustics of porous media. *Physical Review B* 50: 15678–15696. http://dx.doi.org/10.1103/PhysRevB.50.15678.

Pride SR and Morgan FD (1991) Electro-kinetic dissipation induced by seismic waves. *Geophysics* 56: 914–925. http://dx.doi.org/10.1190/1.1443125.

Quincke GH (1859) Ueber eine neue Art elektrischer Ströme. *Annalen de Physik und Chemie* 183(5): 1–47. http://dx.doi.org/10.1002/andp.18591830502.

Rasmus JC (1983) Variable cementation exponent, m, for fractured carbonates. *The Log Analyst* 24(6): 13–23.

Reppert PM (2000) Electrokinetics in the Earth. PhD Thesis, Massachusetts Institute of Technology.

Reppert PM and Morgan FD (2001) Streaming potential collection and data processing techniques. *Journal of Colloid and Interface Science* 233(2): 348–355.

Reppert PM and Morgan FD (2003a) Temperature-dependent streaming potentials: 1. Theory. *Journal of Geophysical Research, B: Solid Earth* 108(11), ECV3-1–ECV3-12.

Reppert PM and Morgan FD (2003b) Temperature-dependent streaming potentials: 2. Laboratory. *Journal of Geophysical Research, B: Solid Earth* 108(11), ECV4-1–ECV4-13.

Reppert PM, Morgan FD, Lesmes DP, and Jouniaux L (2001) Frequency-dependent streaming potentials. *Journal of Colloid and Interface Science* 234: 194–203.

Reuβ FF (1809) Sur un nouvel effet de l'électricité galvanique. *Mémoires de la Société Impériale des Naturalistes de Moskou* 2: 327–337.

Revil A and Cerepi A (2004) Streaming potentials in two-phase flow conditions. *Geophysical Research Letters* 31: L11605. http://dx.doi.org/10.1029/2004GL020140.

Revil A and Florsch N (2010) Determination of permeability from spectral induced polarization in granular media. *Geophysical Journal International* 181(3): 1480–1498.

Revil A and Glover PWJ (1997) Theory of ionic-surface electrical conduction in porous media. *Physical Review B – Condensed Matter and Materials Physics* 55(3): 1757–1773.

Revil A and Glover PWJ (1998) Nature of surface electrical conductivity in natural sands, sandstones, and clays. *Geophysical Research Letters* 25(5): 691–694.

Revil A and Leroy P (2001) Hydroelectric coupling in a clayey material. *Geophysical Research Letters* 28(8): 1643–1646. http://dx.doi.org/10.1029/2000GL012268.

Revil A and Leroy P (2004) Constitutive equations for ionic transport in porous shales. *Journal of Geophysical Research* 109: B03208. http://dx.doi.org/10.1029/2003JB002755.

Revil A and Skold M (2011) Salinity dependence of spectral induced polarization in sands and sandstones. *Geophysical Journal International* 187(2): 813–824.

Revil A, Cathles LM, Losh S, and Nunn JA (1998) Electrical conductivity in shaly sands with geophysical applications. *Journal of Geophysical Research, B: Solid Earth* 103(10): 23925–23936.

Revil A, Pezard PA, and Glover PWJ (1999a) Streaming potential in porous media 1. Theory of the zeta potential. *Journal of Geophysical Research, B: Solid Earth* 104(B9): 20021–20031.

Revil A, Schwaeger H, Cathles LM III, and Manhardt PD (1999b) Streaming potential in porous media. 2. Theory and application to geothermal systems. *Journal of Geophysical Research, B: Solid Earth* 104(B9): 20033–20048.

Revil A, Hermitte D, Spangenberg E, and Cochemé JJ (2002) Electrical properties of zeolitized volcaniclastic materials. *Journal of Geophysical Research, B: Solid Earth* 107(8), ECV3-1–ECV3-17.

Revil A, Linde N, Cerepi A, Jougnot D, Matthäi S, and Finsterle S (2007) Electrokinetic coupling in unsaturated porous media. *Journal of Colloid and Interface Science* 313(1): 315–327.

Revil A, Johnson TC, and Finizola A (2010) Three-dimensional resistivity tomography of Vulcan's forge, Vulcano Island, southern Italy. *Geophysical Research Letters* 37(15), L15308.

Reynolds JA and Hough JM (1957) Formulae for dielectric constant of mixtures. *Proceedings of the Physical Society* 70: 769–775.

Robinson DA, Jones SB, Wraith JM, Ord D, and Friedman SP (2003) A review of advances in dielectric and electrical conductivity measurement in soils using time domain reflectometry. *Vadose Zone Journal* 2(4): 444–475. http://dx.doi.org/10.2136/vzj2003.4440.

Rojo A, Hansen HK, and Monárdez O (2014) Electrokinetic remediation of mine tailings by applying a pulsed variable electric field. *Minerals Engineering* 55: 52–56.

Ross DS and Ketterings Q (2011) *Recommended methods for determining soil cation exchange capacity. Recommended Soil Testing Procedures for the Northeastern United States*. pp. 75–85, Northeastern Regional Publication no. 493.

Ruffet C, Gueguen Y, and Darot M (1991a) Complex conductivity measurements and fractal nature of porosity. *Geophysics* 56(6): 758–768. http://dx.doi.org/10.1190/1.1443093.

Ruffet C, Gueguen Y, and Darot M (1991b) Rock conductivity and fractal nature of porosity. *Terra Nova* 3(3): 265–275. http://dx.doi.org/10.1111/j.1365-3121.1991.tb00144.x.

Sass O and Viles HA (2010) Wetting and drying of masonry walls: 2D-resistivity monitoring of driving rain experiments on historic stonework in Oxford, UK. *Journal of Applied Geophysics* 70(1): 72–83.

Saunders JH, Jackson MD, Gulamali MY, Vinogradov J, and Pain CC (2012) Streaming potentials at hydrocarbon reservoir conditions. *Geophysics* 77(1): E77–E90.

Saunders JH, Jackson MD, and Pain CC (2008) Fluid flow monitoring in oilfields using downhole measurements of electrokinetic potential. *Geophysics* 73(5): E165–E180. http://dx.doi.org/10.1190/1.2959139.

Scales PJ, Grieser F, and Healy TW (1990) Electrokinetics of the muscovite mica-aqueous interface. *Langmuir* 6: 582–589. http://dx.doi.org/10.1021/la00093a012.

Schilling F, Partzsch GM, Brasse H, and Schwartz G (1997) Partial melting below the magmatic arc in the central Andes deduced from geoelectric field experiments and laboratory data. *Physics of the Earth and Planetary Interiors* 103: 17–31.

Schlumberger (1972) *Log Interpretation, Volume 1 – Principles*. New York: Schlumberger Ltd., 113 pp.

Schlumberger (2013) Log Interpretation Charts, Gen-4 (Gen-8 in previous annually issued charts), Schlumberger.

Schmutz M, Revil A, Vaudelet P, Batzle M, Viñao PF, and Werkema DD (2010) Influence of oil saturation upon spectral induced polarization of oil-bearing sands. *Geophysical Journal International* 183(1): 211–224.

Schön JH (2004) Physical Properties of Rocks: Fundamentals and Principles of Petrophysics. In: Helbig K and Treitel S (eds.) *vol. 18* Amsterdam, The Netherlands: Elsevier, ISBN: 008044346X.

Schwartz LM, Sen PN, and Johnson DL (1989) Influence of rough surfaces on electrolytic conduction in porous media. *Physical Review B* 40(4): 2450–2458. http://dx.doi.org/10.1103/PhysRevB.40.2450.

Schwarz G (1962) A theory of the low-frequency dielectric dispersion of colloidal particles in electrolyte solution. *Journal of Physical Chemistry* 66: 2636–2642.

Scott JBT and Barker RD (2003) Determining pore-throat size in Permo-Triassic sandstones from low-frequency electrical spectroscopy. *Geophysical Research Letters* 30(9): 1450. http://dx.doi.org/10.1029/2003GL016951.

Scott JBT and Barker RD (2005) Characterization of sandstone by electrical spectroscopy for stratigraphical and hydrogeological investigations. *Quarterly Journal of Engineering Geology & Hydrogeology* 38: 143–154.

Seager CH and Pike GE (1974) Percolation and conductivity: A computer study II. *Physical Review B* 10: 1435–1446.

Sears AR and Groves JN (1978) The use of oscillating laminar flow streaming potential measurements to determine the zeta potential of a capillary. *Journal of Colloid and Interface Science* 65: 479–482.

Selway K (2014) On the Causes of Electrical Conductivity Anomalies in Tectonically Stable Lithosphere. *Surveys in Geophysics* 35(1): 219–257.

Sen P and Goode P (1992a) Influence of temperature on electrical conductivity on shaly sands. *Geophysics* 57: 89–96.

Sen P and Goode P (1992b) Errata, to: Influence of temperature on electrical conductivity of shaly sands. *Geophysics* 57: 1658.

Sen C, Scala PN, and Cohen MH (1981) A self-similar model for sedimentary rocks with application to the dielectric constant of fused glass beads. *Geophysics* 46(5): 781–795.

Shah C and Yortsos Y (1996) The permeability of strongly disordered systems. *Physics of Fluids* 8: 280–282.

Sheffer MR, Reppert PM, and Howie JA (2007) A laboratory apparatus for streaming potential and resistivity measurements on soil samples. *Review of Scientific Instruments* 78(9): 094502. http://dx.doi.org/10.1063/1.2782710.

Simandoux P (1963) Dielectric measurements on porous media application to the measurement of water saturations: Study of the behavior of argillaceous formations (Mesures dielectriques en milieu poreux, application a la Mewe des saturations en eau, etude du comportement des massifs argileux). *Revue de l'Institut Francais du Petrole* 18: 193–215, Supplementary Issue.

Skold M, Revil A, and Vaudelet P (2011) The pH dependence of spectral induced polarization of silica sands: Experiment and modelling. *Geophysical Research Letters* 38(12), L12304.

Slater L (2007) Near surface electrical characterization of hydraulic conductivity: From petrophysical properties to aquifer geometries—A review. *Surveys in Geophysics* 28: 169–197. http://dx.doi.org/10.1007/s10712-007-9022-y.

Slater L and Glaser D (2003) Controls on induced polarization in sandy unconsolidated sediments and application to aquifer characterization. *Geophysics* 68(5): 1547–1558.

Slater L and Lesmes DP (2002) Electrical-hydraulic relationships observed for unconsolidated sediments. *Water Resources Research* 38(10): 1213.

Slater L, Ntarlagiannis D, and Wishart D (2006) On the relationship between induced polarization and surface area in metal-sand and clay-sand mixtures. *Geophysics* 71(2): A1–A5.

Smith WDM and Rouleau RJ (1977) A modified shaly sand Sw equation for the Western Canada Cretaceous. In: *Canadian Well Logging Society Sixth Formation Evaluation Conference, Paper V,* 4 pp.

Smoluchowski M (1903) Contribution à la théorie l´endosmose électrique et de quelques phénomènes corrélatifs. *Krak. Anz.* 1903: 182–199.

Somerton WH (1992) *Thermal Properties and Temperature-Related Behavior of Rock/Fluid Systems*. Amsterdam, The Netherlands: Elsevier, ISBN: 0444890017.

Speight JG (2011) *An Introduction to Petroleum Technology, Economics, and Politics*. John Wiley & Sons978-1-118-19254-2, 334 pp.

Sposito G (1989) *The Chemistry of Soils*. Oxford: Oxford University.

Sprunt ES, Mercer TB, and Djabbarah NF (1994) Streaming potential from multiphase flow. *Geophysics* 59: 707–711. http://dx.doi.org/10.1190/1.1443628.

Susanto A, Koleva DA, Copuroglu O, Van Beek K, and Van Breugel K (2013) Mechanical, electrical and microstructural properties of cement-based materials in conditions of stray current flow. *Journal of Advanced Concrete Technology* 11(3): 119–134.

Sweeney SA and Jennings HY Jr. (1960) Effect of wettability on the electrical resistivity of carbonate rock from a petroleum reservoir. *Journal of Physical Chemistry* 64(5): 551–553. http://dx.doi.org/10.1021/j100834a009.

Tardif E, Glover PWJ, and Ruel J (2011) Frequency-dependent streaming potential of Ottawa sand. *Journal of Geophysical Research B* 116: B04206. http://dx.doi.org/10.1029/2010JB008053.

Thompson A and Gist G (1993) Geophysical applications of electrokinetic conversion. *The Leading Edge* 12: 1169–1173.

Thomson WT and Dahleh MD (1998) *Theory of Vibration with Applications*, 5th edn. Englewood Cliffs, NJ: Prentice-Hall, 524 pp.

Tiab D and Donaldson EC (2011) *Petrophysics, Theory and Practice of Measuring Reservoir Rock and Fluid Transport Properties*, 3rd edn. Gulf Professional Publishing, ISBN: 9780123838483.

Titov K, Komarov V, Tarasov V, and Levitski A (2002) Theoretical and experimental study of time domain-induced polarization in water-saturated sands. *Journal of Applied Geophysics* 50: 417–433.

Titov K, Tarasov A, Yuri I, Seleznev N, and Boyd A (2010) Relationships between induced polarization relaxation time and hydraulic properties of sandstone. *Geophysical Journal International* 180: 1095–1106.

Ulrich C and Slater L (2004) Induced polarization measurements on unsaturated, unconsolidated sands. *Geophysics* 69(3): 762–771.

Vanhala H (1997) Mapping oil-contaminated sand and till with the spectral induced polarization (SIP) method. *Geophysical Prospecting* 45(2): 303–326.

Vaudelet P, Revil A, Schmutz M, Franceschi M, and Bégassat P (2011a) Changes in induced polarization associated with the sorption of sodium, lead, and zinc on silica sands. *Journal of Colloid and Interface Science* 360(2): 739–752.

Vaudelet P, Revil A, Schmutz M, Franceschi M, and Bégassat P (2011b) Induced polarization signatures of cations exhibiting differential sorption behaviors in saturated sands. *Water Resources Research* 47(2), W02526.

Vinogradov J and Jackson MD (2011) Multiphase streaming potential in sandstones saturated with gas/brine and oil/brine during drainage and imbibition. *Geophysical Research Letters* 38: L01301. http://dx.doi.org/10.1029/2010GL045726.

Vinogradov J, Jaafar MZ, and Jackson MD (2010) Measurement of streaming potential coupling coefficient in sandstones saturated with natural and artificial brines at high salinity. *Journal of Geophysical Research, B: Solid Earth* 115(12).

Volkmann J and Klitzsch N (2010) Frequency-dependent electric properties of microscale rock models for frequencies from one millihertz to ten kilohertz. *Vadose Zone Journal* 9: 858–870. http://dx.doi.org/10.2136/vzj2009.0162.

Waff HS (1974) Theoretical consideration of electrical conductivity in a partially molten mantle and implications for geothermometry. *Journal of Geophysical Research* 79: 4003–4010.

Wagner KW (1914) Erklärung der dielektrischen Nachwirkunsvorgänge auf Grund Maxwellscher Vorstellungen. *Archiv fur Elektrotechnik* 2(9): 371–387.

Walker E and Glover PW J (2010) Characteristic pore size, permeability and the electro-kinetic coupling coefficient transition frequency in porous media. *Geophysics* 75(6): E235–E246.

Walker E, Glover PWJ, and Ruel J (2014) A transient method for measuring the DC streaming potential coefficient of porous and fractured rocks. *Journal of Geophysical Research - Solid Earth* 119. http://dx.doi.org/10.1002/2013JB010579.

Wall S (2010) The history of electrokinetic phenomena. *Current Opinion in Colloid and Interface Science* 15: 119–124. http://dx.doi.org/10.1016/j.cocis.2009.12.005.

Waxman MH and Smits LJM (1968) Electrical conductivities in oil-bearing shaly sands. *SPE Journal* 8(2): 107–122. http://dx.doi.org/10.2118/1863-A.

Weiss J, Snyder K, Bullard J, and Bentz D (2013) Using a saturation function to interpret the electrical properties of partially saturated concrete. *Journal of Materials in Civil Engineering* 25(8): 1097–1106.

Weller A, Breede K, Slater L, and Nordsiek S (2011) Effect of changing water salinity on complex conductivity spectra of sandstones. *Geophysics* 76(5): F315–F327. http://dx.doi.org/10.1190/geo2011-0072.1.

Winsauer WO, Shearin HM, Masson PH, and Williams M (1952) Resistivity of brine-saturated sands in relation to pore geometry. *AAPG Bulletin* 36: 253–277.

Wittmann K, Feuerbacher B, Ulamec S, et al. (1999) Rosetta lander in situ characterization of a comet nucleus. *Acta Astronautica* 45(4–9): 389–395.

Wong PZ (1987) Fractal surface in porous media. In: Banavar JR, Koplik J, and Winkler KW (eds.) *Physics and Chemistry of Porous Media,* vol. 2, *Am. Inst. Phys. Conference Proceedings*, *vol. 154*, pp. 304–318.

Worthington PF (1985) The evolution of shaly-sand concepts in reservoir evaluation. *The Log Analyst* XXVI(1): 23–40.

Wu L, Forsling W, and Schlindler PW (1991) Surface complexation of calcium minerals in aqueous solution. *Journal of Colloid and Interface Science* 147: 178–185. http://dx.doi.org/10.1016/0021-9797(91)90145-X.

Wyllie MRJ and Gregory AR (1953) Formation factors of unconsolidated porous media: Influence of particle shape and effect of cementation. *Transactions of the AIME* 198: 103–110.

Xu Y and Schoonen MAA (2000) The absolute energy positions of conduction and valence bands of selected semiconducting minerals. *American Mineralogist* 85(3–4): 543–556.

Xu Y, Shankland TJ, and Duba AG (2000) Pressure effect on electrical conductivity of mantle olivine. *Physics of the Earth and Planetary Interiors* 118: 149.

Yang X (2011) Origin of high electrical conductivity in the lower continental crust: A review. *Surveys in Geophysics* 32(6): 875–903.

Yoshino T and Noritake F (2011) Unstable graphite films on grain boundaries in crustal rocks. *Earth and Planetary Science Letters* 306(3–4): 186–192.

Yoshino T, Nishi M, Matsuzaki T, Yamazaki D, and Katsura T (2008) Electrical conductivity of majorite garnet and its implications for electrical structure in the mantle transition zone. *Physics of the Earth and Planetary Interiors* 170(3–4): 193–200.

Zakri T, Laurent J-P, and Vauclin M (1998) Theoretical evidence for 'Lichtenecker's mixture formulae' based on the effective medium theory. *Journal of Physics D: Applied Physics* 31: 1589–1594.

Zhang J and Catchmark JM (2011) A catalytically powered electro-kinetic lens, Toward channel-less microfluidics. *Microfluidics and Nanofluidics* 10(5): 1147–1151.

Zhang C, Ntarlagiannis D, Slater L, and Doherty R (2010) Monitoring microbial sulfate reduction in porous media using multipurpose electrodes. *Journal of Geophysical Research, Biogeosciences* 15(G3). http://dx.doi.org/10.1029/2009JG001157.

Zhang C, Slater L, and Prodan C (2013) Complex dielectric properties of sulfate-reducing bacteria suspensions. *Geomicrobiology Journal* 30(6): 490–496. http://dx.doi.org/10.1080/01490451.2012.719997.

Zhang C, Slater L, Redden G, Fujita Y, Johnson T, and Fox D (2012) Spectral induced polarization signatures of hydroxide adsorption and mineral precipitation in porous media. *Environmental Science & Technology* 46: 4357–4364. http://dx.doi.org/10.1021/es204404e.

Zhao JH, Rivera E, Mufti A, Stephenson D, and Thomson DJ (2012) Evaluation of dielectric based and other methods for moisture content measurement in building stones. *Journal of Civil Structural Health Monitoring* 2(3–4): 137–148.